

Multi-Scale Earth Observation of the Arctic Environment

*A Pan-Arctic Climate and Trend Analysis
for the Last Decades*



seit 1558

Dissertation

(kumulativ)

zur Erlangung des akademischen Grades doctor rerum naturalium

(Dr. rer. nat.)

vorgelegt dem Rat der Chemisch-Geowissenschaftlichen Fakultät der
Friedrich-Schiller-Universität Jena

von Marcel Urban (M. Sc.)

geboren am 31. 05. 1983 in Bad-Saarow

Gutachter:

1. Prof. Dr. Christiane Schmullius
2. Prof. Dr. Martin Herold (Wageningen University, Niederlande)

Tag der Verteidigung: 17. Dezember 2014

"Green" has become synonymous with "good" in many circles.

Not inside the Arctic Circle.

By

Heather Goldstone

(The Cape and Islands NPR Station, Woods Hole, MA, United States)

in interview with Scott Goetz (Woods Hole Research Center)

Source:

<http://capeandislands.org/post/new-research-predicts-dramatically-greener-arctic-near-future>

Content

| | |
|--|-------------|
| FIGURES | XI |
| TABLES | XV |
| ABBREVIATIONS | XVII |
| ABSTRACT | XXI |
| ZUSAMMENFASSUNG | XXV |
| | |
| CHAPTER 1 | 1 |
| 1 Introduction..... | 1 |
| 1.1 General Introduction and Outline | 2 |
| 1.2 Research Questions..... | 5 |
| 1.3 Study Area..... | 7 |
| 1.4 Historical Climate Conditions in the Arctic..... | 9 |
| 1.5 Recent Trends in Arctic Ecosystems..... | 13 |
| 1.6 Remote Sensing of Arctic Parameters | 21 |
| | |
| CHAPTER 2 | 25 |
| 2 Identification of Land Surface Temperature and Albedo Trends in AVHRR Pathfinder Data from 1982 to 2005 for Northern Siberia..... | 25 |
| 2.1 Abstract..... | 26 |
| 2.2 Introduction..... | 27 |
| 2.3 Data | 30 |
| 2.4 Methodology | 33 |
| 2.5 Results and Discussion..... | 36 |

| | | |
|-----------------------|---|-----------|
| 2.5.1 | Time series analysis of LST, albedo, NDVI and SWE..... | 36 |
| 2.5.2 | Identification of spatial LST and Albedo trend hot spots..... | 40 |
| 2.5.3 | Comparing Pathfinder LST data and Air Temperature records | 44 |
| 2.6 | Conclusion and Outlook..... | 46 |
| CHAPTER 3..... | | 49 |
| 3 | Comparison of Satellite-Derived Land Surface Temperature and Air Temperature from Meteorological Stations on the Pan-Arctic Scale..... | 49 |
| 3.1 | Abstract | 50 |
| 3.2 | Introduction | 51 |
| 3.3 | Data..... | 54 |
| 3.3.1 | Remote Sensing Data..... | 54 |
| 3.3.2 | Global Surface Summary of Day Data—Version 7..... | 56 |
| 3.4 | Methodology..... | 58 |
| 3.5 | Results and Discussion..... | 61 |
| 3.5.1 | Correlation of Remote Sensing-Based LST Estimates with T_{air} Measurements | 61 |
| 3.5.2 | Inter-Annual Variability of LST Estimates for the Time Period between 2000 and 2005..... | 64 |
| 3.5.3 | Comparison of Land Surface Temperature and Air Temperature for Selected Land Cover Classes..... | 68 |
| 3.5.4 | Pan-Arctic Perspective of the Mean Difference for the Time Period of 2000–2005..... | 72 |
| 3.6 | Conclusion and Outlook..... | 74 |
| 3.7 | Acknowledgments..... | 76 |
| CHAPTER 4..... | | 77 |
| 4 | Pan-Arctic Climate and Land Cover Trends Derived from Multi-Variate and Multi-Scale Analyses (1981 - 2012)..... | 77 |
| 4.1 | Abstract | 78 |
| 4.2 | Introduction | 79 |
| 4.3 | Data and Methods..... | 82 |
| 4.3.1 | Maximum Snow Water Equivalent—ESA DUE GlobSnow | 82 |
| 4.3.2 | Temperature and Precipitation—Climate Research Unit (CRU)..... | 82 |
| 4.3.3 | NDVI3g - GIMMS | 83 |
| 4.3.4 | Arctic Biodiversity Assessment - CAFF..... | 83 |

| | | |
|--------------------------------------|--|------------|
| 4.3.5 | Trend Analysis | 84 |
| 4.3.6 | Vegetation Structure Change Detection Using High Resolution Remote Sensing Data | 84 |
| 4.4 | Results and Discussion..... | 86 |
| 4.4.1 | Pan-Arctic Trends on Monthly Scale..... | 86 |
| 4.4.2 | Monthly Inter-Annual Trend Dynamics for Different Arctic Regions | 91 |
| 4.4.3 | High-Resolution Change Mapping of the Taiga-Tundra Transition Zone in Northern Siberia..... | 93 |
| 4.5 | Conclusions | 97 |
| CHAPTER 5..... | | 99 |
| 5 | Synthesis..... | 99 |
| 5.1 | Concluding Remarks..... | 100 |
| 5.2 | Future Research Needs | 109 |
| REFERENCES | | 113 |
| APPENDIX | | 137 |
| ACKNOWLEDGEMENT..... | | 139 |
| CURRICULUM VITAE..... | | 141 |
| STATEMENT OF AUTHORSHIP | | 147 |

Figures

| | | |
|-------------|---|----|
| Figure 1.1: | Overview of the pan-arctic region including average sea ice extent (yellow line) and minimum sea ice concentration in 2012 (white area), permafrost zones, glacier locations as well as snow cover regimes (modified from Comiso and Hall (2014) and Vaughan et al. (2013)). | 7 |
| Figure 1.2: | Concentration of atmospheric CO ₂ (in ppmv, black) and temperature (unrelated units, red) for the last 420.000 years from Vostok ice core (Antarctica) (based on data from Petit et al. (1999) in Zeng (2003)). | 9 |
| Figure 1.3: | Northern hemisphere temperature anomalies between 1000 and 2000 as described by various sources (based on Mann et al. (2008)) | 10 |
| Figure 1.4: | Time series information from meteorological stations available through the NASA GISS Surface Temperature Analysis network. top: Number of stations and their record length. bottom left: amount of stations since 1880. bottom right: hemispheric area percentage within a 1200 km radius of a station (modified from NASA (2013)). | 11 |
| Figure 1.5: | Global mean temperature anomalies between 1900 and 2100 described by different GCMs (left). Relationship between global and arctic mean temperature anomalies (right) (Kaplan and New 2006). | 14 |
| Figure 1.6: | A schematic illustration describing the snow-albedo feedback (SAF) (modified from Qu and Hall (2007)). | 15 |

| | | |
|--------------|--|----|
| Figure 1.7: | Comparing sea ice concentration, albedo and surface air temperature between 1979 and 2011 (Pistone et al. 2014)..... | 16 |
| Figure 1.8: | Evolution of snow cover extent for the northern hemisphere between 1967 and 2012 for the spring season (Comiso and Hall 2014)..... | 17 |
| Figure 1.9: | Mean values for SOS, EOS and LOS averaged of the period of 2000 - 2011 (top) as well as the linear trend for the same period (bottom) (modified from Zeng et al. (2011))...... | 18 |
| Figure 1.10: | Comparing active layer thickness with shrub cover (<i>Betula nana</i>) for two test sites in 2007 and 2008 (Blok et al. 2010)..... | 19 |
| Figure 2.1: | Methodology flow chart showing the extraction of inter-annual monthly trends from daily AVHRR land surface temperature and albedo information. | 35 |
| Figure 2.2: | Overview of time series information from AVHRR land surface temperature and albedo for the buffer zone of 100 km north and south of the tree line for the summer month June (<i>a</i>) and July (<i>b</i>) within the time period from 1982 to 2005. | 37 |
| Figure 2.3: | Overview of time series information from AVHRR land surface temperature and albedo for the buffer zone of 100 km north and south of the tree line for the summer month August (<i>a</i>) and September (<i>b</i>) within the time period from 1982 to 2005. | 38 |
| Figure 2.4: | Overview of median from AVHRR land surface temperature and albedo time series for the buffer zone of 100 km north and south of the tree line for the summer month (<i>a</i>) and snow water equivalent (SWE) and NDVI time series information for June (<i>b</i>). Missing years of SWE information are marked with a black cross..... | 40 |
| Figure 2.5: | Land surface temperature and albedo trends (correlation coefficient R over time) in northern Siberia for the summer month June, July, August and September. Only significant values are displayed. The dashed line represents the tree line from Walker et al. (2005)..... | 41 |

| | | |
|-------------|--|----|
| Figure 2.6: | Correlation of land surface temperature and albedo trends (correlation coefficient R over time) from three selected regions (Taymir – north and south and Yamal Peninsula). Each month (June (J), July (J), August (A) and September (S)) are displayed in a separate plot..... | 44 |
| Figure 2.7: | Comparison of AVHRR Pathfinder land surface temperature estimates and in-situ air temperature records from meteorological stations (NCDC 2012)..... | 45 |
| Figure 3.1: | Flowchart of the described methodology. | 59 |
| Figure 3.2: | Comparison of (A)ATSR, AVHRR, MODIS Terra and MODIS Aqua LST estimates and T_{air} records from meteorological stations. Each plot shows the complete time period of each product (AATSR = 1991–2009, AVHRR = 1982–2005, MODIS Terra = 2000–2012, MODIS Aqua = 2002–2012). | 62 |
| Figure 3.3: | Inter-annual variability of the correlation coefficient (R), slope, intercept (INT) and mean difference (MD) for the time period of 2000 to 2005..... | 65 |
| Figure 3.4: | Comparing LST and T_{air} for the time period of 2000 to 2005 for selected land cover classes..... | 69 |
| Figure 3.5: | Pan-Arctic mean difference distribution..... | 73 |
| Figure 4.1: | Co-occurrence of different climatic and ecosystem trends on pan-arctic scale between 1981 and 2012 (December to February). The trend findings from monthly temperatures, precipitation, SWE_{max} are combined into one information source, which includes all possible combinations of trend patterns. Only areas showing significant trends (p -value < 0.05) are displayed. | 87 |
| Figure 4.2: | Co-occurrence of different climatic and ecosystem trends on pan-arctic scale between 1981 and 2012 (March to May) (for more explanation see Figure 4.1). The NDVI is shown via plus or minus symbols, which are indicating either positive or negative trends at the location. | 88 |

| | | |
|---------------|--|-----|
| Figure 4.3: | Co-occurrence of different climatic and ecosystem trends on pan-arctic scale between 1981 and 2012 (June to August). The trend findings from monthly temperatures and precipitation were combined into one information source. The NDVI is shown via plus or minus symbols, which are indicating either positive or negative trends at the location..... | 89 |
| Figure 4.4: | Co-occurrence of different climatic and ecosystem trends on pan-arctic scale between 1981 and 2012 (September to November) (for more explanation see Figure 4.1). | 90 |
| Figure 4.5: | Monthly inter-annual variability of the slopes from the multivariate trend calculations. Only trends with a significance level of $p < 0.05$ are shown. | 93 |
| Figure 4.6: | Air-Temperature time series divided by seasons (winter—DJF; spring—MAM, summer—JJA and fall—SON) of the meteorological station Khatanga at the Taymyr Peninsula (71.9°N, 102.5°E)—Additional stations are shown in the supplementary material (see appendix Figure App. 2)..... | 94 |
| Figure 4.7: | Landsat MSS and RapidEye woody vegetation cover (in % per 5 km grid cell) mapping between 1973 (Left) and 2012 (Right)—background based on World Imagery by ESRI. The tree line reference from (Walker et al. 2005) is shown in black. Cloud regions in the Landsat MSS data are shown in grey..... | 95 |
| Figure App.1: | Arctic boundary map produced by the Arctic Biodiversity Assessment as part of the CAFF (Conservation of Arctic Flora and Fauna), 2010..... | 137 |
| Figure App.2: | Air-Temperature time series divided by seasons (winter - DJF; spring - MAM, summer - JJA and fall - SON) of meteorological stations at the Taymyr Peninsula (top: Lake Taymyr (74.5° N, 102.5° E); middle: Saskylah (71.9° N, 114.1° E); bottom: Dzalinda (70.1° N, 113.9° E))..... | 138 |

Tables

| | | |
|------------|--|----|
| Table 1.1: | Low resolution Earth observation data and products for arctic environmental monitoring..... | 22 |
| Table 1.2: | Medium to high resolution Earth observation data for arctic environmental monitoring. | 24 |
| Table 3.1: | Standard deviation of the statistical parameters correlation coefficient and mean difference for selected land cover classes. | 70 |

Abbreviations

| | |
|-----------------|---|
| (A)ATSR | (Advanced) Along Track Scanning Radiometer |
| A.D. | Anno Domini |
| ACIA | Arctic Climate Impact Assessment |
| ALOS | Advanced Land Observing Satellite |
| AMSR-E | Advanced Microwave Scanning Radiometer Earth Observing System |
| ARF | Anisotropic Reflectance Factor |
| ASCAT | Advanced Scatterometer |
| ATCOR | Atmospheric and Topographic Correction |
| AVHRR | Advanced Very High Resolution Radiometer |
| BFAS | Breaks for Additive Seasonal and Trends |
| BP | before present |
| CAFF | Conservation of Arctic Flora and Fauna |
| CAVM | Circumpolar Arctic Vegetation Map |
| CBVM | Circumboreal Vegetation Map |
| CCI | Climate Change Initiative |
| CEC | Commission for Environmental Cooperation |
| CLIP-C | Climate Change Information Platform for Copernicus |
| CMG | Climate Modeling Grid |
| CO ₂ | Carbon Dioxide |
| CRU | Climate Research Unit |
| DJF | winter months |
| DLR | German Aerospace Center |
| DOI | Digital Object Identifier |
| DUE | Data User Element |
| EASE-Grid | Equal Area Scalable Earth Grid |
| ENVISAT | Environmental Satellite |
| EOS | end of season |
| ERS | European Remote Sensing Satellite |

| | |
|---------|--|
| ESA | European Space Agency |
| EVI | Enhanced Vegetation Index |
| FAO | Food and Agriculture Organization |
| FAPAR | Fraction of Absorbed Photosynthetically Active Radiation |
| GCM | Global Climate Model |
| GCOS | Global Climate Observing System |
| GHG | greenhouse gas |
| GIMMS | Global Inventory Modelling and Mapping Studies |
| GISS | Goddard Institute for Space Studies |
| GLC2000 | Global Land Cover 2000 |
| GOES | Geostationary Operational Environmental Satellite |
| GSOD | Global Surface Summary of Day Data |
| GT | gigatons |
| ILST-WG | International Land Surface Temperature working group |
| INT | Intercept |
| IPCC | Intergovernmental Panel on Climate Change |
| ISD | Integrated Surface Database |
| ISH | Integrated Surface Hourly |
| JERS | Japanese Earth Resources Satellite |
| JJA | summer months |
| JRC | Joint Research Centre |
| LAI | Leaf Area Index |
| LC | Land Cover |
| LCCS | Land Cover Classification System |
| LIA | Little Ice Age |
| LOS | vegetation growing period |
| LST | land surface temperature |
| MAM | spring months |
| MD | mean difference |
| MERIS | Medium Resolution Imaging Spectrometer |
| MODIS | Moderate Resolution Imaging Spectroradiometer |
| MTSAT | Multifunctional Transport Satellites |
| MWP | medieval warm period |
| NaN | Not a number |
| NASA | National Aeronautics and Space Administration |
| NCDC | National Climate Data Center |
| NDVI | Normalized Differenced Vegetation Index |
| NELDA | Northern Eurasia Land Dynamics Analysis |
| NITF | National Imagery Transmission Format |
| NOAA | National Oceanic and Atmospheric Administration |
| NSIDC | National Snow and Ice Data Center |

| | |
|-------------|--|
| PAGE21 | Changing permafrost in the Arctic and its Global Effects in the 21st Century |
| PALSAR | Phased Array type L-band Synthetic Aperture Radar |
| ppmv | parts per million by volume |
| PRISM | Panchromatic Remote-Sensing Instrument for Stereo Mapping |
| QA4ECV | Quality Assurance for Essential Climate Variables |
| R | correlation coefficient |
| RESA | RapidEye Science Archive |
| RPC | Rapid Positioning Capability |
| S | slope |
| SAF | snow albedo feedback |
| SE | snow extent |
| SEVIRI | Spinning Enhanced Visible and Infrared Imager |
| SMMR | Scanning Multichannel Microwave Radiometer |
| SON | fall months |
| SOS | start of season |
| SPOT | Satellite Pour l'Observation de la Terre |
| SSM/I | Special Sensor Microwave/Imager |
| SWE | snow water equivalent |
| SWE_{max} | maximum snow water equivalent |
| T_{air} | air temperature |
| TIR | thermal infrared |
| TOA | top-of-atmosphere |
| UNFCCC | United Nation Framework Convention on Climate Change |
| VCF | Vegetation Continuous Fields |
| WCRP | World Climate Research Programme |
| WFA | World Fire Atlas |
| WMO | World Meteorological Organization |

Abstract

The terrestrial ecosystems of the northern high latitudes are subject to significant changes during the last century and highly vulnerable to modifications in the global climate system. Climate models predict increasing global mean temperatures for the 21st century. Changes in temperature, as well as precipitation, are having an impact on snow cover, vegetation productivity and coverage, vegetation seasonality, surface albedo, and permafrost dynamics. The coupled climate-land surface changes in the arctic are thought to be a positive feedback in the Earth system, which can potentially further accelerate global warming. In contrast to other regions, the northern high latitudes are supposed to face the strongest and largest feedbacks for the upcoming decades. Hence, the arctic region has become a major focus in Earth system science and climate related research topics.

The identification of significant modifications of the state and spatio-temporal dynamics of arctic climate and land surface parameters, such as temperature, precipitation, snow and vegetation is a challenging issue. Earth observation information from various sources provides a useful tool to observe and monitor essential climate parameters. Moreover, Earth observation is an indirect measurement technique which allows retrieving spatial information over large areas and compensates for the lack of ground measurements in remote areas. Therefore, the use of remote sensing information has gained high importance for climate change related research studies during the last decades.

This thesis focuses on the analysis of trends and time series information on pan-arctic scale using multi-scale Earth observation data and products describing multiple essential climate and land surface parameters. Remote sensing time series information covering the last 40 years have been utilized to identify spatial and temporal characteristics of land surface temperature (LST) and albedo information in northern Siberia. A comparison of remote sensing derived temperature values with air temperature measurements from climate stations has been carried out to

address uncertainties in Earth observation LST products, which is of high importance for future arctic climate investigations and modeling approaches. The combination of trend findings from multiple sources has been used to analyze the co-occurrence and relationship of different arctic climate and land surface parameters. Changes of the vegetation structure during the last 40 years in the taiga–tundra transition area have been classified using high spatial resolution multispectral remote sensing data.

Analyzing changes in vegetation structure and phenological dynamics within the taiga-tundra ecotone, which is the Earth greatest vegetation transition zone, is of high importance in climate change research. Land surface temperature and albedo time series information, which were derived from the NOAA (National Oceanic and Atmospheric Administration) AVHRR (Advanced Very High Resolution Radiometer) Polar Pathfinder product, have shown significant dependencies for the summer month in the northern parts of central Siberia. In detail, strong negative correlations between LST and albedo values for the start and the end of the vegetation growing period have been identified. The inter-annual dynamics and variations are indicating changes in the vegetation growing period between 1982 and 2005 for the study region. Temporal variations from snow water equivalent and vegetation greenness in this time period emphasize the findings in the AVHRR Polar Pathfinder product.

The use of remote sensing based temperature information is an essential information source for global climate change studies over large areas. Data from various sensor platforms, such as MODIS (Moderate Resolution Imaging Spectroradiometer), AVHRR and (A)ATSR ((Advanced) Along Track Scanning Radiometer), are providing long-term LST time series information (e.g. AVHRR – since the 1980s). Assessing the quality of satellite-based temperature information is important to provide feedback to the climate modeling community and other users. Remote sensing derived LST and air temperature records from meteorological stations covering the entire pan-arctic circle, which were provided by the National Climate Data Center (NCDC), were compared to identify agreements and discrepancies between these variables. The MODIS LST product has shown the highest agreement to the corresponding air temperature records. (A)ATSR and AVHRR have shown the largest biases, high inter-annual variability and inconsistencies in the evaluation approach. Based on these findings it is possible to provide recommendations to user communities, which are utilizing remote sensing

derived temperature information, such as climate and ecosystem modelers as well as meteorologists.

The co-occurrence of temperature, precipitation, snow cover, and vegetation greenness trends in the pan-arctic region between 1981 and 2012 has been analyzed using Earth observation products and ground based measurements. Based on coarse resolution remote sensing and in-situ based data products it was possible to identify regions showing congruent and divergent trends of various parameters. In general, precipitation significantly increases during summer and fall. Temperature conditions in winter are increasing between 1981 and 2012. The parameter snow water equivalent has shown the highest trends during spring and fall. Vegetation greening trends are characterized by a constant increase during the vegetation growing period. Largest dependencies between the parameters are found in spring, fall and winter. The co-occurrence of snow water equivalent and temperature trends in the transition month between summer and winter indicate to have the largest impact to the arctic environment during the last decades. High spatial resolution Earth observation data have been utilized to identify land surface changes in the taiga tundra ecotone for a selected test region in northern Siberia between 1973 and 2012. This region was identified to be characterized by the most significant and largest trends during the last 40 years. By using high spatial resolution remote sensing data, an intensification of the woody vegetation cover have been found at the arctic tree line near the Taymyr peninsula. These climatic and ecosystem changes represent the multi-scale feedbacks in the arctic environment.

Earth observation data and techniques provide a valuable tool to identify and monitor essential climate and land surface variables. The utilization of operational remote sensing data has high potential in future climate change and environmental research. The content of this thesis emphasized, that (1) analyzing the spatial and temporal characteristics of various climate and land surface parameters, (2) addressing the uncertainties in Earth observation data, (3) analyzing the co-occurrence of multiple trend findings, as well as (4) scaling between different satellite platforms, is of high relevance in the assessment and operational monitoring of arctic land surface changes and ecosystem dynamics.

Zusammenfassung

Die arktischen Breiten der nördlichen Hemisphäre sind stark gekennzeichnet durch den Wandel im globalen Klimasystem und durch fortschreitende klimatische Veränderungen, die im Zuge des letzten Jahrhunderts ein historisches Maximum erreichten. Die Veränderung des Klimas und dessen Dynamiken sind dabei zum Großteil auf die Intensivierung der vom Menschen verursachten Treibhausgasemissionen zurückzuführen.

Prognosen von Klimamodellen deuten auf steigende Temperaturen im arktischen Raum in Bezug auf das globale Mittel für das kommende Jahrhundert hin. Durch das Abschmelzen der Dauerfrostböden kommt es zur vermehrten Freisetzung von Treibhausgasen wie Methan und Kohlenstoffdioxid. Folgen des Klimawandels sind nachhaltige Veränderungen der Landoberflächen- und Vegetationsstruktur, der Phänologie sowie der Niederschlagsdynamiken. Die Zusammenhänge zwischen diesen einzelnen klimatischen und erdoberflächigen Parametern können einen positiven Rückkopplungseffekt im arktischen und globalen Klimasystem hervorrufen und die Klimaerwärmung zusätzlich beschleunigen. Im Vergleich zu anderen Regionen der Erde sind der Klimawandel und dessen Auswirkungen in den arktischen Breiten signifikant stärker. Demzufolge liegt der Fokus aktueller Forschungsfragen in verschiedenen Bereichen der Ökologie, Geographie und anderen klimarelevanten Wissenschaftsbereichen vermehrt auf dem arktischen Raum.

Die flächendeckende Analyse und Identifikation von signifikanten raumzeitlichen Veränderungen und Dynamiken von verschiedenen Klima- und Landoberflächenparametern, wie Temperatur, Niederschlag, Schneebedeckung und Vegetation, sind ein wichtiger Bestandteil aktueller Forschungsinitiativen. Die Ableitung von terrestrischen Klimaparametern mit Hilfe verschiedener Fernerkundungssatelliten leistet einen essentiellen Beitrag zur arktischen Klimawandelforschung. Die Erdbeobachtung ist ein indirektes Messverfahren, das die Aufnahme

von räumlichen Informationen verschiedener Variablen über große Gebiete ermöglicht und dadurch fehlende Geländemessungen in abgelegenen Regionen ergänzt. Daher sind Daten von Erdbeobachtungssensoren für aktuelle und zukünftige Forschungsfragen zum arktischen Klima- und Landoberflächenwandel von großer Bedeutung.

Das Ziel dieser Dissertation ist die Trend- und Zeitserienanalyse verschiedener multiskaliger Klima- und Landoberflächenparameter auf der nördlichen Hemisphäre. Dabei wurden sowohl Erdbeobachtungsdaten und -produkte verschiedener Quellen als auch zusätzliche Datensätze, die auf Geländemessungen basieren, verwendet. Im Rahmen dieser Arbeit wurden folgende Forschungsfragen definiert:

- A) Wie sind raum-zeitliche Albedo- und Temperaturdynamiken des AVHRR Polar Pathfinder Datensatzes im Zeitraum von 1982 bis 2005 in Nordsibirien zu bewerten?
- B) Welche Übereinstimmungen und Abweichungen können beim Vergleich von satellitengestützten Temperaturdaten und Lufttemperaturmessungen von Klimastationen im panarktischen Raum abgeleitet werden?
- C) Welche multivariate und multiskaligen Charakteristika verschiedener Klima- und Landoberflächenparameter können durch die Gegenüberstellung der Ergebnisse von Trend- und Zeitserienanalysen abgeleitet werden?

Auftretende Veränderungen in den Dynamiken der Vegetationsperiode und -zusammensetzung im Bereich der nördlichen Baumgrenze, die die größte Vegetationsübergangszone darstellt, sind von hoher Relevanz für die arktische Klimaforschung. Landoberflächentemperatur- und Albedozeitserien des NOAA (National Oceanic and Atmospheric Administration) AVHRR (Advanced Very High Resolution Radiometer) Polar Pathfinder Datensatzes zeigen signifikante Wechselbeziehungen in den Sommermonaten in Zentralsibirien. Insbesondere zu Beginn und Ende der Vegetationsperiode sind starke negative Korrelationen zwischen den beiden Parametern zu messen. Die interannuelle Dynamik und Variabilität deutet auf eine Veränderung der Vegetationsperiode zwischen 1982 und 2005 im nördlichen Teil von Zentralsibirien hin. Weitere Zeitserien, die Informationen über Dynamiken der Schneewasseräquivalenz und der Vegetation bereitstellen, unterstreichen und bestärken die Erkenntnisse des AVHRR Polar Pathfinder Datensatzes.

Operationelle fernerkundungsbasierte Temperaturmessungen sind durch die Abdeckung großer Gebiete und der hohen zeitlichen Auflösung essentiell für die

globale Klimaforschung. Verschiedene Erdbeobachtungssysteme, wie MODIS (Moderate Resolution Imaging Spectroradiometer), AVHRR (Advanced Very High Resolution Radiometer) und (A)ATSR ((Advanced) Along Track Scanning Radiometer), ermöglichen die Analyse von langen Zeitserien rückwirkend bis in die 1980er Jahre. Die Genauigkeitsanalyse von Temperaturinformationen abgeleitet aus Fernerkundungsdaten ist für Klimamodellierer und andere Nutzergruppen von hohem Interesse. In dieser Arbeit wurden Temperaturinformationen aus Fernerkundungsprodukten mit Geländemessungen von Klimastationen des National Climate Data Center (NCDC) gegenübergestellt. Dabei wurde der gesamte panarktische Raum abgedeckt. Ziel war es neben der Analyse von Übereinstimmungen und Abweichungen, raum-zeitliche Charakteristika sowie Informationen verschiedener Landbedeckungsklassen zu extrahieren. Temperaturdaten des MODIS Sensors zeigten die höchste Übereinstimmung mit den Temperaturmessungen der Klimastationen. Die Produkte von (A)ATSR und AVHRR wiesen die höchsten Abweichungen auf. Der Vergleich von verschiedenen Temperaturinformationen ermöglicht es Nutzergruppen, wie Klimamodellierern oder aber Meteorologen, zum einen Aussagen über die Ungenauigkeiten der Produkte, aber auch Empfehlungen in Bezug auf deren Nutzung bereitzustellen.

Die panarktischen Temperatur-, Niederschlags-, Schnee- und Vegetationstrends, abgeleitet aus Fernerkundungsprodukten und Geländemessungen, wurden für den Zeitraum zwischen 1981 und 2012 verglichen. Die Gegenüberstellung und Kombination hatte das Ziel, Regionen von kongruenten und disgruerten Trends verschiedener Klima- und Erdoberflächenparameter zu identifizieren. Im Sommer und Herbst ist im Allgemeinen eine signifikante Zunahme der Niederschlagswerte zu verzeichnen. Die Temperaturtrends weisen den größten Anstieg in den Wintermonaten auf. Im Frühling und Herbst sind insbesondere hohe Dynamiken beim Parameter Schneewasseräquivalenz zu finden. Die Vegetationstrends sind in den Sommermonaten durch einen konstanten Anstieg charakterisiert. Die größten Abhängigkeiten zwischen den einzelnen Parameter sind im Frühjahr, Herbst und Winter zu finden. Dabei ist insbesondere der Zusammenhang zwischen Schnee und Temperatur in den Monaten vor und nach dem Sommer signifikant hoch. Zudem deuten die Ergebnisse darauf hin, dass dieser Zusammenhang den größten Einfluss im arktischen Ökosystem in den letzten Jahrzehnten hatte. Im Bereich der arktischen Baumgrenze in Nordsibirien, die als eine Region mit den signifikantesten Trends und Dynamiken identifiziert wurde, sind optisch hochauflösende Fernerkundungsdaten zur Kartierung der Landoberflächenveränderung hinzugezogen

worden. Ziel war es, Veränderungen der Vegetationsstruktur im Zeitraum von 1973 bis 2012 in der Übergangszone zwischen Taiga und Tundra zu analysieren. Die Ergebnisse zeigen eine Intensivierung der hölzernen Vegetationsarten, zu denen neben Sträuchern auch Bäume zählen können. Diese Veränderung der Vegetationsstruktur und –zusammensetzung ist insbesondere in den einst Tundra dominierten Regionen nördlich der Baumgrenze zu verzeichnen. Diese Ergebnisse der Klima- und Landoberflächenveränderungen zeigen die multiskaligen Rückkopplungseffekte im arktischen Ökosystem.

Für die Beobachtung und Identifikation von verschiedenen Klima- und Landoberflächenparametern besitzen Fernerkundungsdaten und -techniken hohes Potential. Operationelle Fernerkundungsdaten mit hoher räumlicher und zeitlicher Auflösung sind für aktuelle und zukünftige Klima- und Ökosystemforschungen von hohem Interesse. Die Dissertation zeigte, dass (1) die raum-zeitlichen Charakteristika verschiedener Parameter, (2) die Genauigkeitsanalyse von Fernerkundungsdaten, (3) die Kombination von Trends verschiedener Parameter und (4) die Skalierung zwischen verschiedenen Erdbeobachtungssatelliten von hoher Relevanz für die operationelle und konsistente Analyse der arktischen Klima- und Landoberflächenveränderungen sowie Ökosystemdynamiken sind.

Chapter 1

Introduction

General Introduction and Outline

Research Questions

Study Area

Historical Climate Conditions in the Arctic

Recent Trends in Arctic Ecosystems

Remote Sensing of Arctic Parameters

1.1 General Introduction and Outline

During recent decades, climate change in the arctic region has become a major focus in Earth system science and climate related research topics. The terrestrial ecosystems in the arctic are subject to significant changes and highly vulnerable to modifications in the global climate system. Global Climate Models predict an increase in arctic mean temperatures for the upcoming century by a factor between 2 and 4 compared to increasing global mean temperature trends. Changes in temperature, as well as precipitation, have a significant impact on snow cover, vegetation productivity and coverage, vegetation seasonality, surface albedo, greenhouse gas emissions and permafrost dynamics. The coupled climate-land surfaces changes are thought to be a positive feedback in the Earth system, which can potentially further accelerate the warming rates on global scale. In contrast to other regions, the northern high latitudes are supposed to face the strongest and largest feedbacks for the upcoming decades. Even the most optimistic scenarios presented in the IPCC (Intergovernmental Panel on Climate Change) report will have a major impact to the warming rates and vegetation changes of the northern hemisphere. Particularly the changes of vegetation pattern and the phenological cycle in the taiga-tundra transition area are of high importance for climate change research.

The identification of significant modifications in the state and spatio-temporal dynamics of terrestrial parameters, such as temperature, precipitation, snow and vegetation is a challenging issue. Earth observation information from various sources provides a useful tool to observe and monitor essential climate parameters. Moreover, Earth observation is an indirect measurement technique which allows to retrieve spatial information over large areas and compensate for the lack of ground measurements in remote areas. Hence, the use of remote sensing information has gained high importance for climate change related research studies during the last decades.

The main goal of chapter 1 is to provide a general introduction into the framework of this dissertation. The primary part of this chapter gives an overview of the research questions and the study area. Afterwards, historical climate conditions of the arctic ecosystems are described. Within a next step, recent trends in arctic ecosystems from different climate related parameters and variables are highlighted. The last part of chapter 1 shows state of the art remote sensing data and products,

which are used to derive essential climate variables in arctic ecosystems using various Earth observation platforms.

The paper in chapter 2 focuses on the trend analysis of remotely sensed time series data, such as land surface temperature, albedo, snow water equivalent and NDVI between 1982 and 2005. The study have been carried out for the northern parts of central Siberia. The results show strong dependencies between the parameters and their inter-annual dynamics, indicating changes in vegetation growing period.

The manuscript in chapter 3 presents a comparison of state-of-the-art remote sensing-based land surface temperature data with air temperature measurements from meteorological stations on a pan-arctic scale. The main goal was to compare in-situ data (T_{air}) with remote sensed land surface temperature (LST) records from (A)ATSR, MODIS and AVHRR. The in-situ data is based on the database hosted by the National Climate Data Center (NCDC). Within a first step, the entire time series of each individual remote sensing product was compared to the in-situ database. Furthermore, the paper highlights the inter-annual variability of the comparison between T_{air} and LST for the time period between 2000 and 2005, which is the overlapping period of all remote sensing LST products. In addition, land cover information was included in the evaluation approach by using GLC2000.

The paper in chapter 4 focuses on the co-occurrence of temperature, precipitation, snow cover, and vegetation greenness trends between 1981 and 2012. The main goal of this study was to utilize coarse resolution climate data, based on Earth observation techniques and measurements from ground stations for the northern hemisphere as well as to identify land surface changes within the taiga tundra ecotone at the Taymyr peninsula in Russia using high spatial resolution Earth observation data. The climatic and ecosystem changes of this study has emphasized the multi-scale feedbacks in the arctic ecosystems.

The conclusion and discussion of the findings achieved by the three manuscripts is part of chapter 5. The last part of the synthesis is providing information about future research needs and potential applications as well as upcoming scientific milestones.

1.2 Research Questions

The main focus of this thesis is the analysis of different climate parameters from multi-scale Earth observation information to monitor arctic land surface dynamics using time series and trend analysis with respect to global climate change. Moreover, the goal is to identify spatio-temporal dynamics of climate related parameters extracted from Earth observation time series data for the northern hemisphere.

The structure of the thesis is based on three main research questions, which have been divided into sub-questions referring to the peer-reviewed publications (section 2-4):

A) What are the spatio-temporal dynamics of the AVHRR Polar Pathfinder land surface temperature and albedo time series information for northern Siberia between 1982 and 2005?

A.1: What inter-annual temperature and albedo dynamics are found within the taiga-tundra transition zone of northern Siberia?

A.2: How to characterize land surface temperature and albedo trends in northern Siberia during the summer month?

A.3: Is there a connection between land surface temperature and albedo trend findings in selected hot spot regions?

B) What (dis-)agreements are found comparing satellite derived land surface temperature products from various sources with air temperature measurements from meteorological stations for the pan-arctic region?

B.1: What correlation can be found between remote sensing based land surface temperature and air temperature for the entire time series of each Earth observation product?

B.2: How to characterize the inter-annual variability between different land surface temperature products and air temperature measurements for the time period between 2000 and 2005?

B.3: What are the characteristics and differences comparing land surface temperature and air temperature for different land cover types?

B.4: What are the spatial patterns of the mean difference parameter on pan-arctic scale?

C) What information can be extracted from a multi-variate and multi-scale analyses of different land surface and climate parameters for the last decades?

C.1: Which spatio-temporal information can be derived analyzing the co-occurrences of monthly trends from Earth Observation and ground measured parameters?

C.2: What are the monthly inter-annual trend dynamics for different arctic regions?

C.3: What vegetation structure changes at the taiga-tundra transition zone can be identified using high-resolution Earth observation data?

1.3 Study Area

The studies presented in this dissertation are covering the pan-arctic area, which includes the northern parts of Europe, Russia, Alaska and Canada. The main focus of the investigations was put on the regions north of 60 degree in latitude. An overview of the entire pan-arctic areas is shown in Figure 1.1. In general, the arctic is characterized by permafrost soils, the boreal forest in the south (taiga), the low vegetated tundra with barren ground, rocks and ice in the north as well as the arctic coast with the coastal plains and deltas bordering the Arctic Ocean. Moreover, seasonal freeze-thaw, permafrost and snow dynamics as well as climate change induced modifications are forming the arctic land surface.

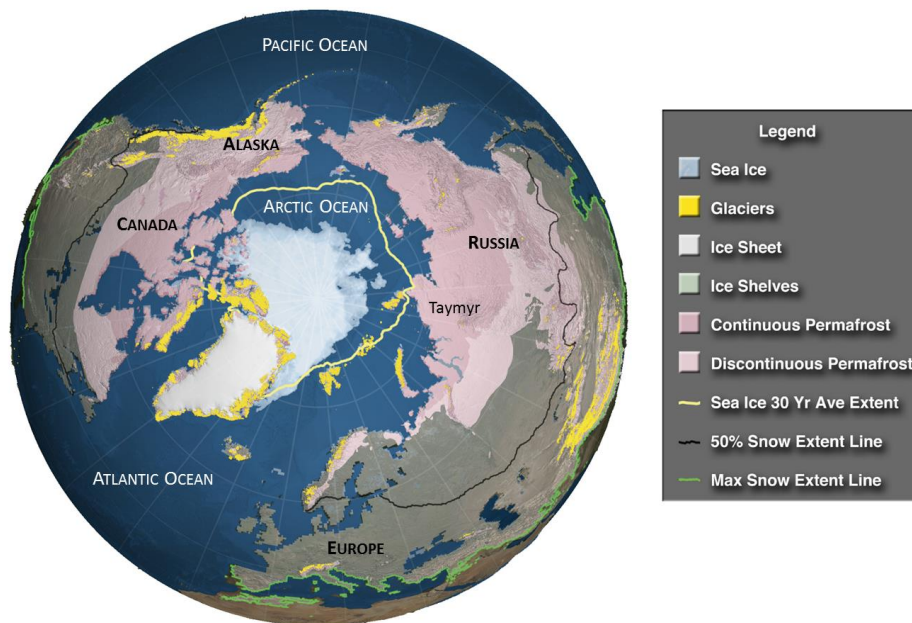


Figure 1.1: Overview of the pan-arctic region including average sea ice extent (yellow line) and minimum sea ice concentration in 2012 (white area), permafrost zones, glacier locations as well as snow cover regimes (modified from Comiso and Hall (2014) and Vaughan et al. (2013)).

Besides the analyses on pan-arctic scale, central Siberia has been identified to be highly affected by impacts from recent changes in the climate system. Based on this, regional investigations have been focused on the Taymyr peninsula, which part of

the Krasnoyarsk Krai in northern Siberia (Figure 1.1), covering an area of about 400.000 km². This region is dominated by continental climate conditions and represents the northernmost larch forest regions (*larix gmelinii*) (Jacoby et al. 2000), acting as a carbon sink (Shvidenko et al. 2013). The Khatanga River represents the border between the taiga and tundra vegetation (Walker et al. 2005).

The vegetation transition zone between taiga and tundra, known as the tree line, is of high importance in climate research. The latitudinal tree line is the earth's greatest vegetation transition zone and stretches approximately 13.000 km around the entire northern hemisphere (Callaghan et al. 2002). Modifications in these regions are potential indicators and drivers for changes within the regional and global climate system (Beringer et al. 2001; Holtmeier and Broll 2007; Harsch et al. 2009; Olthof and Pouliot 2010; Pearson et al. 2013).

1.4 Historical Climate Conditions in the Arctic

The climate system of the high latitude regions is multifaceted. Modifications in the arctic climate system have a significant impact on global scale and vice versa. In historical perspective, the polar climate was characterized by large dynamics resulting in cold- and warm phases (Mcbean et al. 2005) (Figure 1.2).

The reconstruction of the historical climate conditions in the polar regions are assessed through natural archives such as tree rings, fluvial sediments and ice cores (Overpeck et al. 1997; Crowley 2000; Briffa et al. 2001; Juday et al. 2005; Miller et al. 2010). Due to the lack of additional information, the outcomes are defined as paleontological proxies. For further investigations and usage of reconstructed historical climate data, different calibration and cross-evaluation steps are required (Mcbean et al. 2005).

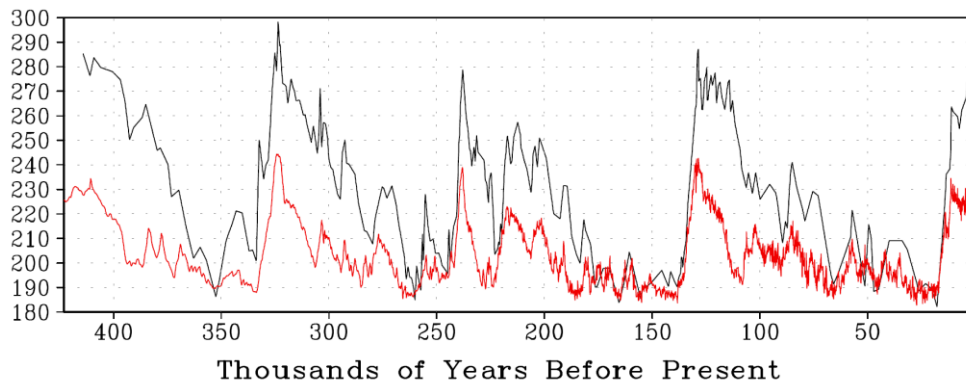


Figure 1.2: Concentration of atmospheric CO₂ (in ppmv, black) and temperature (unrelated units, red) for the last 420.000 years from Vostok ice core (Antarctica) (based on data from Petit et al. (1999) in Zeng (2003)).

During the last millions of years, the polar climate system was characterized by the alternation of cold and warm periods. Between approximately 120 and 90 million years before present (BP) the polar regions faced a cycle of extreme warm events. During the quaternary period, which represents the last 1.6 million years BP, the arctic climate conditions are undergone various intervals of warm and cold phases (up to 50 times), which varying in timing and magnitude. However, the ice age periods ended 20.000 years BP (Mcbean et al. 2005). The dynamics of the atmospheric CO₂ concentration and temperature conditions of the last 420.000 years BP, extracted from the Vostok ice core, are shown in Figure 1.2. Here the rapid abrupt changes between cold and warm periods are clearly visible.

One of the main reason causing these changes are due to orbital modifications of the Earth. These changes, also known as the Milankovitch cycles (Milanković 1941), are divided into three periods. The longest, with a 100.000 year cycle, describes the changes in the eccentricity of the earth. A cycle of 41.000 years describes modifications in the inclination angle of the earth. The last cycle, with a 23.000 yearly dynamic, is describing the elliptical orbit of the earth around the sun, caused by gravitations from other planets from the solar system. All of these factors are causing variations in incoming solar radiation, which are then leading the modifications in the climate system (Mcbean et al. 2005).

The climate reconstructions for the last 1000 years allow the identification of two main epochs. The first is the *medieval warm period* (MWP), which extends between the 9th and 15th century. This period was then followed by the so called *little ice age* (LIA), which lasted until the 19th century (Naurzbaev et al. 2002; Gerber et al. 2003; Jansen et al. 2007; Mann et al. 2008) (Figure 1.3). The coldest temperatures in the Holocene on the northern hemisphere during the LIA have been found between 1400 and 1700 (Mann et al. 2009; Miller et al. 2010).

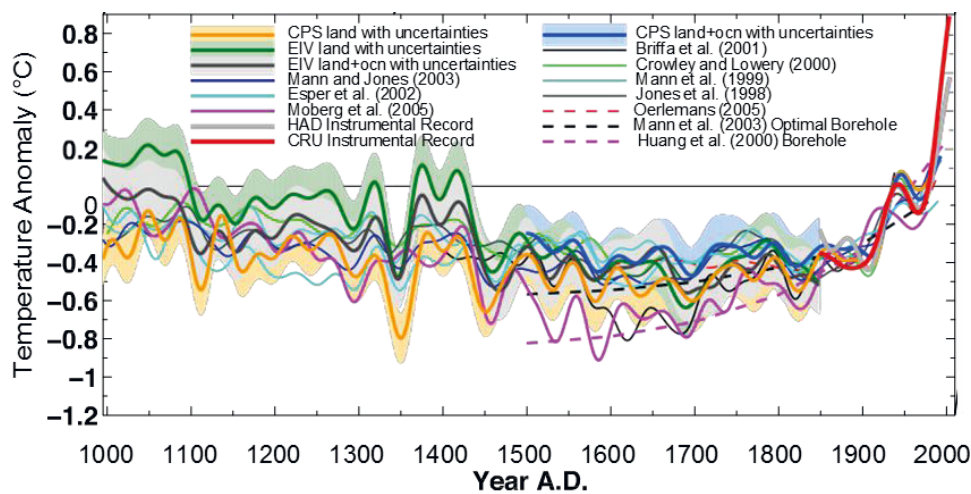


Figure 1.3: Northern hemisphere temperature anomalies between 1000 and 2000 as described by various sources (based on Mann et al. (2008)).

The surface temperature conditions in the arctic regions have never been as high as in the 20th century compared to measurements of the past 300 years (Moritz et al. 2002). A direct attribution and connection to the increase in GHG emissions has still uncertainties, as the climate system is characterized by rapid warming and cooling phases observing the last few thousands of years (Mcbean et al. 2005). However, the influence of the industrialization and therefore the human impact is

obvious when comparing recent climate dynamics to historical climate conditions (Kaplan and New 2006).

The climate information from natural archives, e.g. ice cores or fluvial sediments, are a source for the derivation of an approximation of the environmental conditions during the past thousands of years. The development of different climate observation methods and measurement systems during the last two centuries, has led to an improvement of measuring the global climate. However, the amount of available station data has changed during the past decades (Jones et al. 1982; Jones and Moberg 2003). The observation time period of climate stations started around 1860 with the installation of the first meteorological measurement units (Figure 1.4).

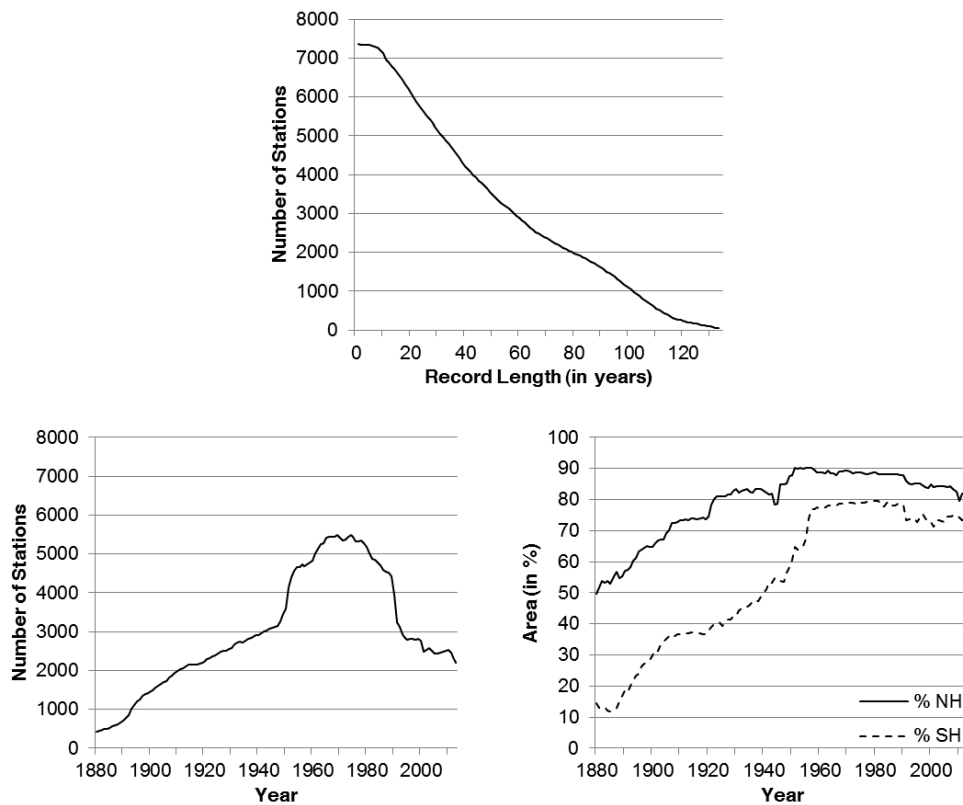


Figure 1.4: Time series information from meteorological stations available through the NASA GISS Surface Temperature Analysis network. top: Number of stations and their record length. bottom left: amount of stations since 1880. bottom right: hemispheric area percentage within a 1200 km radius of a station (modified from NASA (2013)).

Today there are around 1000 stations available, which are able to provide data for the last 100 years. Since the 1880s, the amount of stations has increased rapidly until the 1970s, where a decline in available meteorological stations is found, due to the removal of stations as result of improving measurement techniques (Menne et al. 2009). In the years before the middle of the 20th century, the coverage of stations on the southern hemisphere was lower than on the northern hemisphere. In-situ temperature information from meteorological stations are an important source for the monitoring and prediction of changes in the global climate system. The climate conditions of the arctic are found to be highly variable in space and time. The ground station distribution in the arctic regions is sparse (Overpeck et al. 1997).

Earth observation sensors and techniques for temperature applications, which are available since the 1980s, are a promising solution to overcome this problem. A major advantage in using remote sensing data for temperature applications is the spatial coverage. However, a high revisiting rate (< 1 day) is also of high importance for temperature studies. Temperature information, assessed by Earth observation data, is a very powerful tool for future arctic climate monitoring and modelling strategies, which also might be used in combination with in-situ measurements for calibration and validation purposes.

1.5 Recent Trends in Arctic Ecosystems

Changes in the arctic temperature system of the high northern latitudes, which are rapidly increasing during the last centuries, especially after the pre-industrial phase (Section 1.4), have been found to be the major source and cause for modifications of terrestrial and marine arctic ecosystems. Impacts and modifications of the arctic climate and ecosystems have been addressed by various scientific studies during the recent years (ACIA (Arctic Climate Impact Assessment) 2004; Hinzman et al. 2005). Numerous methods and applications using ground measurements, Earth observation techniques and modelling approaches have been utilized to detect, monitor and predict changes in the arctic in order to analyze global climate trends and anomalies by characterizing their impacts to the arctic environment as well as identifying sources of these changes.

Temperature

The study from Kaplan and New (2006) focused on the comparison of different global climate models (GCMs) using various data inputs. The results from these GCM runs have shown positive trends of global mean air temperature and CO₂ concentration for the upcoming century. According to the model comparison, the 2 °C target, which is defined by the UN Framework Convention on Climate Change (UNFCCC) parties as goal to prevent dramatic climate induced environmental consequences (Knopf et al. 2012), will be reached between 2026 and 2060 (Figure 1.5 - left). Even if succeeding this target, the impact to the arctic climate system will be much higher. Kaplan and New (2006) conclude an increase in mean air temperature for the arctic between 3.3 °C - 6.6 °C, within a 2 °C global mean temperature increase (Figure 1.5 - right).

The increase in mean air temperature is causing modifications in various terrestrial and marine parameters, such as permafrost soil temperatures, snow cover dynamics, sea ice concentration, surface albedo, vegetation growth, vegetation structure, and phenological dynamics (Myneni et al. 1997; Moritz et al. 2002; Romanovsky et al. 2002; Stow et al. 2004; Post et al. 2009; Langer et al. 2013). As a consequence of global warming these effects will have influences on the energy budget, storage capacity, the permafrost dynamics and the climate system on regional and global scale.

Changes in snow cover, sea ice extent and sea ice concentration are found to have a critical impact on the environmental, hydrological and ecological dynamics in

the arctic regions (Post et al. 2009). The active layer dynamics, represented by seasonal freeze-thaw variations, are subject to significant changes during the last years (Anisimov and Reneva 2006), resulting in thermokarst lake changes and permafrost melting, which are the major carbon and methane source in the arctic regions (Kozlenko and Jeffries 2000; Christensen et al. 2004; Frohn et al. 2005).

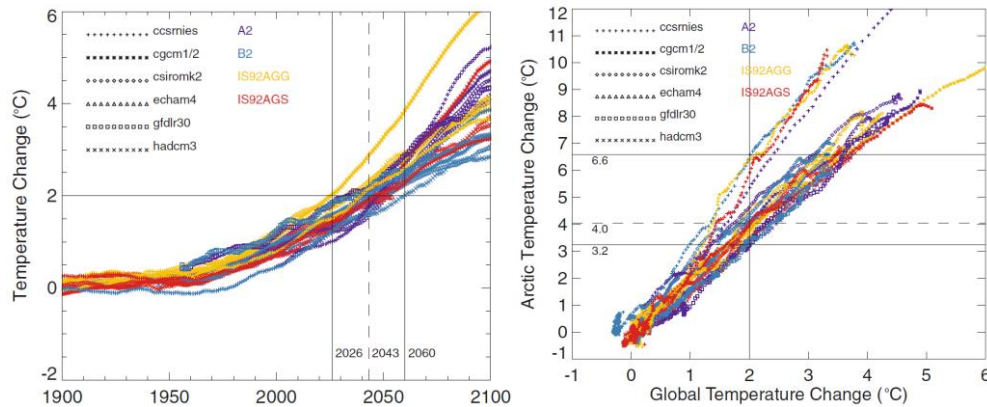


Figure 1.5: Global mean temperature anomalies between 1900 and 2100 described by different GCMs (left). Relationship between global and arctic mean temperature anomalies (right) (Kaplan and New 2006).

Some of the changing parameters are thought to result in a bilateral positive feedback. Among others, the increasing GHG emissions, released by melting permafrost soils, and changes in vegetation structure, such as the recruitment of woody vegetation species to the northernmost regions, are assumed to result in a positive feedback (Overpeck et al. 1997; Crowley 2000; Serreze et al. 2000; Beringer et al. 2001; Chapin et al. 2005; Schuur et al. 2008; Cuevas-Gonzalez et al. 2009; Blok et al. 2011b; Lorantý et al. 2011; Xu et al. 2013).

Albedo

The albedo is a measure of the reflected incoming solar radiation by the Earth surface. On the northern hemisphere surface albedo acts as important boundary component between the high and mid-latitudes and their energy exchange (Stroeve et al. 2001). Albedo is characterized and influenced by the spectral and structural attributes of a surface, e.g. vegetation types, bare ground, snow cover, etc. (Dorman and Sellers 1989). This parameter is of high interests in arctic related climate studies. Especially, the transition times between snow-covered and snow-free periods are of high importance in analyzing the impact of albedo changes to the arctic environment (Pearson et al. 2013). The snow albedo feedback (SAF) can be

described in general by the following interactions (Figure 1.6): (1) Increasing temperatures lead to a reduction of snow cover, (2) reducing the surface albedo while (3) decreasing the reflection of the incoming solar radiation and (4) increasing of the heat absorption (Qu and Hall 2007).

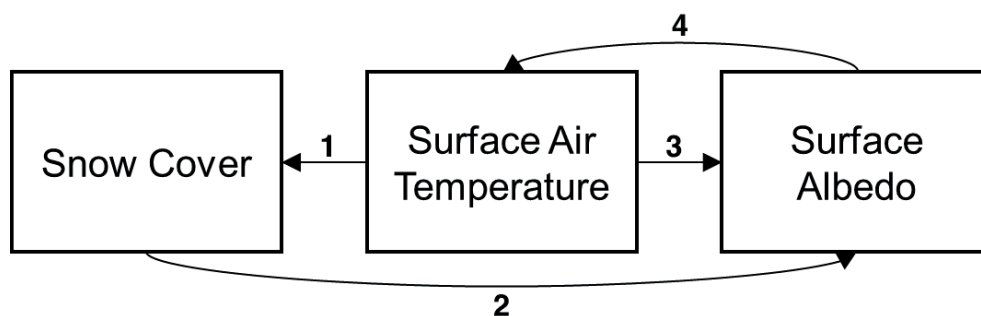


Figure 1.6: A schematic illustration describing the snow-albedo feedback (SAF) (modified from Qu and Hall (2007)).

Figure 1.7 shows the evolution of albedo, sea ice concentration and surface air temperature between 1979 and 2011 over the Arctic Ocean. A detailed overview of feedback mechanisms in arctic ocean albedo dynamics, which have not been addressed in this thesis, but are also important with respect to the arctic ecosystem, are given in Curry et al. (1996).

The surface albedo in the northern hemisphere is characterized by an ongoing decrease during the last decades, with an annual rate of -0.14 % (Wang and Key 2005). A synergetic analysis using Earth observation data and field measurements to monitor albedo changes over the last three decades has been carried out by Flanner et al. (2011). The results have shown a significant linear decreasing trend in surface albedo, which have been driven by both sea ice and terrestrial snow cover changes, leading to vast changes in the net radiation and energy budget. The amplification of these changes has been larger than predicted by various climate models (Flanner et al. 2011). Sturm et al. (2005) found a decrease in albedo of about 30 % by comparing regions with tall and low shrubs. Low shrubs, which are below the snow layer, do not influence the albedo, whereas branches which are only surrounded by snow having a larger influence (Sturm et al. 2005). Thus, changes in snow cover dynamics and vegetation are likely to influence the surface albedo and thereby the energy budget (Lorantý et al. 2011). However, Blok et al. (2011b) found an indirect connection of increase in summer temperature and albedo trends. He found other parameters such as surface water and bare ground to have larger impact on albedo

changes. With respect to the arctic and global climate system, surface albedo appears to be not the major driver in climate change (Winton 2006). Studies from Pithan and Mauritsen (2014) show that climate model predictions conclude the parameter temperature to be the major driver in climate change, as the arctic temperature amplification remains similar, even without changes in terrestrial snow and sea ice cover.

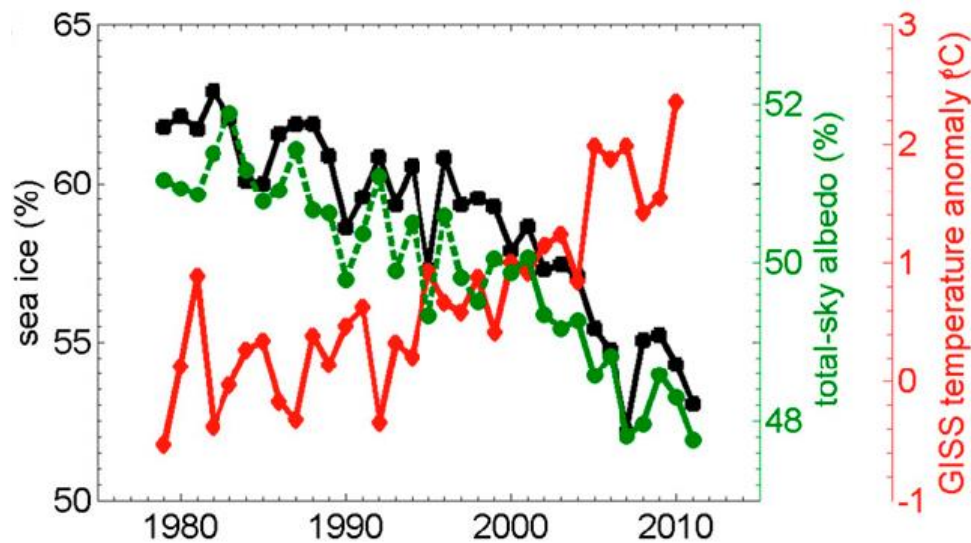


Figure 1.7: Comparing sea ice concentration, albedo and surface air temperature between 1979 and 2011 (Pistone et al. 2014).

Snow Cover

Changes in arctic snow accumulation have been identified by various studies (Déry and Brown 2007; Brown and Robinson 2011; Comiso and Hall 2014). However, the trends in snow cover extent are varying in space and time. Déry and Brown (2007) found a transition from positive to negative snow cover extent anomalies in the years after 1985 for the entire northern hemisphere. These findings are similar for both the Eurasian and Northern American continent. Approximately, 7.3 GT (gigatons) per year of snow mass have been lost during the last three decades (Takala et al. 2011).

Trend analyses from snow cover extent time series have shown evidence of decreasing snow cover extent during spring season over the last 90 years on the northern hemisphere by approximately 10 % (Brown and Robinson 2011). Figure 1.8 is showing the changes between 1967 and 2012 for the spring season. Snow covered areas in the arctic have been declined by about -2.75 % (± 0.45 %) per decade. In detail, higher decreasing rates are found in Eurasia (-2.72 % ± 0.63 %) when

compared to Northern America, which is characterized by a decline of $-1.27\% \pm 0.53\%$ per decade (Comiso and Hall 2014).

Besides this, Cohen et al. (2012) found increasing snow accumulations for October during the last three decades. Similar results using AVHRR satellite time series have been published by Brown and Derksen (2013). However, as this is in conflict with increasing air temperature trends at the northern hemisphere, Brown and Derksen (2013) compared the trend findings to additional snow cover datasets and identified inconsistencies in the AVHRR time series due to the cloud detection algorithm and other calibration issues. Nevertheless, Brown and Derksen (2013) also argue that Cohen et al. (2012) followed another methodology analyzing anomalies and other snow parameter such as snow depth, making both studies only partly comparable. This highlights the importance of monitoring snow cover processes and detecting snow cover dynamics during the transition seasons in a changing arctic environment.

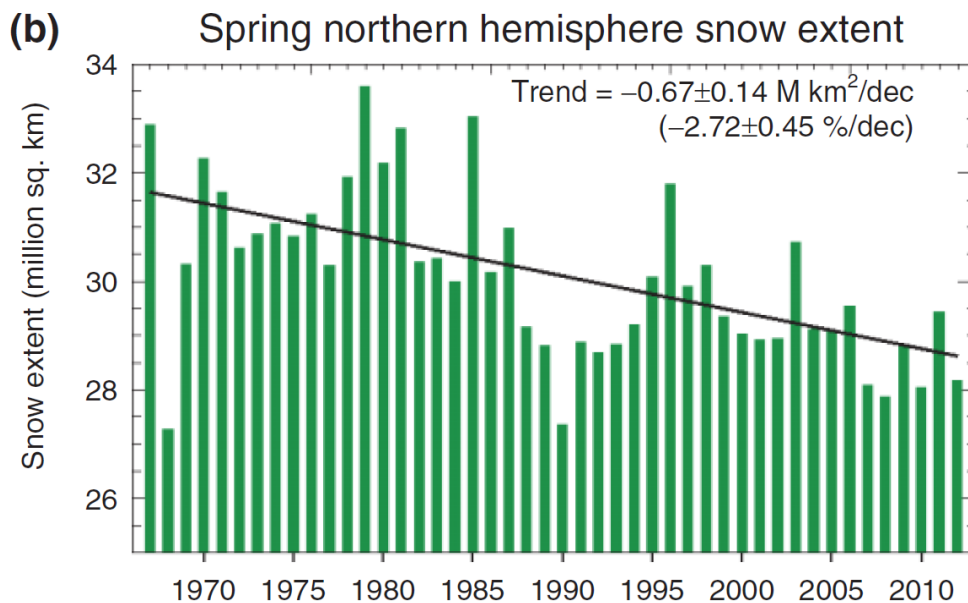


Figure 1.8: Evolution of snow cover extent for the northern hemisphere between 1967 and 2012 for the spring season (Comiso and Hall 2014).

Vegetation

Vegetation cover, as well as snow cover, is acting as insulation layer for the underlying permafrost, by protecting the active layer from direct incoming solar radiation and heat absorption (Walker et al. 2003; Yi et al. 2007). In the high latitudes, the phenological cycle and its dynamics are influenced by various factors,

such as temperature and the presence of snow cover (Raynolds et al. 2008; Zeng et al. 2011; Dutrieux et al. 2012).

There is clear evidence of modifications to the phenological cycle on the northern hemisphere during the last decades, seen by Earth observation data (Bunn and Goetz 2006; White et al. 2009; Zeng et al. 2011). The onset of the vegetation growing (SOS) period has shifted towards earlier days whereas the end of season (EOS) postponed to later days. This results in an enlargement of the vegetation growing period (LOS) and vegetation activity (Zeng et al. 2011). Even during the last 10 years there is evidence of an increase in vegetation growing length of more than two days for some regions (Figure 1.9).

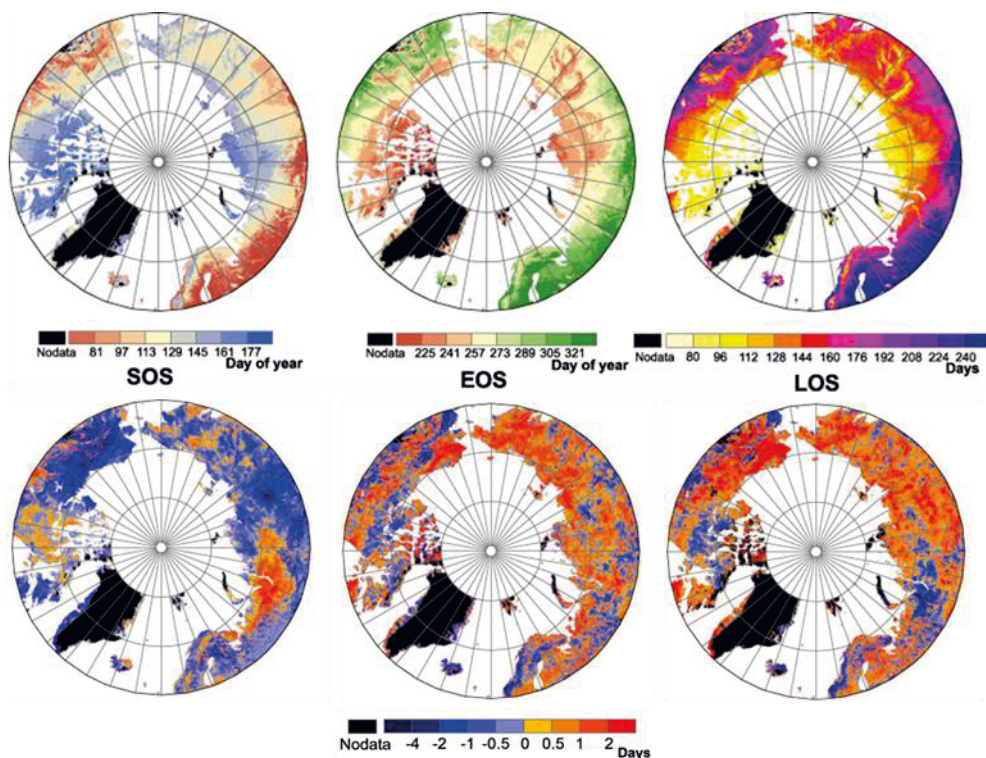


Figure 1.9: Mean values for SOS, EOS and LOS averaged of the period of 2000 - 2011 (top) as well as the linear trend for the same period (bottom) (modified from Zeng et al. (2011)).

Changes in arctic phenological dynamics, based on external input drivers, such as snow cover and temperature, are leading to vast modifications of the vegetation compositions, e.g. greening (Lucht et al. 2002; Forbes et al. 2010; de Jong et al. 2011). However, there is also evidence of browning, which is a regional effect caused

external effects such as drought stress, decreasing temperatures, and fires (de Jong et al. 2011; Piao et al. 2011; Xu et al. 2013).

To address vegetation changes in the arctic, which are rather slow, some studies use photographs or, if available, aerial photos taken during the middle of the 20th century and in recent years and compare them in order to identify changing vegetation pattern (Stow et al. 2004; Tape et al. 2006; Naito and Cairns 2011; Ropars and Boudreau 2012). Besides ground surveys, which are intensive in cost and time and can only cover a small area, additional information, such as remote sensing data, is used to detect vast and cumulative changes over a large regions.

One of the first studies using Earth observation data to map plant growth over the entire arctic region was done by Myneni et al. (1997), highlighting the regions above 45 degree in latitude to be the most affected in terms of climate change induced vegetation changes on the northern hemisphere.

The detection of changes in vegetation structure, composition as well as dynamics is of high importance and has been accentuated in numerous scientific studies during the last years (Peddle et al. 1993; Moritz et al. 2002; Laidler and Treitz 2003; Stow et al. 2004).

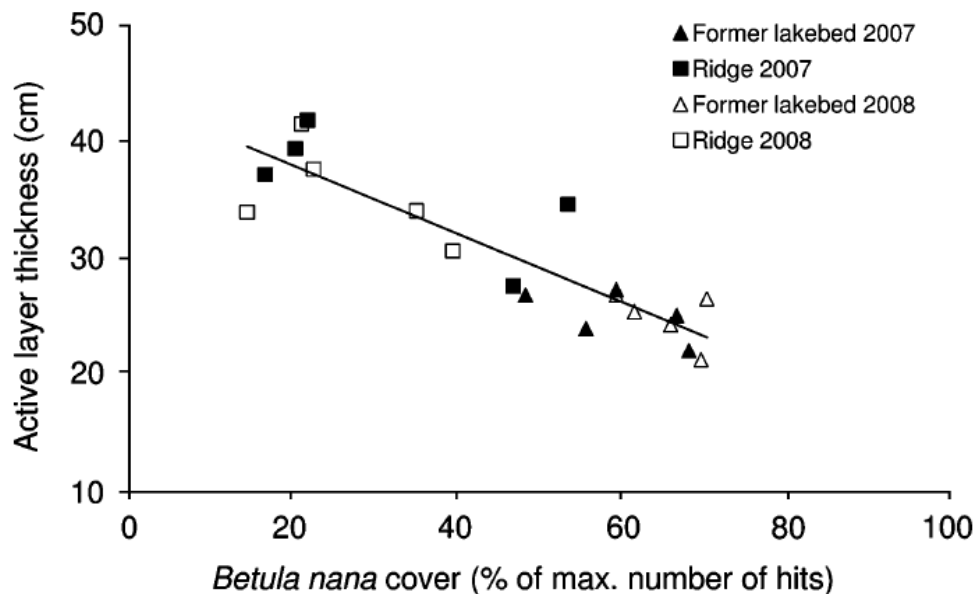


Figure 1.10: Comparing active layer thickness with shrub cover (*Betula nana*) for two test sites in 2007 and 2008 (Blok et al. 2010).

Particularly, the observation of vegetation transition zones, such as the latitudinal tree line is of high importance in the arctic regions. Modifications in these

regions are potential indicators of changes within the regional and global climate system (Beringer et al. 2001; Holtmeier and Broll 2007; Harsch et al. 2009; Olthof and Pouliot 2010; Pearson et al. 2013).

The modification of the vegetation structure and composition at the taiga-tundra transition area has a major impact on various ecosystem functions, such as energy budget, snow properties and dynamics, soil temperatures, nutrients cycle, carbon storage as well as biodiversity (Myers-Smith et al. 2011). Blok et al. (2010) demonstrated in a local experiment in eastern Siberian tundra that an increase in shrub cover will reduce the active layer thickness significantly during the summer month (Figure 1.10). Besides an encroachment of shrubs, other vegetation types also tend to migrate to the northern parts in a changing arctic environment. Kharuk et al. (2006) has shown the increase in larch forest cover in the tundra area at a test region on the Taymyr Peninsula using ground based measurements and remote sensing data. A change in vegetation structure at the taiga tundra transition area is also found for Alaska (Tape et al. 2006; Blok et al. 2011b).

1.6 Remote Sensing of Arctic Parameters

Remote sensing data provides a useful tool observing and monitoring various essential climate parameters and variables for arctic climate research. An overview of ground based, airborne and spaceborne Earth observation data and techniques for permafrost monitoring are given in Kääb (2008).

Optical Earth observation platforms (passive systems) are measuring the solar radiation reflected by the Earth surface, covering the visible, infrared and thermal parts of the electromagnetic spectrum (Albertz 2009). Remote sensing platforms, covering the microwave part of the electromagnetic spectrum, are operating in active or passive mode. Active systems measuring different physical properties of the earth surface such as backscatter intensity, phase and polarization. Passive systems detecting microwave emissions of the earth, while having a lower spatial resolution compared to active systems. Additionally, radar remote sensing platforms work independently from cloud cover or solar illumination and can even penetrate the upper surface layer (Woodhouse 2006).

Important Earth observation products and datasets, which are of high interest in recent and future climate related studies, are summarized in Table 1.1 and Table 1.2. Table 1.1 is giving an overview of available data and products, which are used for large scale monitoring and observations, such as LST, snow, albedo, land cover, phenology, fire, and soil moisture. Parameters, which are used for detecting changes and dynamics on regional and local scale, such as vegetation, water bodies and subsidence, are listed in Table 1.2. The papers of this thesis (Chapter 2 to Chapter 4) are focusing on multi-scale Earth observation parameter such as LST, albedo, snow water equivalent, vegetation, and phenology. Hence, some of the listed optical remote sensing data have been utilized as additional information source (e.g. publications) during the research process.

The arctic region is characterized by significant land surface variations during the year. The seasonal dynamics of different land surface variables are one of the major challenges in monitoring the arctic environment using Earth observation data. One example is the short snow and ice free period of only few month per year. Hence, rapid vegetation and phenological processes are prevalent and need to be observed within a small time frame (Olthof et al. 2008). Moreover, increasing cloud cover in the summer season due to sea ice loss (Liu et al. 2012) are likely to cause data gaps in optical Earth observation data.

Table 1.1: Low resolution Earth observation data and products for arctic environmental monitoring.

| low resolution Earth observation data and products MODIS, MERIS, AVHRR, SPOT, (A)ATSR, SMMR, SSM/I, AMSR-E, ASCAT | | |
|---|---|--|
| Variables & Parameters | Temporal Resolution & Spatial coverage | Sensors & Products |
| Land Surface Temperature | since 1982 / 8 km / daily since 2000 / 1 km / twice-daily since 1991 / 9 km / twice-daily | AVHRR - Pathfinder MODIS (A)ATSR - GlobTemperature |
| Snow Properties | since 1978 / 25 km / day to month since 1995 / 1 km / day to month since 2000 / 500 m / day to month | SMMR, SSM/I, AMSR-E – GlobSnow (A)ATSR – GlobSnow MODIS |
| Albedo | since 1982 / 8 km / daily since 2000 / 500 m / bi-weekly | AVHRR - Pathfinder MODIS |
| Vegetation Dynamics & Phenology | since 1982 / 8km / bi-weekly 1998 - 2007 / 1km / monthly 2000 - 2010 / 250 m / yearly since 2000 / 250 m / bi-weekly since 2000 / 1 km / weekly 2001 - 2010 / 500 m / yearly | NOAA-AVHRR - GIMMS NDVI(3g) GlobCarbon FAPAR, LAI MODIS VCF MODIS EVI, NDVI MODIS FAPAR MODIS Land Cover Dynamics |
| Land Cover | 1990 - 2000 / 1 km / - since 2000 / 500 m / yearly 2000 / 1 km / - 2000 & 2005 / 500 m / - 2005 & 2009 / 300 m / - 2005 / 500 m / - 2005 / 250 m / - 2008 - 2012 / 300 m / - | SYNMAP MODIS LAND COVER GLC2000 Terra Norte (Russia) GLOBCOVER MODIS NELDA North American LC (CEC) ESA CCI Land Cover |
| Fire | since 1995 / 1 km / monthly 1996 - 2002 / 1 km / yearly 1998 - 2007 / 1 km / yearly 2000 - 2006 / 1 km / monthly since 2000 / 500 m / monthly | GLOBSCAR (ATSR WFA) AVHRR (Russia) GLOBCARBON – following ESA CCI Fire Terra Norte (Russia) MODIS burned area |
| Snow Moisture & Freeze-Thaw | since 2000 / 250 m / daily since 2006 / 12.5 - 25.5 km / daily | AMSR-E ASCAT |

Nevertheless, one major advantage of using coarse resolution remote sensing data is the retrieval of spatial information of various parameters covering large areas. Earth observation platforms with a low geometric resolution (> 1 km) have

short revisiting rates (< 1 day), which enables the user to receive consistent temporal information within a narrow time steps.

Since the early 1980s, the first operational satellite platforms, such as AVHRR onboard of NOAA, are covering the entire globe with high revisiting rates. Since this time numerous NOAA satellites were carried into space to ensure the continuation of the AVHRR time series. AVHRR has 5 spectral channels, covering the red, near and mid-infrared and thermal infrared spectrum, with a geometric resolution of 1 km (Pedelty et al. 2007).

During the mid-1990s and the early 2000s additional platforms, such as MODIS onboard of TERRA and AQUA and MERIS onboard of ENVISAT were in orbit to acquire information for different parameters, such as vegetation, snow, albedo, fire, etc. on high temporal resolution. Henceforth, the availability of remote sensing information for a large range of climate related parameters increases. Besides AVHRR, MODIS is the main sensor used for the creation of various coarse resolution Earth observation products with a high temporal resolution. MODIS has 36 spectral channels with a spatial resolution ranging from 250 m in visible, 500 m in near and mid-infrared and 1 km for the longwave infrared channels (Pedelty et al. 2007).

The use of remote sensing time series information to derive temporal dynamics and changes of climate related parameters in the arctic regions becomes essential for recent and future research (Stow et al. 2004; Kääb 2008). Different approaches and techniques to derive trends of land surface parameters from satellite-derived time series are existing. A common method is a linear regression between the annual aggregated time series and the yearly time steps. The slope coefficient of the regression is used as a metric for the trend. Many studies have shown the potential of identifying trends in long-term time series Earth observation data (Goetz et al. 2005; de Jong et al. 2011; Piao et al. 2011).

Earth observation data with medium to high spatial resolution (from few meters to less than 100 m) are important for the monitoring and change detection on regional and local scale. Especially the analysis of the taiga tundra boundary using optical and radar remote sensing data are of high importance (Ranson et al. 2004; Sun et al. 2011; Simms and Ward 2013). Additionally, Earth observation data with medium or high geometric resolution are often used for evaluation, validation and scaling approaches in comparison with coarse resolution remote sensing data and products. Using high resolution Earth observation data acquired at individual time steps are essential for monitoring and change detection methods in the arctic

regions, e.g. vegetation species, water bodies, fires, subsidence, etc. (Bartsch et al. 2012). Future research investigations will benefit from upcoming satellite missions, e.g. the Sentinel missions as well as ALOS continuation, which will cover a wide range of applications.

Table 1.2: Medium to high resolution Earth observation data for arctic environmental monitoring.

| medium to high resolution Earth observation data Landsat, RapidEye, ALOS, ASAR, JERS, ERS, Radarsat, Ikonos, Quickbird, TerraSAR-X, Corona, Sentinel | | |
|--|---|--|
| Variables & Parameters | Temporal Resolution & Spatial coverage | Sensors & Products |
| Land Cover Vegetation Species & Structure Disturbances | since 1982 / 15, 30, 60, 80 m / 16 days 1992 – 1998 / 50 m / yearly 1995 – 1998 / 25 m / 1-day repeat pass cycle since 1995 / 11, 28 m / 24 days 2002 – 2012 / 12.5, 25, 300, 1000 m/ 35 days 2006 – 2011 / 10 m / 46 days since 2005 / 6.5, 12, 25 m / 46 days since 2006 / 1 - 4 m / bi-weekly since 2006 / 2.5 m / 46 days since 2007 / 1, 3, 7 m / 11 days since 2008 / 5 m / daily in 2014 / 5 - 50 m / > 6 days planned / 10, 100 m /3 days | Landsat JERS-1 ERS Tandem Radarsat ENVISAT ASAR ALOS PALSAR Ikonos Quickbird ALOS PRISM TerraSAR-X RapidEye Sentinel - 1 ALOS 2 PALSAR |
| Water Bodies & Changes | 1959 – 1975 / 2 - 7.5 m / - since 1982 / 15, 30, 60, 80 m / 16 days since 2008 / 5 m / daily | Corona Landsat RapidEye |
| Subsidence & Elevation | 1995 – 1998 / 25 m / 1-day repeat pass cycle 2002 – 2012 / 12.5, 25, 300, 1000 m/ 35 days 2006 – 2011 / 10 m / 46 days since 2007 / 1, 3, 7 m / 11 days in 2014 / 5 - 50 m / > 6 days planned / 10, 100 m /3 days | ERS Tandem ENVISAT ASAR ALOS PALSAR TerraSAR-X Sentinel - 1 ALOS 2 PALSAR |

Chapter 2

Identification of Land Surface Temperature and Albedo Trends in AVHRR Pathfinder Data from 1982 to 2005 for Northern Siberia

M. URBAN¹, M. FORKEL², C. SCHMULLIUS¹, S. HESE¹, C. HÜTTICH¹ & M. HEROLD³

¹Friedrich-Schiller-University Jena, Department for Earth Observation

²Max Planck Institute for Biogeochemistry, Biogeochemical Model-Data Integration Group

³Wageningen University, Centre for Geo-Information

Published in:

International Journal of Remote Sensing (2013), 34, 12, 4491-4507

(Received 23 May 2012; Accepted 20 January 2013)

DOI: 10.1080/01431161.2013.779760

This is the authors accepted manuscript of an article published as the version of record in

International Journal of Remote Sensing® 25 Mar 2013

<http://www.tandfonline.com/doi/full/10.1080/01431161.2013.779760>

2.1 Abstract

The arctic regions are highly vulnerable to climate change. Climate models predict an increase in global mean temperatures for the upcoming century. The arctic environment is subject to significant changes of the land surface. Especially the changes of vegetation pattern and the phenological cycle in the taiga-tundra transition area are of high importance in climate change research. This study focuses on time series and trend analysis of land surface temperature, albedo, snow water equivalent, and normalized difference vegetation index information in the time period of 1982–2005 for northern Siberia. The findings show strong dependencies between these parameters and their inter-annual dynamics, which indicate changes in vegetation growing period. We found a strong negative correlation between land surface temperature and albedo conditions for the beginning (60–90%) of the growing season for selected hot spot trend regions in northern Siberia.

2.2 Introduction

The arctic environment is subject to significant changes (Grace et al. 2002; Moritz et al. 2002; Nelson 2003). Historically, surface temperature conditions in the arctic regions have never been as high as in the twentieth century when compared to measurements of the past 300 years (Moritz et al. 2002). The arctic environment is highly vulnerable to impacts of global climate changes caused by increase in greenhouse gas (GHG) emissions (Overpeck et al. 1997; Crowley 2000; Chapin et al. 2005).

Results of global climate modelling runs have shown an increasing trend in the global land surface temperature for the twenty-first century. Findings from the global climate models (GCMs) expose that a significant increase in global mean temperatures of 2 °C will occur in the years from 2026 to 2060. Even if the 2 °C target will be adhered to, the temperature conditions in the arctic regions will be increased by approximately 3.3–6.6 °C. This scenario will have dramatic impacts on the arctic environment (Kaplan and New 2006).

As a result of the arctic warming, measurements from changes in snow cover and sea ice extent have been found to have a critical impact on the environmental and ecological dynamics in the arctic regions during the last decades (Post et al. 2009). Rising temperatures will lead to an intensification of vegetation activity, changes of land surface structures, and phenological dynamics (Myneni et al. 1997; Moritz et al. 2002; Stow et al. 2004). These processes decrease the surface albedo, which is related to a higher absorption of solar radiation. This positive feedback in the climate system can then accelerate the warming of the arctic environment. The identification, analysis, and interpretation of changes in structures, composition, and dynamics of different arctic vegetation types, with special focus on the arctic tree line region, has been more and more emphasized in scientific studies during the last decade (Moritz et al. 2002; Olthof and Pouliot 2010; Harsch and Bader 2011).

The increase in vegetation activity is related to a recruitment of trees and an increase in shrub cover. Thus, these vegetation changes and their dynamics are indicators for present modifications in the arctic climate system (Sturm et al. 2001; Epstein et al. 2004; Bunn and Goetz 2006; Tape et al. 2006).

Recent studies have been carried out analysing the increase in shrub cover in Siberia (Blok et al. 2010), Alaska (Tape et al. 2006), and the Pan-Arctic Circle (Tape et al. 2006; Myers-Smith et al. 2011). These effects as a consequence of global

warming will have influences on the energy budget, storage capacity, the permafrost dynamics, and the climate system on regional and global scale.

The recruitment of trees into the northern regions, which are controlled by summer temperature conditions and the length of the growing season, is of high importance for the global climate system. Changes in tree cover and its northwards expansion will lead to a positive feedback in climate conditions since dark forest areas will reduce the albedo which leads to higher warming rates (ACIA (Arctic Climate Impact Assessment) 2004) and is influencing the inter-annual albedo dynamics (Blok et al. 2011b; Loranty et al. 2011).

Trends on satellite-derived time series of land surface parameters were estimated with different approaches. A common method is a linear regression between the annual aggregated time series and the yearly time steps. The slope coefficient of the regression is used as a metric for the trend. Many studies have shown the potential of identifying trends in long-term time series Earth observation data (Goetz et al. 2005; de Jong et al. 2011; Piao et al. 2011).

This article presents results from time series and trend analysis of land surface temperature, surface albedo, and snow water equivalent (SWE) as well as a vegetation parameter in northern Siberia with special focus on the arctic taiga–tundra transition zone. The study area covers the area from the Yamal Peninsula in the west to the far eastern parts of the Laptev Sea region. The main objective of this article is to analyse long-term time series Earth observation data for the arctic regions of northern Siberia. Other more specific objectives are as follows:

- land surface temperature, albedo, SWE, and normalized difference vegetation index (NDVI) time series information analysis for the taiga–tundra transition zone with a special focus on the summer months June, July, August, and September;
- identification of large cumulative trends in Advanced Very High Resolution Radiometer (AVHRR) Pathfinder land surface temperature and albedo information; and
- extraction of the dependencies between the land surface temperature and albedo trends for selected hot spot regions.

The findings show strong dependencies between land surface temperature and albedo time series information, especially at the beginning of the growing season. A comparison of time series information from land surface temperature, albedo, NDVI,

and SWE are applied for a detailed analysis, with a special focus on the taiga–tundra transition area. This comparison shows the inter-annual dynamics as well as the significant dependencies between different land surface characteristics captured by remote-sensing satellites.

2.3 Data

This article presents time series analysis of AVHRR Polar Pathfinder land surface temperature and albedo measurements. In the following section, the described data and algorithms are referred to the AVHRR Polar Pathfinder product documentation (Fowler et al. 2007). The data can be acquired free of cost through the National Snow and Ice Data Center (NSIDC) and is provided as a twice-daily product. The product includes five AVHRR channels, covering one visible, one infrared, and three thermal infrared bands, as well as surface albedo, skin surface temperature, solar zenith angle, satellite elevation angle, azimuth angle, surface type, and a cloud mask. The data covers the polar regions of the northern and southern hemisphere with a spatial coverage of 48° N and 53° S in latitude. The AVHRR Pathfinder product is available for the time period from 24 July 1981 to 30 June 2005. Since it is a twice-daily data set, the acquisition time of the imagery was 4 am in the morning and 2 pm in the afternoon on the northern hemisphere. The data is available in Equal Area Scalable Earth Grid (EASE-Grid) projection with spatial resolution of 5 km.

To retrieve the land surface temperature information from the National Oceanic and Atmospheric Administration (NOAA)–AVHRR data, two different algorithms, which are based on a regression modelling approach, have been used. The first is suitable for the extraction of land surface temperature information over high-latitude oceans and snow-covered area and the second for other land surfaces. Both of the algorithms are based on the remarks from Key et al. (1997). Thus, the land surface temperature information is based on the measurements of the brightness temperature from channels 4 and 5. These bands have a spectral bandwidth of 1 μm covering the thermal infrared spectrum from 10.3–11.3 μm (band 4) and 11.5–12.5 μm (band 5).

The extraction of clear sky albedo information from AVHRR Pathfinder data is done by a four step methodology. The approach utilizes the reflection properties from the visible (band 1, 0.58–0.68 μm) and infrared channel (band 2, 0.725–1.05 μm). First, both channels are normalized according the solar zenith angle. Second, the channels are converted from narrowband to broadband reflectance using regression coefficients based on surface type properties from special sensor microwave/imager (SSM/I) (Key and Schweiger 1998). The correction of anisotropy effects was done by top-of-atmosphere (TOA) anisotropic reflectance factors (ARFs)

derived from Suttles et al. (1988). Afterwards, the broadband reflectance from channels 1 and 2 are converted to clear sky surface albedo information.

Maslanik et al. (1997) evaluated the accuracy of the land surface temperature and albedo information from AVHRR Pathfinder data by using field observations for a selected test site in Alaska. Due to the large spatial coverage and temporal resolution, an estimation of the overall accuracy of the product requires a large validation database, which was not available at this time. Nevertheless, Maslanik et al. (1997) obtained an accuracy of ± 2 K for land surface temperature and ± 0.05 for albedo (Maslanik et al. 1997). Another evaluation over Greenland was done by Stroeve et al. (2001). The results have shown a 10% underestimation of the AVHRR albedo measurements when comparing to ground-based station values.

The NOAA satellites are influenced by an orbital drift during their lifetime. Thereby the satellite equator-crossing time is shifted towards the afternoon, which brings a cooling effect to the land surface temperature estimates. However, it has been shown that this drift effect has a stronger influence on the southern hemisphere and non-vegetated areas (Gleason et al. 2002; Julien and Sobrino 2012).

The Circumpolar Arctic Vegetation Map (CAVM) represents a vegetation classification of tundra regions on a pan-arctic scale (Walker et al. 2005). This map was derived by using Earth observation data from AVHRR imagery and expert knowledge. The southern border of this data set represents the tree line. This northern tree limit was derived from existing maps, e.g. an ecoregion map of Alaska, and expertise from a variety of arctic research groups. For this specific study here, the CAVM was used as a reference to identify the taiga–tundra transition area in the study region of northern Siberia.

In addition to the time series information from AVHRR land surface temperature and albedo measurements, NDVI information from Global Inventory Modelling and Mapping Studies (GIMMS) and SWE data from the European Space Agency (ESA) GlobSnow project were integrated.

The GIMMS database provides bi-monthly NDVI information on a global scale with a resolution of 8 km since July 1981. The product is based on NOAA–AVHRR satellite imagery with a spatial resolution of 4 km. The derived vegetation index NDVI describes the relation of solar reflections from the red and near-infrared spectral band of the AVHRR sensor (Tucker et al. 2005). The NDVI is mostly used to interpret the photosynthetic activity of vegetation based on measurements of the chlorophyll and water content within plants (Myneni et al. 1997). Additionally,

detailed information about the GIMMS NDVI data set can be found in Tucker et al. (2004), Tucker et al. (2005) and Pinzon et al. (2005).

The ESA GlobSnow project provides information about different snow parameters such as snow extent (SE) and SWE for the northern hemisphere. The SWE data, which was used in this study, provides information within a time period from 1978 to 2010. The product has a spatial resolution of 25 km and is available in EASE-Grid projection. The SWE product is available in daily, weekly, and monthly resolution. For this specific analysis, monthly SWE information was integrated into the time series analysis. The acquisition of time series SWE is done by using remote-sensing data from the Scanning Multichannel Microwave Radiometer (SMMR), SSM/I, and the Advanced Microwave Scanning Radiometer Earth Observing System (AMSR-E). The methodology and algorithms utilized for the extraction of snow parameters from remote-sensing data can be found in Pulliainen (2006).

2.4 Methodology

The methodology for extracting monthly trends for the summer season from daily AVHRR land surface temperature and albedo measurements is based on the following five processing steps (Figure 2.1):

- 1) cloud removal and conversion of temperature values from kelvin to degree Celsius;
- 2) aggregation of data to monthly mean values;
- 3) combination of monthly data sets to yearly layer stacks;
- 4) trend analysis based on a linear regression; and
- 5) relationship of land surface temperature and albedo trends for selected test regions.

Due to a problem with the scan motor on NOAA-16 (2001–2005), which causes a shift of the spectral channels, the data for the known dates of error were removed prior to processing steps 1–5. More information on bad data can be found in Fowler et al. (2007).

(1) Cloud and haze information was obtained from the cloud mask, which is included as a data set in the AVHRR Polar Pathfinder product, to eliminate these pixels from the daily land surface temperature and albedo images. The cloud mask is based on three algorithms. One, the Cloud and Surface Parameter Retrieval (CASPR) algorithm, uses a multi-day and multi-channel technique. Another approach is utilizing time series information from AVHRR-channel 4. The last is based on a combination of both. Each of these approaches has a certain quantity of uncertainty (Fowler et al. 2007). For this study, all cloud masks, which were provided by the database, were used to reduce the amount of uncertainty. For the raw land surface temperature and albedo data, a scaling factor of 0.1 was used to make the database more efficient in storage. This factor was applied to each image. The land surface temperature data, which were provided in kelvin, were converted to degree Celsius values. The images were combined with daily to monthly multi-layer stacks with regard to leap and no leap years.

(2) For a better visualization of the data, monthly means from the multi-layer stacks with regard to Not a number (NaN) values were calculated resulting in a monthly data set for the time period 1982–2005.

(3) These files were aggregated with an annual stack (Figure 2.1). In detail, one layer stack for each summer month (June, July, August, and September) was created for the whole time period, which resulted in 24 layers per data set. The northern tree limit is not a line as it is drawn on a map. It, rather, characterizes a transition zone between the taiga and tundra ecosystems. Based on this assumption, a buffer zone of 100 km north and south of the tree line (Walker et al. 2005) was defined. This buffer was utilized to extract this transition zone from data to analyse the time series information from the remote-sensing data. The data were used to extract the inter-annual dynamics from the land surface temperature, albedo, NDVI, and SWE information using boxplot (see Section 2.5.1).

(4) Temporal trends were analysed for the individual growing season months of the land surface temperature and albedo time series for each grid cell using the statistical software R (<http://www.r-project.org/>). The correlation coefficient of the AVHRR Pathfinder land surface temperature and albedo signal over time was used as a trend measure. This allows interpretation of the magnitude of the trend signal, where a value of -1 indicates a strong negative trend over time and vice versa. The significance of the trend was computed from the signal-to-noise ratio of the trend and estimated from the density function of a normal distribution. It was not necessary to remove the seasonal cycle from the time series because we focused on annual trends for each individual month. Since we are interested in long-term changes in land surface temperature and albedo, further analysis was carried out for trends that are significant for the full 24 year time period. The potential of identifying hot spot trend regions was indicated by the strength of the correlation over time and the significance of these trends. This allows the extraction of regions showing significant trends, which was supported by the p-value information coming from the trend calculation.

(5) The results of both land surface temperature and albedo trends were compared. The aim was to identify dependencies between these parameters in their identified hot spot regions. Therefore, a pixel by pixel comparison of the two parameters (land surface temperature trends and albedo trends) was done. Point density cloud graphs are used to represent the relation of each pixel pair, which allows a better interpretation of the dependencies of the trend findings. The visualization of different parameters by a point density cloud graph is feasible if working with large and spatial distributed data sets (Eilers and Goeman 2004).

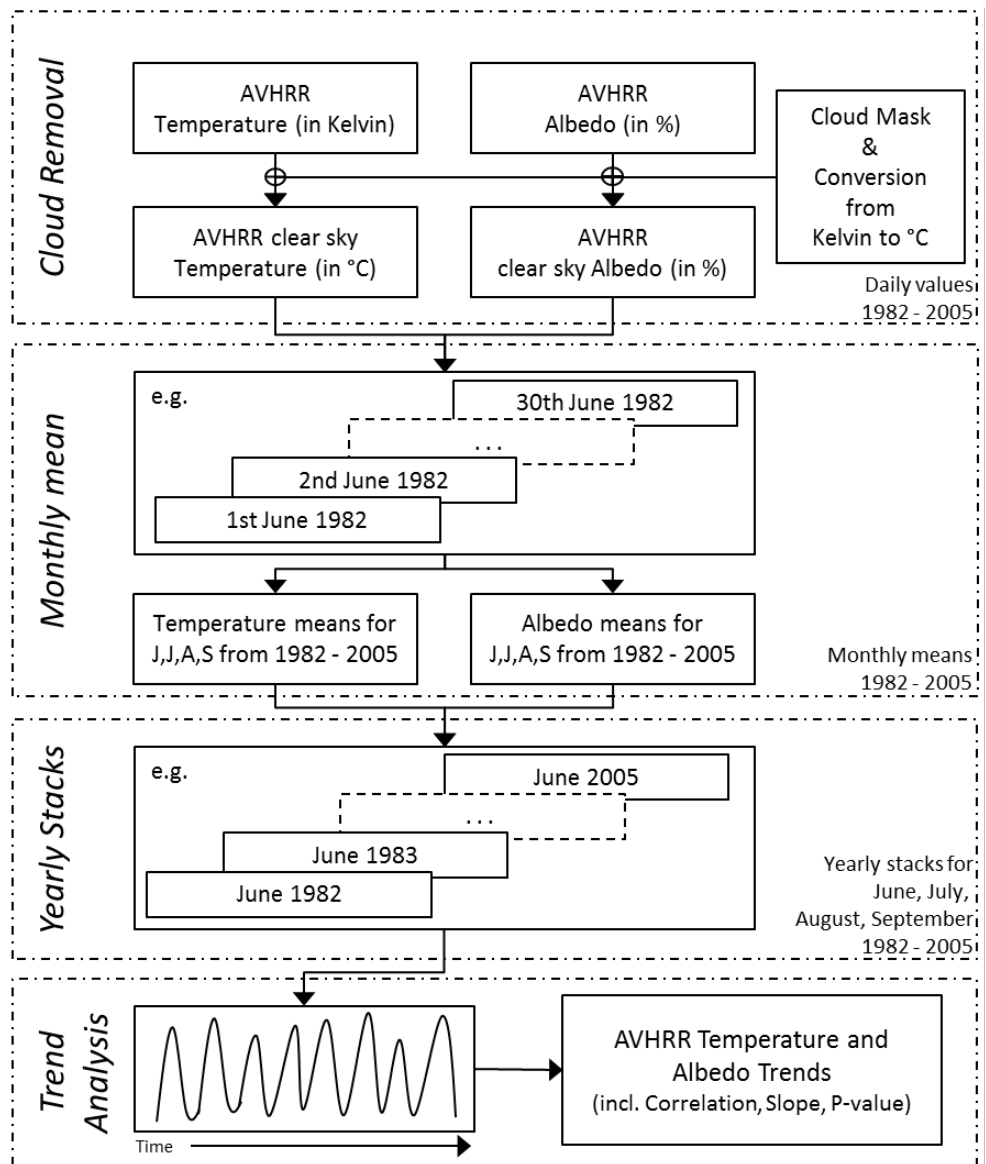


Figure 2.1: Methodology flow chart showing the extraction of inter-annual monthly trends from daily AVHRR land surface temperature and albedo information.

2.5 Results and Discussion

2.5.1 Time series analysis of LST, albedo, NDVI and SWE

The results are based on the derived buffer zone of 100 km north and south of the tree line for the whole study area. Each boxplot, which is presented in the following section, represents the variability of pixel values for this buffer zone per month. The whiskers on each side of the box correspond to approximately 99.3% of the data distribution that are not captured by the upper and lower quartile. Land surface temperature and albedo time series information from AVHRR Pathfinder data for the summer months June, July, August, and September are shown in Figures 2.2 and 2.3.

The land surface temperature and albedo time series plot for June (Figure 2.2 – A) shows the highest inter-annual dynamics in comparison with July, August, and September. Intervals of significant increasing and decreasing land surface temperature and albedo conditions are observable. For example, the land surface temperature shows a slight positive trend within the 10 year period between 1992 and 2002. Moreover, land surface temperature drops in 1992 in comparison with the other years. One reason could be the eruption of Pinatubo in 1991, which increased the amount of aerosols in the atmosphere and had a cooling effect on a global scale (Lucht et al. 2002). The years prior to 1992 are characterized by both increasing and decreasing inter-annual temperature conditions. This fact is obvious between the years 1988 and 1992. The albedo time series shows segments of high and low values. The years between 1984 and 1987 as well as 1992 and 1996 are characterized by high albedo conditions in comparison with the other years. This becomes clear if observing the periods between 1988 and 1991 and between 1997 and 2005, which show low albedo values in the study area. Two peaks of high albedo conditions can be found in the years 1987 and 1992.

If comparing the time series information from June, uniform dynamics between land surface temperature and albedo conditions are observable. In detail, an increase in the temperature conditions leads to a decrease in albedo values. Especially, the years between 1998 and 1991 as well as 2003 and 2005 are characterized by these circumstances. The high values in albedo can be seen as a potential indicator for the appearance of snow cover in June of this specific year. This assumption is consistent when comparing high albedo with land surface temperature conditions, which are lower than in years with low albedo values.

The results for the time series information from July (Figure 2.2 – B) show high land surface temperature and low albedo conditions for the entire study area. The median of the boxplot from the land surface temperature data is characterized by low dynamics with values over 20 °C for the whole time period. There are no dynamics within the albedo time series. In detail, the median of the albedo data is less than 20% for the entire period. Based on these findings, no significant trends can be found in the data for July.

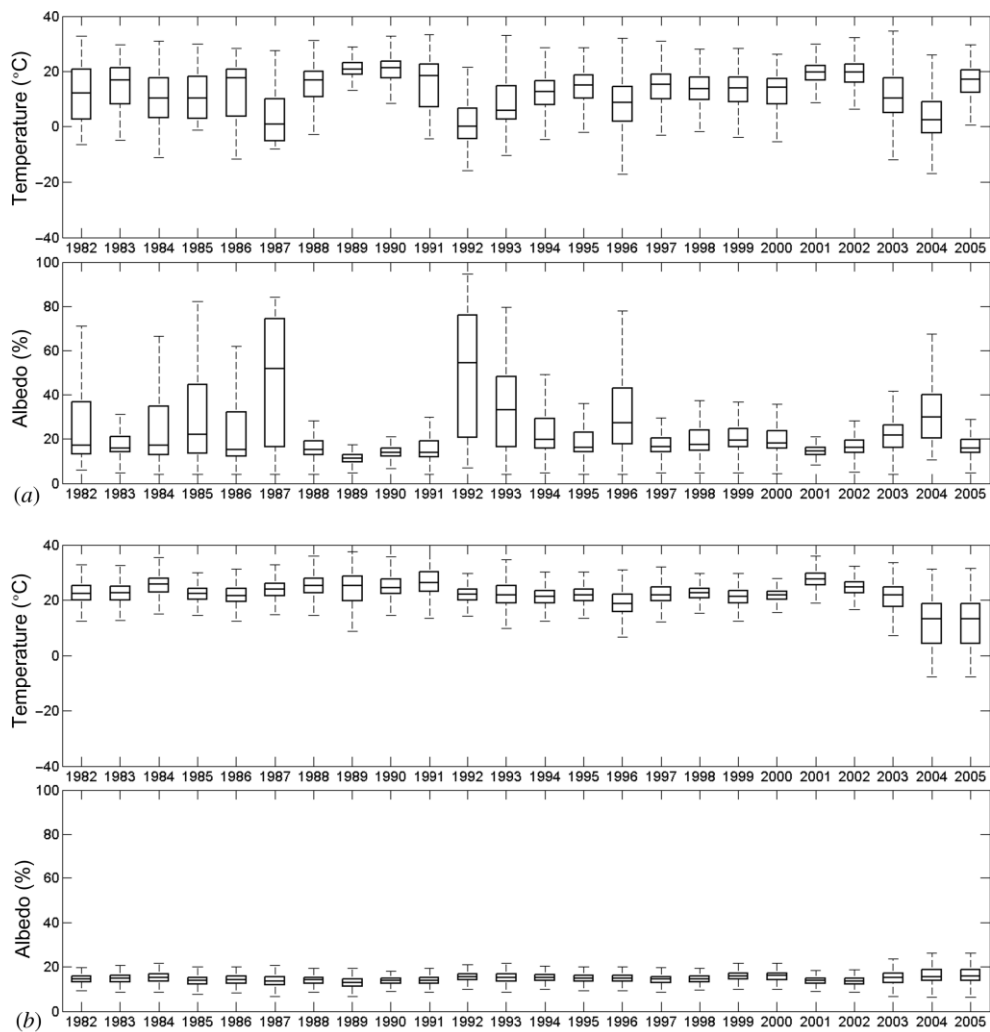


Figure 2.2: Overview of time series information from AVHRR land surface temperature and albedo for the buffer zone of 100 km north and south of the tree line for the summer month June (a) and July (b) within the time period from 1982 to 2005.

The time series information for August is displayed in Figure 2.3 (A). In comparison with July, the same dynamics and inter-annual variability are present.

Beside this, some dynamics in temperature conditions can be seen between 1991 and 1997. These circumstances are also visible in the albedo values for the same period. In general, two periods of slight increase in land surface temperature prior to and after 1992/1993 are observable, which can be also related to the Pinatubo Eruption in 1991 (Lucht et al. 2002). The years 2004 and 2005 show the lowest land surface temperature values, which can be caused by data quality. This fact becomes also visible in the albedo values, which show higher variance in 2004 and 2005.

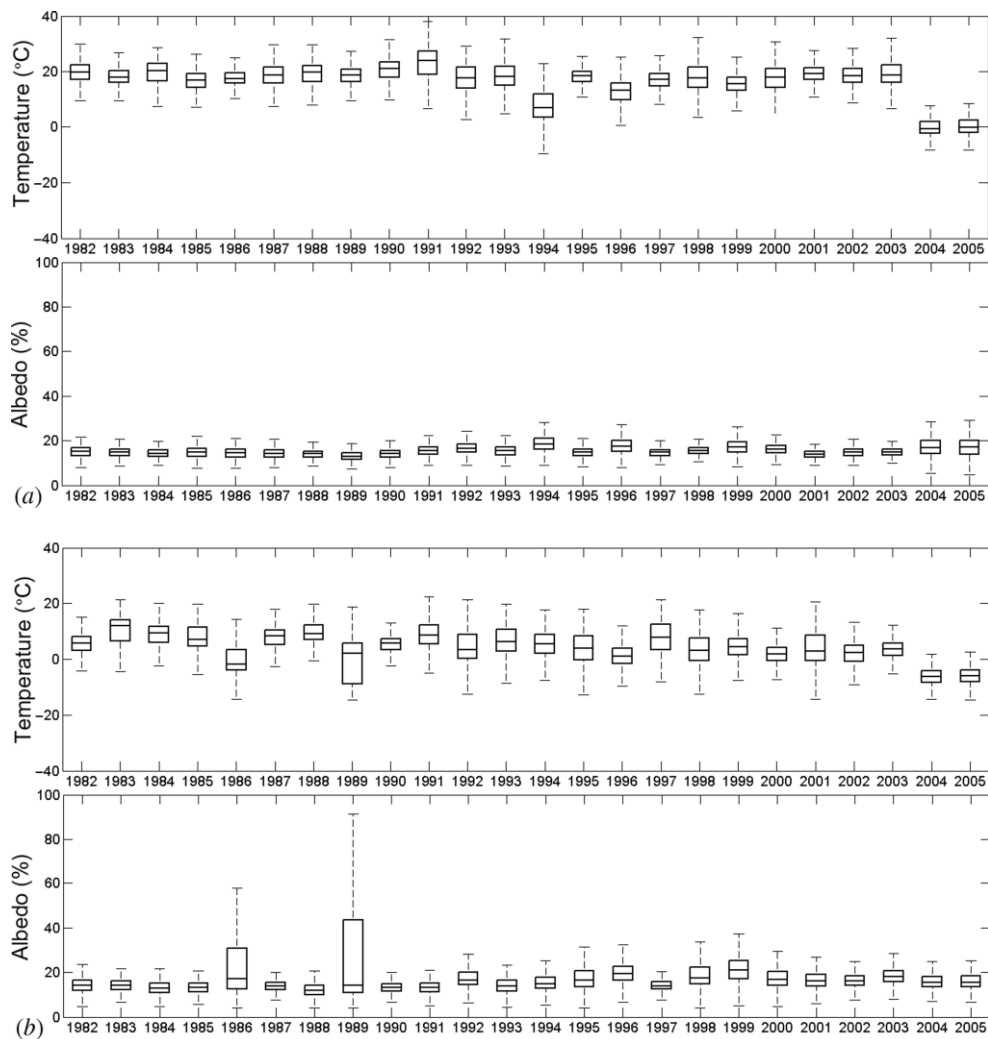


Figure 2.3: Overview of time series information from AVHRR land surface temperature and albedo for the buffer zone of 100 km north and south of the tree line for the summer month August (a) and September (b) within the time period from 1982 to 2005.

The time series information for the land surface temperature and albedo of September is displayed in Figure 2.3 (B). In comparison with July and August,

higher inter-annual dynamics are visible. The years 1986 and 1989 show the highest variance in the land surface temperature values. These conditions are also visible in the albedo measurements, which show peak events in these years. Moreover, this fact can be attributed to the influence of snow appearance, which has taken part in the study areas in the years 1986 and 1989. The time period since 1993 also shows the dependencies between temperature and albedo. In detail, the inter-annual dynamics show that a decrease in temperature results in lower albedo values and vice versa.

An overview of the median values from land surface temperature and albedo are displayed in Figure 2.4 (A). This graph gives a detailed insight into the inter-annual dynamics of the time series information from the buffer zone around the treeline. Especially, the information from June shows high dependencies between the land surface temperature and albedo dynamics. In detail, extreme events of low temperature conditions result in high albedo values, which become obvious in the years 1987, 1992, 1996, and 2004. If these events are compared to the SWE information for June produced by the GlobSnow project, which is a direct indicator for snow cover, the occurrence of high SWE values conform with high albedo and low land surface temperature information (Figure 2.4 – B). When comparing the albedo and SWE time series, it becomes clear that years with SWE values above 50 mm result in high albedo values (>30%). These conditions are visible in the years 1992, 1995 to 1997 as well as 1999. Unfortunately, no SWE values for 1987 are available, which have also shown low temperature and high albedo information. In 2004, a low SWE is detected, which might be the result of inaccuracies from the GlobSnow product. However, if SWE is compared to the other parameters in 2004, the relationship is captured. A comparison with GIMMS NDVI values for June is given in Figure 2.4 (B). As a result of the low land surface temperature and high albedo and SWE conditions in 1987, 1992, and 1996, lower NDVI values were acquired. Figure 2.4 shows time periods where all four parameters show strong dependencies on each other. This relationship is obvious in the years between 1991 and 1998 as well as 2003 and 2005, where the inter-annual dynamics of different land surface parameters are acquired by different satellite sensors showing an equal response to each other.

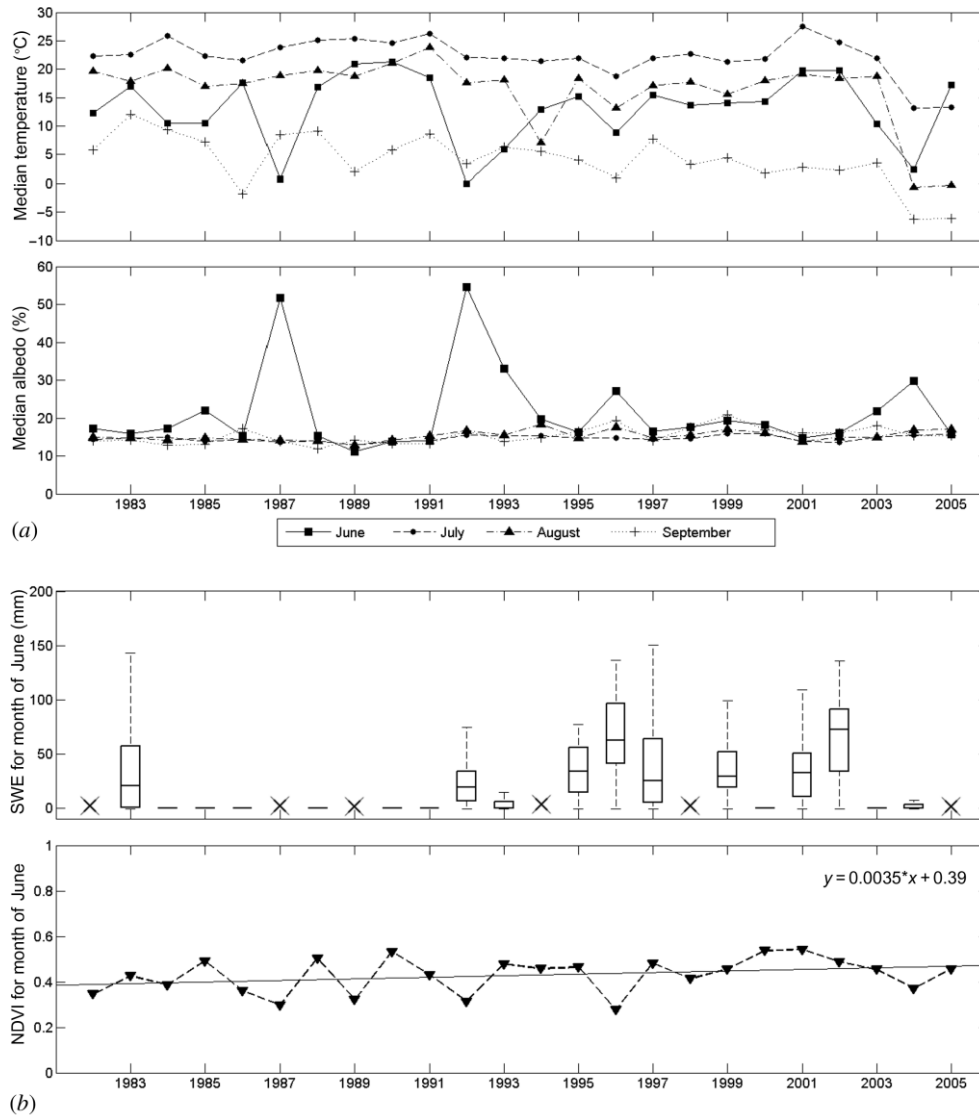


Figure 2.4: Overview of median from AVHRR land surface temperature and albedo time series for the buffer zone of 100 km north and south of the tree line for the summer month (a) and snow water equivalent (SWE) and NDVI time series information for June (b). Missing years of SWE information are marked with a black cross.

2.5.2 Identification of spatial LST and Albedo trend hot spots

The following section presents the results from the AVHRR Pathfinder land surface temperature and albedo time series trend analysis for the time period of 1982–2005. Only areas that show significant trends, are visualized. The correlation coefficient as a measure of the trend over time, with a range of -1 to 1 , of the time series for June, July, August, and September are shown in Figure 2.5. This visualization gives the

opportunity to identify potential regions with significant increasing or decreasing trends.

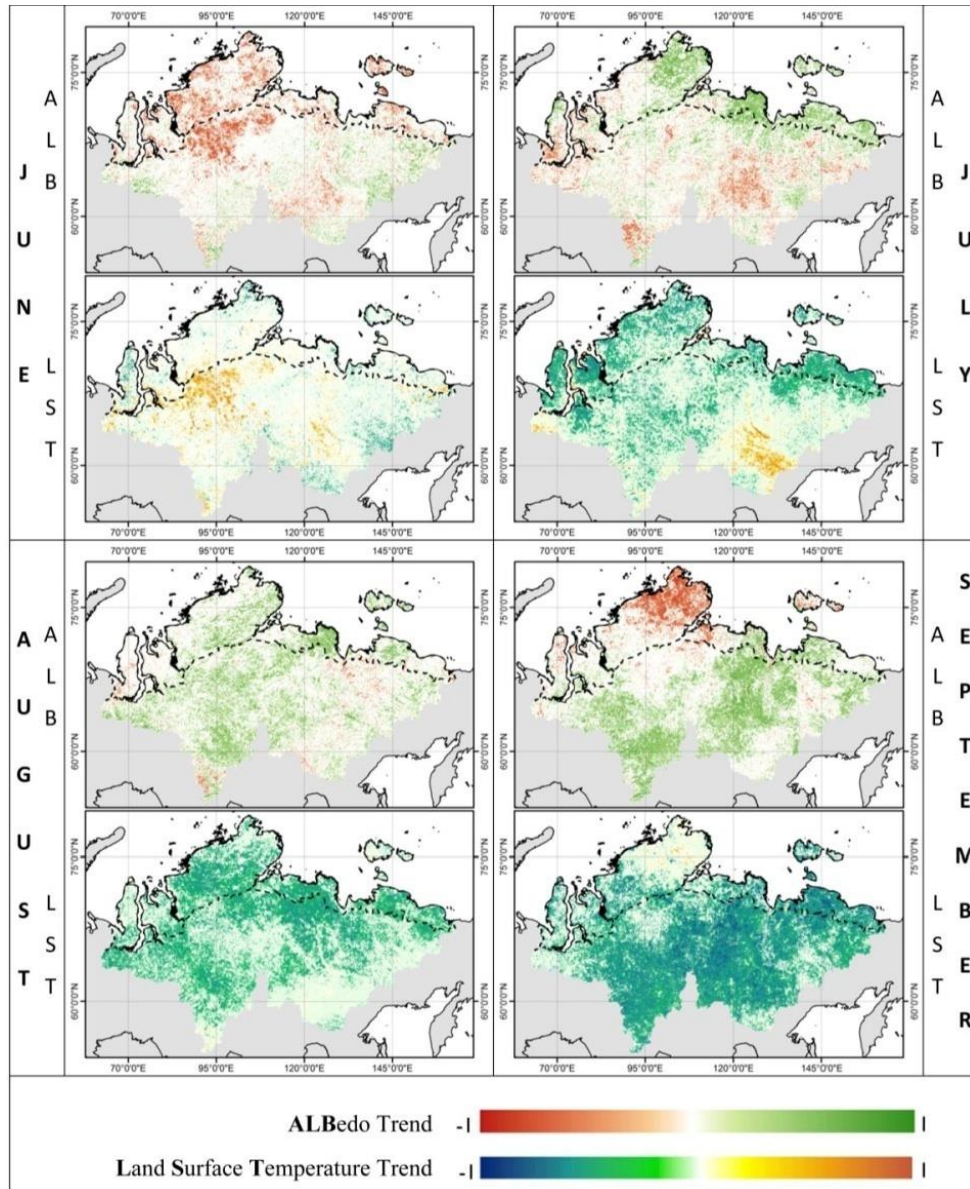


Figure 2.5: Land surface temperature and albedo trends (correlation coefficient R over time) in northern Siberia for the summer month June, July, August and September. Only significant values are displayed. The dashed line represents the tree line from Walker et al. (2005).

The results for June show larger areas of the Taymir Peninsula, indicating significant negative albedo trends. Further east, the Lena River Delta and Yana Delta system show slight positive trends in albedo. Additionally, a second trend area

of decreasing albedo trends can be seen between the Laptev and East Siberian Sea (70° N and 140° E). A strong increase in land surface temperature is situated south of the Taymir Peninsula, close to the taiga–tundra transition area. Despite this, a slight decreasing trend of land surface temperature becomes visible for the Yamal area, north of the taiga tundra transition area.

The land surface temperature and albedo conditions in July are found to be less strong than in June. Hence, regions of low positive and negative trends become visible. An increase in albedo can be found on the eastern part of the Taymir Peninsula as well as the Lena River Delta system. Nevertheless, slightly decreasing albedo conditions are found on the western regions of the Taymir and the Yamal area. The results from the land surface temperature trend analysis indicate stable conditions over time for most of the test region. The majority of the region shows a slight decrease in land surface temperature. However, a significant strong increase in land surface temperature conditions during the time period of 1982–2005 becomes visible for southern Yakutia. In the same area, a hot spot of decreasing albedo trends can be found. This part of Yakutia was highly affected by a transformation and degradation of permafrost soil due to global warming during the last decades (Iijima et al. 2009).

Despite all other months, the findings for August show only low trends in land surface temperature and albedo conditions. Albedo seems to be characterized by a slight increasing trend, whereas the land surface temperature indicates a moderate decrease.

In September, a significant albedo hot spot of strong negative trends can be found at the Taymir Peninsula. Besides this, some areas of decreasing albedo trends become visible south of the taiga–tundra transition area. For the remaining part of the whole study regions, the boreal forest regions, an increase in albedo conditions is observable. Moderate increasing of land surface temperature trends can be found on the Taymir Peninsula. But only some parts show a significance concerning the trend findings. The remaining areas indicate decreasing land surface temperature trends. Additionally, a strong decreasing land surface temperature hot spot is situated at the boreal forest regions of central Siberia.

Figure 2.6 shows the relationship of both land surface temperature and albedo trends for selected hot spot test regions. Particularly, the regions of the Taymir and Yamal peninsulas have been found to show the most significant trends in northern Siberia between 1982 and 2005. The visualization of this comparison is done via a point density cloud. Conventional scatter plots would not allow a detailed insight

into the distribution of points by a comparison of a large number of pixels, since large parts of the chart will be displayed as a black area, caused by the amount of overlapping pixel values (Eilers and Goeman 2004). Hence, the colour bar describes the quantity of pixel pairs for a specific value, where red stands for a high and white for a low density of compared values/pixels within the selected hot spot region.

Since the results of the time series analysis in Section 2.5.1 have shown significant dependencies of land surface temperature and albedo conditions, similar relationships are found for three selected trend hot spot regions. Moreover, positive land surface temperature trends result in negative albedo trends and vice versa. This fact becomes visible, especially for June, which shows the highest correlation between the land surface temperature and albedo trends. Furthermore, this month presents the beginning of the vegetation growing period in the arctic regions. Since albedo is related to the amount of snow cover, which shows a decreasing trend, these results give a potential indicator for an earlier start of the vegetation growing period in these regions. July and August indicate no significant trends, as was previously described in Section 2.5.1 and visualized in Figure 2.5. In September, only the northern parts of the Taymir Peninsula indicate increasing land surface temperature and decreasing albedo conditions, which could be also linked to a decrease in snow cover, as was found in June. Within this context, an expansion of the vegetation growing period might be expected for this specific part of the Taymir Peninsula (e.g. Bokhorst et al., 2008; Bunn and Goetz, 2006; Tucker et al., 2001).

The results of the trend analysis for three selected hot spot regions in Figure 2.6 provide a detailed insight into the derived trends for the summer period. Particularly, the amount of land surface temperature and albedo trends for the selected test sites become clearer. The findings indicate changes in the length of the vegetation growing period, since June shows the highest correlation of land surface temperature and albedo trends for all selected test regions. This could be an indicator of the absence of snow cover, which is the cause of the reduction of the surface albedo. Additionally, warmer June land surface temperature conditions are expected in these regions. These circumstances are also visible in Figures 2.2 and 2.3. Thus, the results indicate changes in the length of the growing season for these regions in northern Siberia. The results for July and August indicate both increasing and decreasing albedo trend areas. Despite this, all test regions show a decrease in land surface temperature trends, which indicates cooling conditions in this time period. The relation of land surface temperature and albedo result in very low correlations for July and August, as no direct dependency between these two

parameters becomes visible. In September, only the northern parts of the Taymir Peninsula show a significant increase in land surface temperature, whereas decreasing albedo conditions are observed.

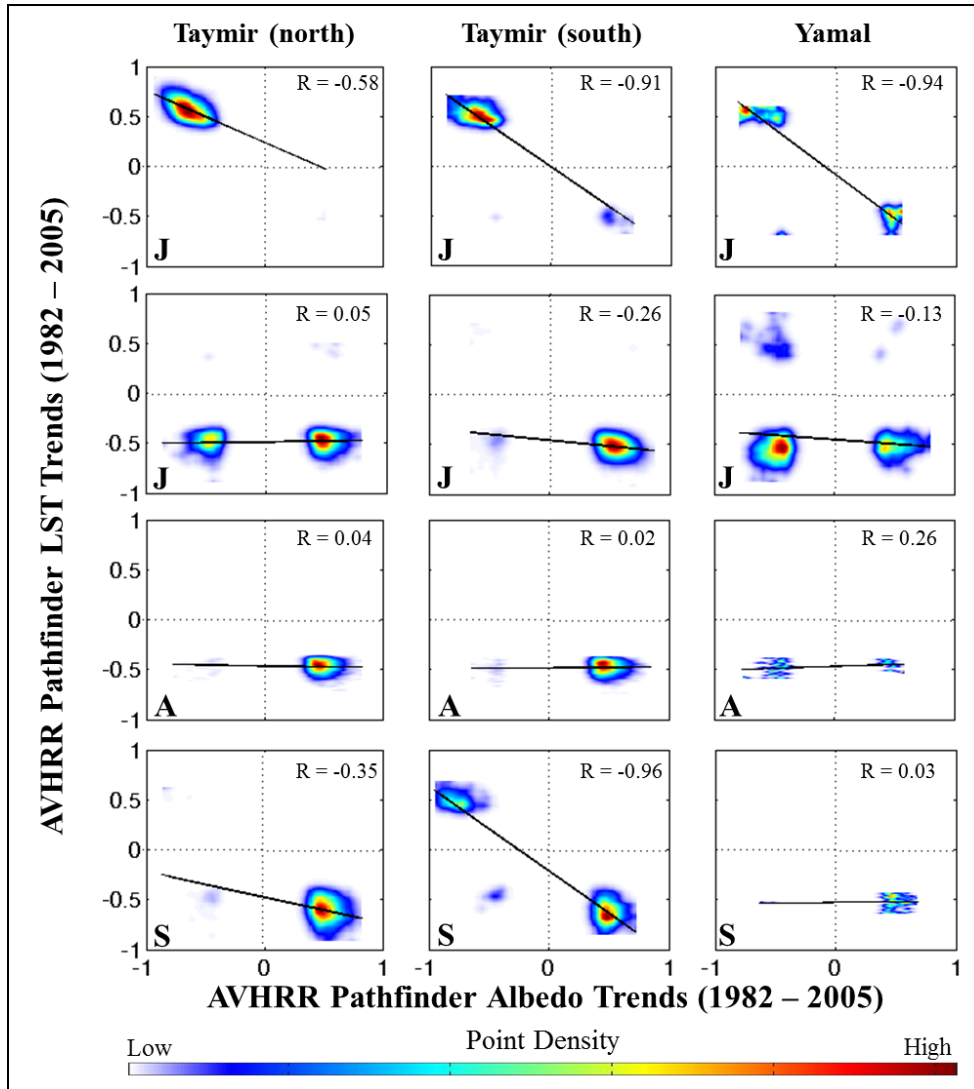


Figure 2.6: Correlation of land surface temperature and albedo trends (correlation coefficient R over time) from three selected regions (Taymir – north and south and Yamal Peninsula). Each month (June (J), July (J), August (A) and September (S)) are displayed in a separate plot.

2.5.3 Comparing Pathfinder LST data and Air Temperature records

The land surface temperature estimates from the AVHRR Pathfinder product were compared with air temperature measurements to address the quality of the remote-sensing data used. The daily mean air in-situ temperature was derived from 79

meteorological stations situated within the study area covering the time series from 1982 to 2005 (NCDC 2012).

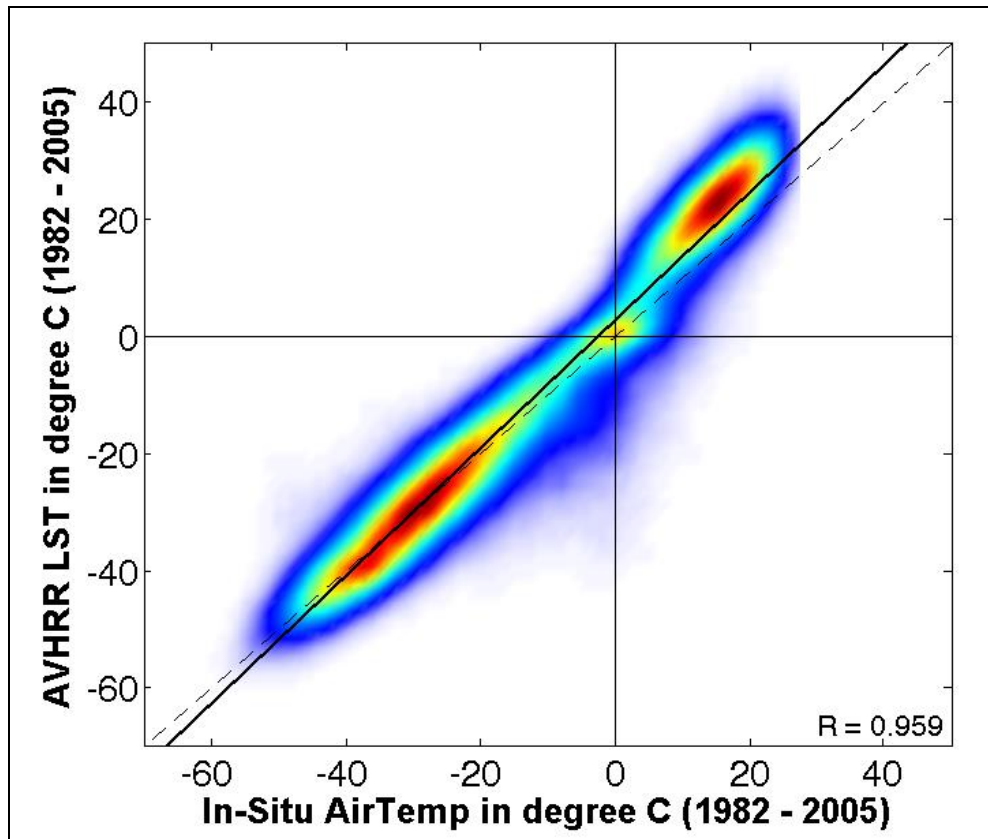


Figure 2.7: Comparison of AVHRR Pathfinder land surface temperature estimates and in-situ air temperature records from meteorological stations (NCDC 2012).

The comparison of land surface temperature and air temperature is shown in Figure 2.7, represented by a point density cloud, due to the high amount of data (red = high concentration of points, blue = low concentration of points). A correlation coefficient of $R = 0.96$ shows a very good agreement between remote-sensing-derived land surface temperature and temperature from meteorological stations. However, a minor overestimation of the air temperature can be found for values above $0\text{ }^{\circ}\text{C}$. This overestimation is the result of the temperature derived from land surface emissions, which are slightly warmer in comparison with air temperature measured at approximately 2 m height. For the negative temperature range, the correlation is higher, with a slight underestimation below $-40\text{ }^{\circ}\text{C}$.

2.6 Conclusion and Outlook

In this study, the relationship of AVHRR Pathfinder land surface temperature and albedo products for the summer months June, July, August, and September as well as SWE and NDVI information for June in the time period 1982–005 were analysed. The spatial focus of this investigation is the taiga–tundra transition area of northern Siberia. The findings show significant trends of various land surface parameters extracted from Earth observation time series.

Section 2.5.1 shows the inter-annual variability of land surface temperature, albedo, SWE, and NDVI conditions in the time period 1982–2005. The highest variability of land surface temperature and albedo is found in June, followed by September. The months July and August show practically no inter-annual variability during this time period. Additional information from SWE and NDVI information is integrated for June. The inter-annual dynamics of these parameters correlate with the land surface temperature and albedo time series information. In detail, low temperature and high albedo conditions are accompanied by high SWE and low NDVI values, and vice versa.

The spatial localization of AVHRR Pathfinder land surface temperature and albedo trends is shown in Section 2.5.2. We found a significant indirect proportional correlation of land surface temperature and albedo trends. Especially, at the start and end of growing season, June and September, high trends and correlation are observable. The negative correlation of land surface temperature and albedo information in June and September indicate changes of snow cover and the length of growing season. Since snow-covered areas produce a high surface albedo, decreasing albedo trends indicate the absence of a snow layer. Thus, longer snow free periods are expected, especially for the regions Taymir and Yamal. On the other hand, an increase in land surface temperature conditions indicates an extension of the vegetation growing cycle.

This study shows the feasibility and potential of using time series information for trend analysis for various land surface parameters extracted from Earth observation data. Hence, the synergetic comparison of different parameters appears to provide a detailed insight into the land surface dynamics. Future satellite missions, such as the Sentinel-3 mission by ESA, will contribute to upcoming climate change studies through the continuation of a sustainable acquisition of coarse resolution time series information (Aguirre et al. 2007).

This article focuses on the linear trends in AVHRR Pathfinder land surface temperature and albedo time series information. Linear regression models cannot separate the time series signal in increasing and decreasing trends. To solve this problem, Wang et al. (2011) and Piao et al. (2011) used a piece-wise linear regression to estimate turning points and trend changes. The aggregation of time series to annual values causes a loss of temporal information. An alternative is to decompose the original time series in different components. The Breaks for Additive Seasonal and Trends (BFAST) algorithm (Verbesselt et al., 2010) removes seasonal effects and short-term deviations from the time series and estimates breakpoints in the remaining series with the application of a piece-wise linear regression model. Future studies will be carried out using additional trend analysis tools, such as BFAST (Verbesselt et al. 2010), to address a multiple regression analysis. Moreover, the detection of trend breakpoints provides valuable information for the analysis of satellite time series of vegetation activity (de Jong et al. 2012), which requires the definition of short-term trends, which are not the focus of this study.

Since, this investigation is part of a multi-scale approach, remote-sensing data with higher spatial resolution will be integrated to map potential vegetation changes in the regions showing the highest and most significant trends. Therefore, recent remote-sensing data from Rapideye and historical Corona Keyhole imagery with a spatial resolution of few metres will be used to provide a detailed insight into the changes of vegetation structures and compositions in the study area.

Chapter 3

Comparison of Satellite-Derived Land Surface Temperature and Air Temperature from Meteorological Stations on the Pan-Arctic Scale

M. URBAN¹, J. EBERLE¹, C. HÜTTICH¹, C. SCHMULLIUS¹ & M. HEROLD²

¹Friedrich-Schiller-University Jena, Department for Earth Observation

²Wageningen University, Centre for Geo-Information

Published in:

Remote Sensing (2013), 5, 2348-2367

(Received 20 March 2013; Accepted 7 May 2013)

DOI: 10.3390/rs5052348

3.1 Abstract

Satellite-based temperature measurements are an important indicator for global climate change studies over large areas. Records from Moderate Resolution Imaging Spectroradiometer (MODIS), Advanced Very High Resolution Radiometer (AVHRR) and (Advanced) Along Track Scanning Radiometer ((A)ATSR) are providing long-term time series information. Assessing the quality of remote sensing-based temperature measurements provides feedback to the climate modeling community and other users by identifying agreements and discrepancies when compared to temperature records from meteorological stations. This paper presents a comparison of state-of-the-art remote sensing-based land surface temperature data with air temperature measurements from meteorological stations on a pan-arctic scale (north of 60° latitude). Within this study, we compared land surface temperature products from (A)ATSR, MODIS and AVHRR with an in situ air temperature (T_{air}) database provided by the National Climate Data Center (NCDC). Despite analyzing the whole acquisition time period of each land surface temperature product, we focused on the inter-annual variability comparing land surface temperature (LST) and air temperature for the overlapping time period of the remote sensing data (2000–2005). In addition, land cover information was included in the evaluation approach by using GLC2000. MODIS has been identified as having the highest agreement in comparison to air temperature records. The time series of (A)ATSR is highly variable, whereas inconsistencies in land surface temperature data from AVHRR have been found.

3.2 Introduction

Land surface temperature (LST) is a supporting information source for the generation of the Essential Climate Variable defined by the Global Climate Observing System (GCOS), to support the United Nations Framework Convention on Climate Change (UNFCCC), the World Climate Research Programme (WCRP) and the Intergovernmental Panel on Climate Change (IPCC) (GCOS 2011). Global climate change, caused by increasing greenhouse gas (GHG) emissions, results significant changes to global ecosystems (Overpeck et al. 1997; Chapin et al. 2005).

The arctic environment is highly vulnerable to modifications in the global climate system and currently subject to dramatic changes (Grace et al. 2002; Moritz et al. 2002; Nelson 2003). Predictions are indicating a significant increase of temperature conditions in the arctic regions for the upcoming century (Kaplan and New 2006), which leads to changes in permafrost temperature regimes, snow cover, sea ice, vegetation activities and phenological dynamics (Myneni et al. 1997; Romanovsky et al. 2002; Stow et al. 2004; Post et al. 2009). Increasing greenhouse gas emissions from thawing permafrost soils will accelerate rising temperature for the upcoming decades, due to positive feedback mechanisms in the global climate system (Serreze et al. 2000; Moritz et al. 2002). These circumstances are showing the high importance of a consistent and operational monitoring of climate conditions, such as temperature, within the arctic regions. Thus, the problem is the availability of records from meteorological stations, as well as their spatial coverage in these territories. The integration of those ground measurements in climate research, such as modeling and trend analysis, will evoke different problems. The analysis will suffer from the spatial coverage and will not capture the heterogeneity of the arctic climate system. Hence, remote sensing provides a useful tool to retrieve different land surface characteristics over large areas, such as LST (Hachem et al. 2012).

The Data User Element Permafrost (DUE Permafrost), funded by the European Space Agency (ESA), highlighted the needs for a permafrost monitoring system. The aim of this project was to facilitate the cooperation between remote sensing experts and the permafrost science community. To create an observation strategy, various permafrost relevant parameters, such as LST, land cover, subsidence, thermokarst lake changes, soil moisture, *etc.*, which are measurable by satellite systems, were defined. Land surface temperature is one important variable, used as an indicator of the thermal state of the subsurface phenomenon permafrost, which cannot be directly measured with satellite platforms (Bartsch et al. 2010). Hence, there is an

increasing demand for integrating LST estimates in arctic research, such as permafrost modeling systems (Soliman et al. 2012).

This paper presents the comparison of state-of-the-art remote sensing-based LST data with air temperature measurements (T_{air}) for the pan-arctic regions north of 60 degrees latitude. Within this study, we compared LST products from Advanced Very High Resolution Radiometer (AVHRR), Moderate Resolution Imaging Spectroradiometer (MODIS) and (Advanced) Along Track Scanning Radiometer ((A)ATSR) with an *in situ* T_{air} database provided by the National Climate Data Center (NCDC). In the context of this paper, the term LST is used for the remote sensing-based temperature information, while T_{air} refers to the measurement of the meteorological station. The aim is to analyze the agreement between LST and T_{air} for (1) the complete available period of each product, (2) for the overlapping time period from 2000 to 2005, (3) based on different land cover classes from GLC2000, as well as (4) the spatial distribution of the agreement on the pan-arctic scale.

This paper presents a comparison of LST with T_{air} records, rather than validation approach. A validation approach of LST requires *in situ* data, which are based on emissivity measurements of the earth surface using an thermal infrared radiometer (TIR) or comparable systems (Hachem et al. 2012). Particularly, this paper presents a comparison of two parameters, which have a different physical meaning.

Land surface temperature refers to the radiation properties of the earth surface and determines the intensity of the radiation of long waves emitted by it, which can be detected by aircrafts or satellite-based remote sensing platforms. There are different terms describing the same variable, such as land surface temperature or surface skin temperature. The air temperature or surface air temperature is measured at 1.5–2 m height, where the measurements are done by the contact of the sensor and the surrounding air. Land surface temperature and T_{air} are correlated to a certain degree, with some drawbacks depending on factors, such as land cover type (Jin and Dickinson 2010; Mildrexler et al. 2011).

The comparison is done by using statistical parameters such as the Pearson correlation coefficient (R), the slope (S) and the intercept (INT) with the y-axis of the regression line and the mean difference (MD), also known as bias. The first three parameters were derived by comparing the pixel of the LST data with the corresponding T_{air} measurements from the meteorological station. Each meteorological station is situated within a pixel of the different remote sensing

products. The statistics are based on the scatter cloud derived from the analyzed comparison pairs and time step. The MD is calculated by the difference between T_{air} and LST divided by the amount of observed time steps. If the MD is negative, the LST detects warmer temperatures than the measured T_{air} , and *vice versa* (Hachem et al. 2012).

3.3 Data

3.3.1 Remote Sensing Data

3.3.1.1 AVHRR Polar Pathfinder Land Surface Temperature

The AVHRR Polar Pathfinder product covers the polar regions of the northern and southern hemisphere with a spatial coverage north of 48° and south of 53° in latitude and have been used for several studies (Maslanik et al. 1997; Green and Hay 2002; Ouaidrari et al. 2002; Julien et al. 2006; Sobrino et al. 2006). The product includes five AVHRR channels, covering one visible, one infrared and three thermal infrared bands, as well as surface albedo, skin surface temperature, solar zenith angle, satellite elevation angle, azimuth angle, surface type and a cloud mask. The product covers the time period from July 1981 to June 2005 and is based on data from NOAA-7, 9, 11, 14 and 16. It is a twice-daily dataset acquiring the imagery at 4 a.m. and 2 p.m. in the northern hemisphere. For this study, only daytime LST estimates have been used. The data is available in EASE-Grid projection (Equal Area Scalable Earth-Grid) with spatial resolution of 5 km (Fowler et al. 2007). The LST is extracted by two algorithms, which utilize the brightness temperature of spectral channels 4 (10.3–11.3 μm) and 5 (11.5–12.5 μm) (Key et al. 1997).

The data quality of the AVHRR Polar Pathfinder product is influenced by an orbital drift of each NOAA satellite during their lifetime, which causes a shift of the equator crossing time to the afternoon. This orbital drift evokes a cooling effect to the LST estimates. The effect was found to be stronger on the southern hemisphere and non-vegetated regions (Gleason et al. 2002; Julien and Sobrino 2012). Since this study focuses on the cold regions of the northern hemisphere, the effect of the orbital drift is negligible and not part of its scope.

3.3.1.2 MODIS Land Surface Temperature (MOD11C1, MYD11C1)

The LST products from MODIS Terra and Aqua are widely used for remotely sensed temperature research such as (Guangmeng and Mei 2004; Liu et al. 2006; Hulley and Hook 2009; Julien and Sobrino 2009; Langer et al. 2010; Lei et al. 2010; Mildrexler et al. 2011; Zhang et al. 2011; Crosson et al. 2012; Hengl et al. 2012). The product covers a range of different datasets ranging from 1 km to 0.05° (approx. 5.6 km at equator; CMG - Climate Modeling Grid) spatial resolution, as well as daily, eight-day and monthly temporal resolution. Both satellite platforms have sun-

synchronous orbits. MODIS Terra acquires the data at 10:30 a.m./p.m. (daytime/nighttime), whereas MODIS Aqua collects the imagery at 1:30 p.m./a.m. (daytime/nighttime) (Savtchenko et al. 2004). For this study, daily MODIS LST products MOD11C1 and MYD11C1 (Version 5) with a resolution of 0.05° were used. The MODIS LST products (MOD11C1, MYD11C1) were derived from MOD11B1, which has a daily resolution with 6 km pixel size in sinusoidal projection. This product is developed from algorithms defined in (Wan and Li 1997), whereby the temperature and emissivity extraction from 7 of 16 emissivity bands from MODIS that cover the thermal infrared spectrum (TIR) are described. In detail, the bands 20 (3.66–3.84 μm), 22 (3.93–3.98 μm), 23 (4.02–4.08 μm), 29 (8.40–8.70 μm), 31 (10.78–11.28 μm), 32 (11.77–12.27 μm) and 33 (13.18–13.48 μm) were used for the approach. Compared to the other channels from MODIS, these channels, also known as window bands, remain virtually unaffected by changes in temperature and amount of water vapor within elevations above 9 km (Wan and Li 1997).

The retrieval of LST from MODIS is based on various input parameters, which were also available as individual products. In general, only swaths, which have a valid Level 1B radiance in channels 31 (10.78–11.28 μm) and 32 (11.77–12.27 μm), are over land (including water bodies) and are acquired under clear sky conditions, in addition to being used to derive LST information. The extraction is done by a classification-based algorithm developed by (Snyder and Wan 1998), in which emissivity estimates from band 31 and band 32 are used. Additional input parameters, such as cloud mask (MOD35_L2), atmospheric profiles (MOD07_L2), geo-location (MOD03), land cover (MOD12Q1) and snow cover (MOD10_L2), are integrated into the algorithm.

3.3.1.3 Land Surface Temperature from AATSR

The LST product by the European Space Agency (ESA), which was provided for this study, was derived using ATSR-1 on ERS-1, ATSR-2 on ERS-2 and AATSR on ENVISAT earth observation data. All satellites have sun-synchronous orbits, where ERS-1 and ERS-2 acquire data at 10:30 a.m. and ENVISAT at 10 a.m. (Mutlow et al. 1999; Coll et al. 2009). The LST product is produced using a nadir-split window approach calculating brightness temperature from 11 μm and 12 μm described in (Prata 2002). Coefficients depending on the atmospheric water vapor, the viewing angle and the land-surface emissivity are considered in the algorithm (Dorman and Sellers 1989; Prata 2002; Scarpino and Cardaci 2009). The ESA is planning to develop a GlobTemperature program based on the data from ERS-1 and 2,

ENVISAT and upcoming missions during the next year. A first user workshop, to address the user's needs for a global LST dataset, was held in Edinburgh in mid-2012 (Pinnock 2012).

This global product covers the time period from August 1991 to December 2009 with a spatial resolution of 9.28 km in sinusoidal projection. The product has monthly resolution, where each month is covered by approximately 430 orbits at a resolution of 1 km. The final product resolution of 9.28 km is based on a composite and consists of pixels marked as land and cloud-free. The discrimination between day and nighttime data was done using sun elevation information (Mutlow et al. 1999; Kogler et al. 2012).

Some issues about the data quality due to anomalies of the sensors during their data acquisitions times were identified. In May 1992, the 3.7 μm channel from ATSR-1 was lost. There were no data between January and June 1996 due to problems with the downlink and the tape capacity followed by a reduced swath within the visible channels since June 2001. AATSR onboard of ENVISAT suffered from a spectral drift in the 0.55- μm channel from December 2005 to December 2006, which was corrected *a priori* by a model defined by (Smith 2006). Since all three sensors are using identical thermal infrared channels, which are used deriving LST information, it has to be mentioned that all of the sensors are onboard of three different platforms with individual orbits and acquisition times. This is an important point to highlight in a product combined from similar but unique sources (Kogler et al. 2012).

3.3.2 Global Surface Summary of Day Data—Version 7

The comparison of the daily and monthly remote sensing-based LST estimates with ground measurements were done using the Global Surface Summary of Day Data (GSOD), an *in situ* database from NOAA (National Oceanic and Atmospheric Administration) National Climate Data Center (NCDC). The product provides daily information about 18 meteorological parameters, such as T_{air} (min, mean and max), wind speed, wind gust, and amount of precipitation, from over 8,000 stations worldwide. This GSOD dataset is based on the Integrated Surface Database (ISD), an initiative developed in 1998 by a cooperation of NCDC, US Air Force and US Navy. The aim of this program is to provide hourly consistent climate measurements back to the 19th century to address the needs of global climate studies (Lott et al. 2008; NCDC 2012; Ruff and Neelin 2012).

The database of the Global Summary of Day Data is updated on a daily frequency. In general, the majority of the temporal availability of the meteorological stations goes back to the 1970s, for some cases even back to the 1930s and earlier. There are known issues about the data availability for some regions, which could be interrupted for some time periods due to data restrictions or communication problems. However, all available daily data records are based on a minimum of four observations per day. The data quality is automatically controlled and corrected, which prevents larger data gaps within the database (NCDC 2012).

3.4 Methodology

The comparison of remote sensing-based LST estimates and T_{air} records from the meteorological station is performed with six processing steps:

- (1) Extraction of meteorological stations on pan-arctic scale (above 60 degrees north).
- (2) Identification of geographic location of meteorological stations and extraction of data from pixels in remote sensing-based LST products.
- (3) Comparison of LST and T_{air} time series for the whole temporal coverage of each product.
- (4) Reduction of both databases to the overlapping time period of the remote sensing products (2000–2005).
- (5) Inter-annual comparison of LST and T_{air} data based on the overlapping time period.
- (6) Link of the results to land cover classes extracted for each meteorological stations based on GLC2000 (Global Land Cover 2000).

I. The extractions of the meteorological stations, which are situated north of 60 degrees, are done by metadata file, which was provided by the NCDC. This file includes additional information for each station, such as station ID, starting time of acquisition, geographic coordinates, country and measured parameters. This extraction results in over 600 stations suitable for this analysis. After an automated consistency check, identifying missing daily data, the data gaps were filled to create a consistent database. Meteorological stations, which have shown a significant number of missing data, were not used for this study.

II. To develop a comprehensive validation database, the geographic coordinates of each of the selected meteorological stations was extracted from the metadata and applied to the remote sensing time series product. Afterwards it was possible to convert the pixel stack from the LST products, which are including each time step, into a single vector. For each meteorological station, a matrix was developed, which included the time, the LST that was based on the remote sensing data, and the T_{air} values.

III. In a first step, the remote sensing-based LST was compared to T_{air} measurements for the complete time series of each product (Section 3.5.1). Only

daytime temperature information was used in this study. This analysis should give an impression about the agreement between both parameters.

IV. To derive a detailed insight in the comparison and to assure the comparability of this study, the overlapping period of the remote sensing products (2000–2005) was analyzed (Section 3.5.2).

V. For this time period, the inter-annual variability between LST and T_{air} were analyzed, using different statistical parameters, such as the Pearson correlation coefficient (R), the slope (S) and the intercept of the regression line (I), as well as the mean difference (MD).

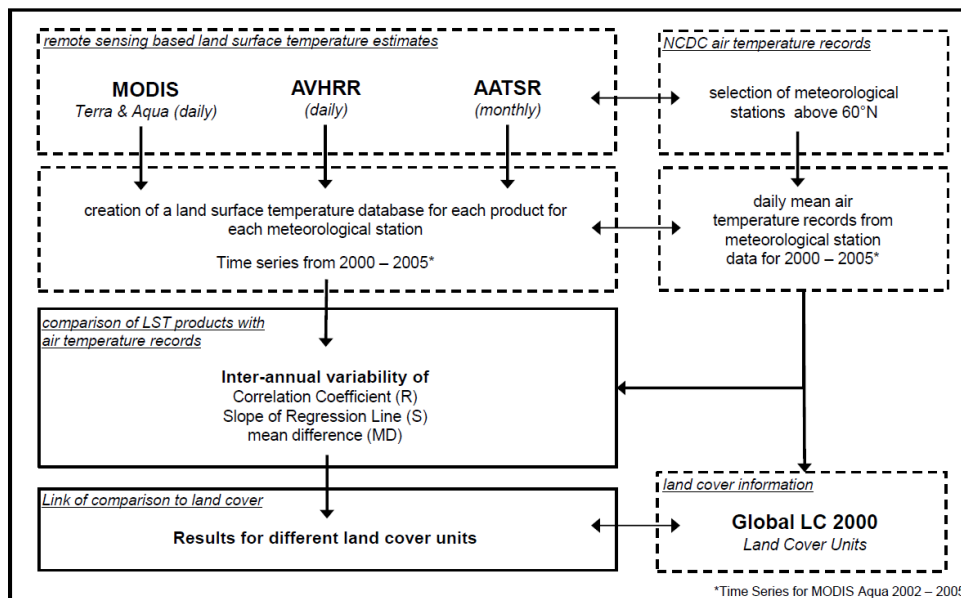


Figure 3.1: Flowchart of the described methodology.

VI. Prior to the inter-annual variability by comparing LST and T_{air} time series information, the results were linked to land cover units (Sections 3.5.3 and 3.5.4). The goal was to provide information about land cover classes, which are showing the highest variability and discrepancies between remote sensing and ground temperature measurements. The aim was to use the most recent global land cover product GlobCover 2009, developed by ESA (Bontemps et al. 2011). Unfortunately, this classification is not suitable for this analysis, since the land cover class “needle-leaved deciduous forest” (80) does not appear in the final product. The reason for that is that this class needs a seasonal observation from a remote sensing satellite, which was not sufficient for this classification (Bontemps et al. 2011). Thus, the Global Land Cover Classification 2000 (GLC2000), produced by the Joint Research

Centre (JRC), was used for this study. This classification is based on satellite data from VEGETATION on SPOT-4 and uses the standardized Land Cover Classification System (LCCS) developed by FAO (Food and Agriculture Organization) as land cover legend (Bartholomé and Belward 2005). A brief overview of the methodology is shown in Figure 3.1.

3.5 Results and Discussion

3.5.1 Correlation of Remote Sensing-Based LST Estimates with T_{air} Measurements

The following chapter presents the results from the comparison of LST from (A)ATSR (monthly mean values), AVHRR and MODIS (both daily mean values) with daily mean *in situ* measurements from meteorological stations. Each plot shows the correlation of the comparison based on the time series of each product with T_{air} data (Figure 3.2). The density cloud plot is divided into temperatures above and below 0 degree Celsius ($^{\circ}\text{C}$), while showing the corresponding regression line as well as the Pearson's correlation coefficient (R).

The LST product from (A)ATSR covers the time period of 1991 to 2009 with a monthly temporal resolution. When compared to T_{air} measurements, a correlation of $R = 0.89$ is achieved. The remote sensing data detects colder temperatures than those measured on the ground within a range of 0 to 15 $^{\circ}\text{C}$. Above 15 $^{\circ}\text{C}$, the opposite becomes visible. The agreement between LST and T_{air} for temperatures above 0 $^{\circ}\text{C}$ are described by a correlation coefficient $R = 0.75$. Observing the negative temperature range, LST is showing colder temperatures until approximately -30 $^{\circ}\text{C}$. Below this value, LST appears to be warmer. The negative temperature range results in a correlation coefficient of $R = 0.81$. Thus, higher correlations are found for temperatures below the freezing point.

The LST estimates from the AVHRR Polar Pathfinder dataset results in an overall correlation of $R = 0.9$, which is comparable to the correlation coefficient of (A)ATSR. However, AVHRR has a larger temporal coverage (1981–2005) and has a daily temporal resolution. Similar to (A)ATSR, LST from AVHRR results in colder temperatures compared to the corresponding T_{air} measurements within a temperature range from 0 and 5 $^{\circ}\text{C}$ and the opposite above this range, causing a correlation coefficient of $R = 0.74$. For temperature values below 0 $^{\circ}\text{C}$, (A)ATSR and AVHRR are showing similarities. Until a value of -30 $^{\circ}\text{C}$, LST is slightly colder than T_{air} . Afterwards, LST values are warmer than the corresponding T_{air} values. The correlation coefficient is $R = 0.82$.

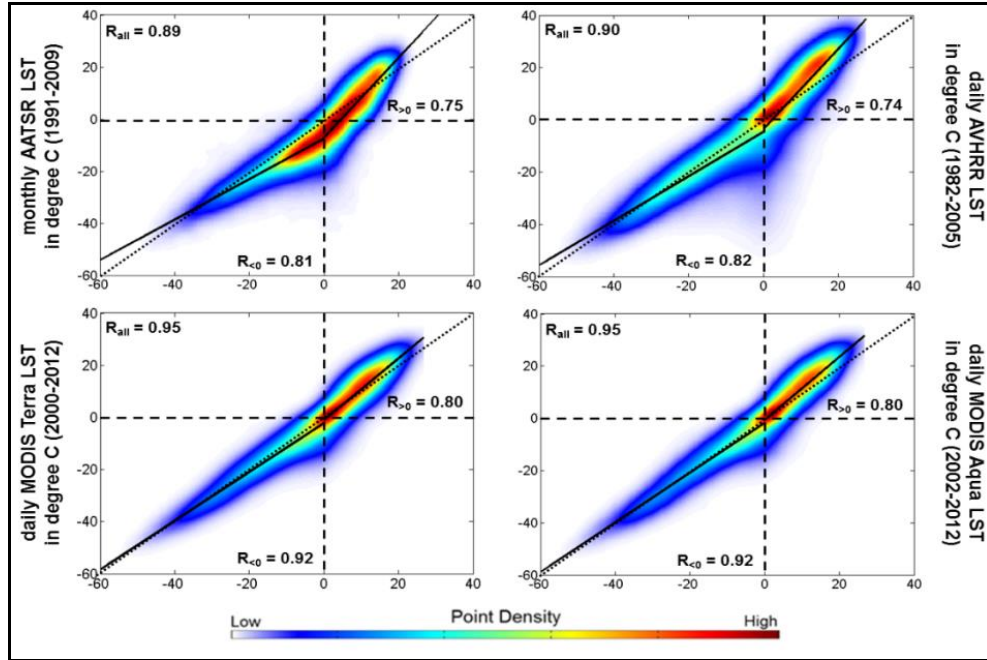


Figure 3.2: Comparison of (A)ATSR, AVHRR, MODIS Terra and MODIS Aqua LST estimates and T_{air} records from meteorological stations. Each plot shows the complete time period of each product (AATSR = 1991–2009, AVHRR = 1982–2005, MODIS Terra = 2000–2012, MODIS Aqua = 2002–2012).

The overall correlation coefficient of MODIS Terra and Aqua is higher than for (A)ATSR and AVHRR ($R = 0.95$). However, MODIS Terra and Aqua are covering a shorter time period. The correlation of temperature above $0\text{ }^{\circ}\text{C}$ shows a slight overestimation with a very close fit of the regression line to the 1:1 line. The correlation coefficient is higher ($R = 0.80$) than for (A)ATSR and AVHRR. The correlation of negative temperature is very high with $R = 0.92$, which also results in a very close fit of the regression line and the 1:1 line.

In summary, MODIS Terra and Aqua LST estimates display a higher correlation when compared to T_{air} records, followed by (A)ATSR and AVHRR. The concentration of the point density within the scatter cloud is close to the 1:1 line, which is also the case for AVHRR. Values around $0\text{ }^{\circ}\text{C}$ and slightly warmer seems to show the highest concentration of compared data pairs, except for (A)ATSR. AVHRR and (A)ATSR show outliers at $0\text{ }^{\circ}\text{C}$ of the x-axis ranging down to $-60\text{ }^{\circ}\text{C}$ of the y-axis. These artifacts may be caused by the cloud and ice detection algorithm of the products. Since temperature conditions in the lower atmosphere (top of clouds) are much lower (Vardavas and Taylor 2012) than the temperature of snow or ice covered surfaces, confusion between cloud and ice detection during the winter season could cause this problem.

In general, LST appears to result in warmer values compared to T_{air} within the positive temperature range for all remote sensing products. This problem exists due to the fact that LST and T_{air} are based on different physical processes (Jin and Dickinson 2010), as described in the introduction. Land surface temperature is warmer in positive temperature ranges than T_{air} , which is measured at a height of 2 m, as standardized for meteorological stations. Increased solar irradiance (e.g., during the summer month), causes higher land surface temperatures, thereby leading to this overestimation (Sun and Mahrt 1995).

3.5.2 Inter-Annual Variability of LST Estimates for the Time Period between 2000 and 2005

This chapter highlights the inter-annual variability of different statistical parameters extracted by the comparison of LST and T_{air} . Due to the large amount of data, each time step represents the median of all measurements. Figure 3.3 gives an overview of the variation between the time periods of 2000 to 2005, which is the overlapping time period of the used remote sensing products and enables a refined comparability.

The correlation coefficient (R) describes the variance of the point cloud around the regression line, showing the dependencies between LST and T_{air} . The variability of R during the time period of 2000 to 2005 is quite similar for all products, with the majority ranging between 0.6 and 0.9 during the yearly cycle. Higher correlations can be found in the winter season and lower during the summer month. An explanation could be the higher turbulences between land surface and atmosphere in the summer month in comparison to the winter month with lower incoming solar radiation (Zhang et al. 2011). AATSR is showing the highest inter-annual dynamics compared to the other products. Since 2003, AATSR is not capturing the yearly dynamics of the other products. Land surface temperatures from MODIS are showing similar inter-annual variations when compared to T_{air} measurements. The dynamics of AVHRR are comparable to the variability identified for MODIS. However, AVHRR is resulting in larger amplitudes of the dynamics.

In general, MODIS results in consistent inter-annual dynamics in contrast to more variations identified in AATSR and data inconsistencies for some months in the AVHRR product. A drop of the correlation coefficient is found at the end of 2004 for the AVHRR data. This might be due to the data quality, consistence of acquired data and algorithm processing chain. Known issues include problems with the scan motor on NOAA-16, which causes sporadic, irregular shifts within the derived spectral information (Fowler et al. 2007), as well as the orbital drift of the NOAA satellites, which in turn causes a delay in overflying time (Gleason et al. 2002; Julien and Sobrino 2012). Another reason could be that the data from AATSR has a monthly temporal resolution. The number and the time of observations may vary from month to month during this time period.

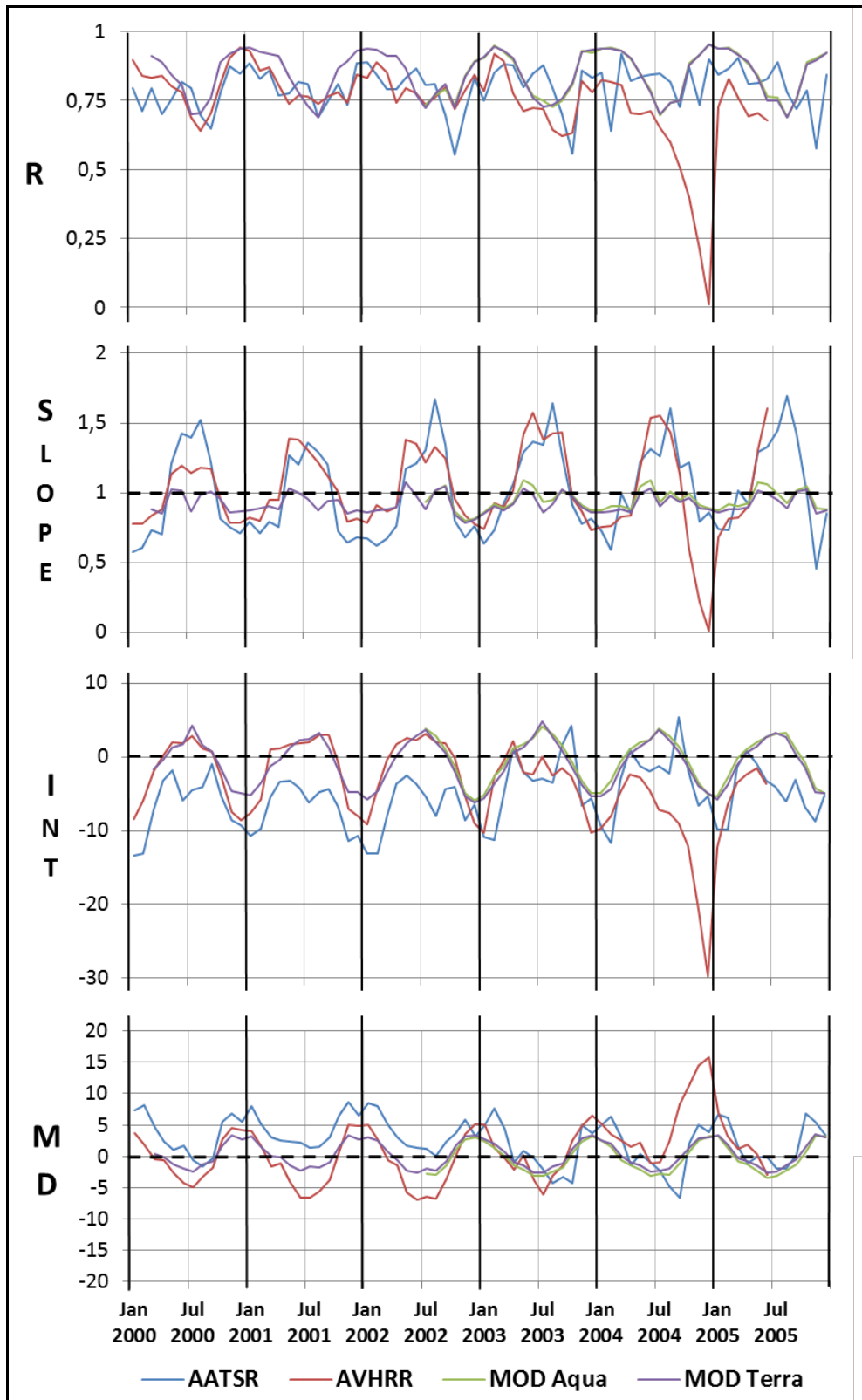


Figure 3.3: Inter-annual variability of the correlation coefficient (R), slope, intercept (INT) and mean difference (MD) for the time period of 2000 to 2005.

The statistical parameters Slope (S) and Intercept (Int) describe the dynamics of the point clouds. A slope of 1 exists when the regression line is parallel to the line of best fit (x equals y). If the intercept equals 0, the regression line and the line of best fit are congruent. In combination with the correlation coefficient, which describes the variance around the regression line, these three statistical parameters allow for a detailed interpretation comparing LST and T_{air} . AVHRR and AATSR display large variability observing the slope. During the wintertime, the products have resulting slopes of -0.5 , which is an indicator of lower dynamics during this time of the year. In the summer months, higher dynamics can be found by slopes with the value of 1.5. MODIS LST is very close to slopes of 1, which indicates low dynamics during the year. This is applicable during the summer season, while the winter season is showing fairly lower slopes of 0.8.

The statistical parameter Intercept (Int) is congruent for the AVHRR and MODIS data for the years 2000–2002. AATSR shows the same dynamics, but is fairly lower. For the year 2003 and beyond, AATSR and AVHRR have the same variability, while MODIS continues the dynamic patterns of the previous years. The decrease of the slope and intercept statistic values for the AVHRR at the end of 2004 data also becomes visible.

The relation of the correlation coefficient, the slope as well as the intercept indicates that LST was lower than the equivalent T_{air} during the wintertime for all LST products. This assumption is based on slopes, which are below 0 while showing a negative intercept with the y-axis. The summer season is characterized by slopes above a value of 1 in combination with positive intercepts, which indicates an overestimation of the positive temperature range and an underestimation of negative temperatures.

The correlation coefficient during the summer is lower in comparison to the winter month, indicating higher variances in differences between LST and T_{air} . In general, the diurnal temperature magnitude is lower in winter as in the summer season. This causes larger variations between day and night temperatures (Seidel and Free 2005; Zhang et al. 2011). It needs to be mentioned that the diurnal cycle is also influenced by different moisture conditions of the earth surface (Langer et al. 2010), as well as water vapor within the lower atmosphere (Zhang et al. 2011). Nevertheless, the findings illustrate lower dynamics between LST and T_{air} for negative temperatures. The positive temperature range, influenced by larger diurnal temperature differences, results in higher divergences between LST and T_{air} measurements.

The mean difference (MD) is an indicator describing whether remote sensing-based LST data detects warmer or colder temperature in comparison to T_{air} . If the MD is negative, the LST detects warmer temperatures than the measured T_{air} , and *vice versa* (Hachem et al. 2012). All products show a similar inter-annual variability. The MODIS product is close to 0 for the whole time period. AVHRR is showing similar bias values in comparison to MODIS. In detail, higher differences between MODIS and AVHRR are found in the summer than during the winter season, which have been recently identified by (Frey et al. 2012). AATSR detects solely colder temperatures for the first three years, which is followed by an adaption to the seasonal cycle of the other products, but still higher variations.

In general, the summer months are showing a slightly negative bias, which indicates that the land LST estimation results in warmer temperature than the measured T_{air} . For the winter season, the opposite is found. The positive mean difference values are caused by colder LST estimates than measured by the meteorological station at 2 m height. The lowest bias can be found for spring and autumn, which was also found for the other statistical parameters.

The observed variability and derivations between LST and T_{air} could be caused by the different pixel sizes of the products. MODIS and AVHRR have a spatial resolution of approx. 5 km, whereas AATSR has a resolution of about 9 km. This is changing the influence of the heterogeneity of the land surface in the LST pixel. Moreover, the LST values from AATSR are based on monthly mean. Hence, a comparison to daily values from MODIS and AVHRR is a challenging issue.

The findings are indicating low agreements between LST and T_{air} during peak temperatures events for both positive and negative ranges, which are found in summer and winter. Besides this, spring and autumn, which are characterized by moderate temperatures and diurnal differences, are showing a higher agreement and a lower bias between LST and T_{air} .

In summary, MODIS seems to show the best fit between LST and T_{air} . Data from AATSR is affected by high inter-annual variability, which reduces the consistency of the dataset. Comparing LST from AVHRR with T_{air} , inconsistencies are also found in the time series, such as the drop of in the end of 2004.

3.5.3 Comparison of Land Surface Temperature and Air Temperature for Selected Land Cover Classes

The statistical parameters comparing LST with T_{air} estimates are linked to land cover classes for each station. As it was done in Section 3.5.2, only the median is displayed in Figure 3.4. The land cover information was derived using GLC2000 global land cover classification (Bartholomé and Belward 2005). Only classes, including more than 20 stations, are shown below (Figure 3.4). The standard deviation of each data point is shown in Table 1.

The correlation coefficient R was above 0.7 for all selected classes and products, which is an indicator for a good agreement between LST and T_{air} . However, MODIS showed the highest correlation for all classes (>0.9) while AVHRR results in lower coefficients for all classes. The range between the correlation coefficient of the products is low for classes, which are dominated by forest classes. Land cover units characterized by lower vegetation and sparse vegetation were showing a higher range of R -values. From the perspective of land cover classification, forest classes were defined as stable, whereas shrub land and herbaceous vegetation classes, characterized by a mixture of plant species, were known to be heterogeneous landscape units (Herold et al. 2008). Additionally, the heterogeneity is also an effect of the large pixel size of the remote sensing-based LST products, affecting the estimation of the LST for specific land cover types (Lu et al. 2011).

The majority of the land cover classes resulted in slopes above 1, except for water bodies, as well as needle-leaved deciduous trees, one of the dominant vegetation types in Siberia. Both land cover types resulted in slope values close to 1, indicating a nearly identical dynamic between the observed and the measured variables. Slopes above 1 resulted if LST was showing higher dynamics than T_{air} . In combination with the intercept, it is possible to derive information about whether LST is warmer or colder than the corresponding T_{air} measurements.

Land cover types such as needle-leaved evergreen forest, mixed forest, mosaic forest with other natural vegetation, shrubs, herbaceous and sparse vegetation, as well as flooded areas and water bodies, resulted in slopes above 1 and negative intercepts. This indicated that LST is warmer than T_{air} in positive and negative temperature range. In detail, the remote sensing sensors detect warmer temperature in positive temperature range and colder temperatures in negative range. For all these classes, AATSR and AVHRR had a stronger influence over this circumstance.

Good agreement of LST and T_{air} was found for the needle-leaved deciduous forest, mosaic forest and other vegetation, sparse vegetation and flooded areas.

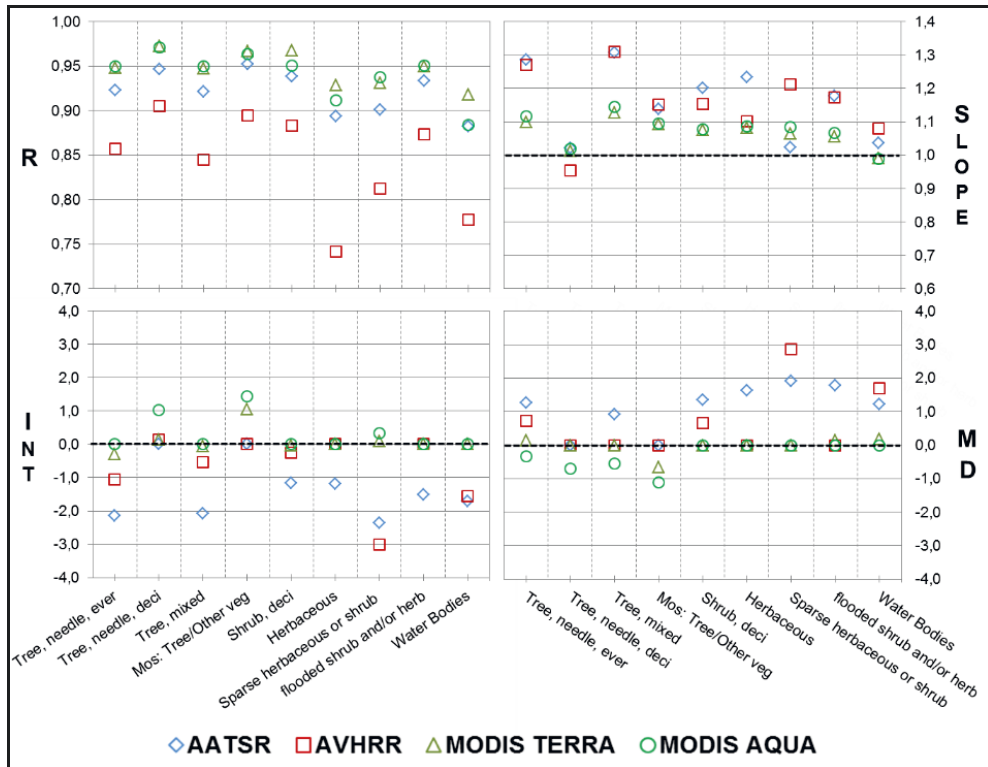


Figure 3.4: Comparing LST and T_{air} for the time period of 2000 to 2005 for selected land cover classes.

The statistical parameter mean difference is zero or positive for non-forest classes. These land cover types also showed the highest range between the products, where AATSR showed the highest values for this statistical parameter. The positive mean difference values thus indicate that LST estimates colder temperatures than those measured in the field. In comparison, the forest classes showed a negative bias, thereby indicating that warmer temperatures have been detected by the remote sensing data. In general, MODIS results in low mean difference values, which suggests the measured LST estimates to be close to the T_{air} (see Section 3.5.2). The needle-leaved deciduous forest land cover class, which is one of the major vegetation types, showed high agreement between LST and T_{air} by a low bias for all products. The standard deviations of the correlation coefficient as well for the mean difference for each product and land cover type are shown in Table 1.

Table 3.1: Standard deviation of the statistical parameters correlation coefficient and mean difference for selected land cover classes.

| Land Cover | AATSR | AVHRR | MOD Terra | MOD Aqua | \emptyset |
|------------------------|----------|-------|--------------|-------------|-------------|
| | R | | | | |
| tree, needle, ever | 0.38 | 0.29 | 0.29 | 0.33 | 0.32 |
| tree, needle, deci | 0.49 | 0.48 | 0.50 | 0.50 | 0.49 |
| tree, mixed | 0.39 | 0.37 | 0.36 | 0.38 | 0.38 |
| mos: tree/other veg | 0.46 | 0.42 | 0.43 | 0.45 | 0.44 |
| shrub, deciduous | 0.42 | 0.30 | 0.24 | 0.35 | 0.33 |
| herbaceous | 0.45 | 0.41 | 0.40 | 0.42 | 0.42 |
| sparse herb or shrub | 0.33 | 0.24 | 0.27 | 0.29 | 0.28 |
| flood shrub/herb | 0.42 | 0.38 | 0.41 | 0.44 | 0.41 |
| water bodies | 0.42 | 0.35 | 0.38 | 0.40 | 0.39 |
| Mean Difference | | | | | |
| tree, needle, ever | 2.66 | 2.70 | 1.49 | 1.78 | 2.16 |
| tree, needle, deci | 1.51 | 1.46 | 1.17 | 1.51 | 1.41 |
| tree, mixed | 1.76 | 2.86 | 0.98 | 1.19 | 1.70 |
| mos: tree/other veg | 1.44 | 1.59 | 0.82 | 1.21 | 1.26 |
| shrub, deciduous | 3.04 | 3.96 | 1.59 | 1.75 | 2.59 |
| herbaceous | 3.03 | 3.96 | 1.52 | 1.72 | 2.56 |
| sparse herb or shrub | 2.05 | 3.13 | 1.47 | 1.75 | 2.10 |
| flood shrub/herb | 2.13 | 1.87 | 1.22 | 1.13 | 1.59 |
| water bodies | 2.92 | 3.20 | 1.56 | 1.65 | 2.33 |

AATSR results had the highest standard deviation values for the correlation coefficient. For the mean difference, AVHRR had the highest standard deviation, while MODIS Terra showed the lowest. The ranges of the standard derivations for the slope, which are not shown in the table, were similar for all products and land cover classes (0.44–0.62). In contrast, the correlation coefficient, intercept (not shown in Table 3.1) and mean difference were characterized by larger derivation of the standard deviation between the products for the selected land cover classes. The forest classes showed the lowest differences for the standard deviations, particularly for the mean difference. Moreover, sparse vegetated classes, as well as herbaceous

and shrub lands, had larger discrepancies in standard deviation values. As discussed in Section 3.5.3, the heterogeneity of the land surface has a major impact on the derived agreement between LST and T_{air} . Thus, comparing LST and T_{air} for different land cover units, heterogeneous land cover units seem to be rather variable and differ from more stable classes, such as tree cover classes. Additionally, the coarse pixel size of the LST products enhances the effect of heterogeneity (Frey et al. 2012).

In general, MODIS LST estimates resulted in the lowest standard deviations when compared to AATSR and AVHRR. As it was identified in Sections 3.5.1 and 3.5.2, the LST estimates from MODIS showed the agreement with T_{air} measurements and also had the lowest magnitude variability within the observed time series. Thus, the MODIS products are defined as consistent and having the highest confidence compared to the other products.

3.5.4 Pan-Arctic Perspective of the Mean Difference for the Time Period of 2000–2005

Figure 3.5 presents the mean difference for all meteorological stations, covering the pan-arctic circle. The values of the legends are ranging from -2 °C to 2 °C (Note: higher positive and negative values might occur). The colors are ranging from orange (warmer) to blue (colder). The size of the circles provides information about the height of the mean difference. Larger circles indicate higher mean differences in both directions, positive and negative. In general, maritime-dominated regions, such as coastal areas, indicate that the remote sensing-based LST detects colder temperature conditions than those acquired by the meteorological stations. Furthermore, stations within a continental climate regime show that LST is warmer than T_{air} . This is the case for all products. Moreover, the magnitude of positive and negative peaks is higher in continental regions, which indicates higher variations within the LST retrieval. The stability of temperature conditions in maritime regions around the arctic coastline in comparison to continental areas have been highlighted by (Dutrieux et al. 2012).

Comparing the products, AATSR and AVHRR showed larger values in both directions than MODIS, indicating a higher bias especially in Europe and the western part of Russia. AATSR detects colder temperatures over large areas when compared to *in situ* measurements. AVHRR and MODIS Terra are also showing this phenomenon in these areas. However, the biases are quite low. MODIS Aqua does not reflect these findings for Europe and the western part of Russia. The mean difference values were negative, which indicates that LST is warmer than T_{air} . These findings are reasonable, since the acquisition time of MODIS Aqua is in the afternoon, which causes warmer temperatures during the day. Thus, the solar irradiance has changed during both acquisition times, causing an increase in LST. It is expected that AVHRR also shows the same bias than MODIS Aqua, since AVHRR also acquires the satellite data during the afternoon. One reason for these dissimilarities could be the orbital drift of the NOAA satellite, which causes a delay in overflying time. Since the data is acquired later during the day, the temperature conditions could already decline towards the late afternoon. Hence, the temperature conditions could be similar to those during the morning time (MODIS Terra, AATSR). In the far eastern parts of Russia, all products showed a similar bias. However, some differences in the height of mean difference values can be found when AVHRR is compared with the other products. The territories of North America are

showing the same patterns between AATSR and AVHRR. Moreover, a different distribution of the mean difference values was found for both MODIS products. In contrast to AATSR and AVHRR, the LST estimates were detected to be warmer than T_{air} (negative MD). This is already the case for the morning data (MODIS Terra) and increases during the afternoon, which can be found for the MODIS Aqua data.

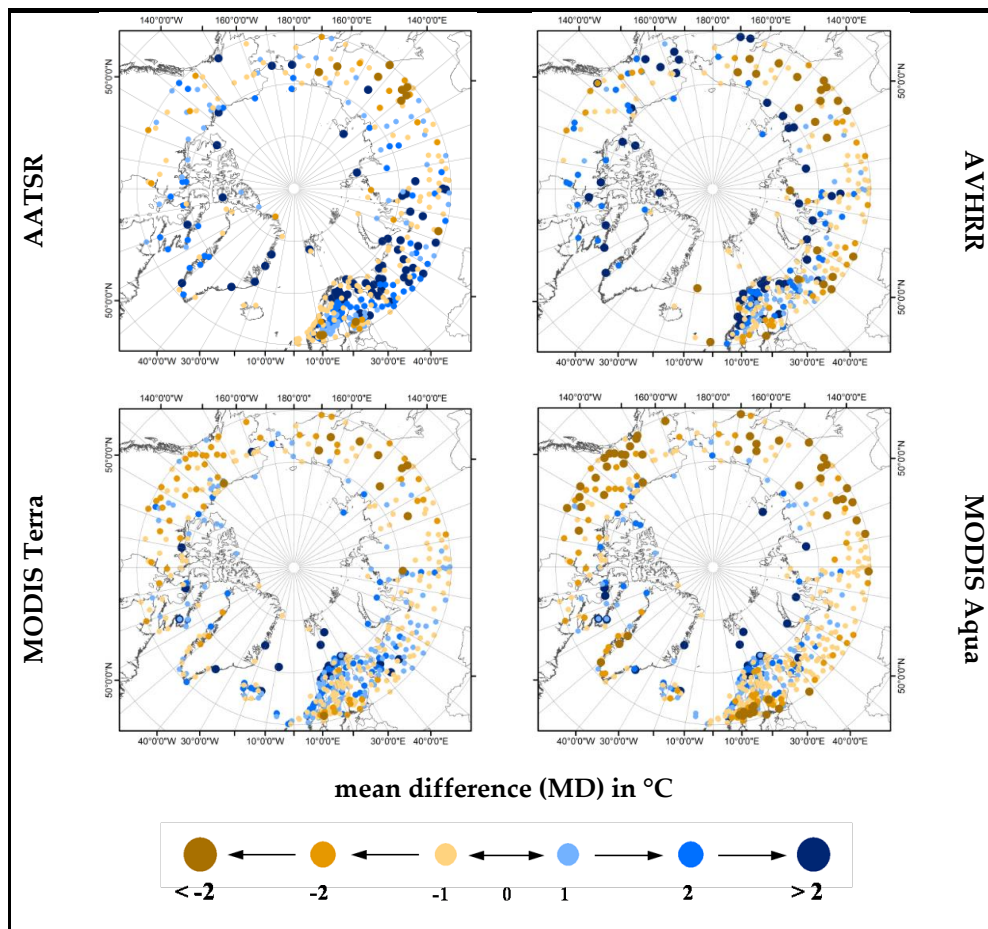


Figure 3.5: Pan-Arctic mean difference distribution.

3.6 Conclusion and Outlook

Land surface temperature information (LST) from AVHRR (Advanced Very High Resolution Radiometer), MODIS (Moderate Resolution Imaging Spectroradiometer) and (A)ATSR ((Advanced) Along Track Scanning Radiometer) were compared to *in situ* air temperature measurements (T_{air}) from the National Climate Data Center (NCDC). The quality characteristics are addressed to the climate modeling community, as well as other climate-related research groups.

MODIS LST has shown the highest agreement in comparison to T_{air} . (A)ATSR and AVHRR tend to detect warmer and colder temperatures for the positive and negative temperature ranges. MODIS is showing minor overestimations in the positive temperature range. (A)ATSR and AVHRR indicate outliers around the freezing point. These artifacts are referred to errors in the processing chain, when differentiating between clouds and snow, as well as ice-covered regions.

High agreements between LST and T_{air} can be found for the winter season with a decline towards the summer months (Frey et al. 2012). AATSR has the highest inter-annual variability. Some issues can be found for AVHRR, induced by a decrease of the agreement at the end of 2004. The bias of MODIS LST is close to zero for the entire time, whereas larger variability is found for AATSR and AVHRR.

High correlations are found for all land cover classes. The ranges of the correlation coefficient between the products are low for tree cover classes. Heterogeneous land surfaces, such as herbaceous and shrub lands, result in higher discrepancies. MODIS LST results in the lowest bias, emphasizing the quality of the product. Differences between maritime and continental areas are found. The results have shown coastal regions to be characterized by positive mean difference values, indicating LST to be colder than T_{air} . Continental areas are characterized by an overestimation of the T_{air} .

Coarse resolution LST information was compared to point measurements on the ground. The comparison between pixel and point values can bring uncertainties to the analysis caused by land cover, snow cover, topography, soil moisture and surface water, *etc.* (Hachem et al. 2012). The arctic regions are characterized by a high density of thermokarst lakes, non-vegetated surfaces (rocks), as well as snow and ice, which have a strong influence over the emission characteristics of the earth's surface. Additionally, the diurnal cycle is a challenging issue which needs to be addressed in LST studies. Investigations are carried out by combining daytime and nighttime

LST observations, which have shown the potential to reduce the discrepancies (Soliman et al. 2012).

As daily and monthly mean temperatures are compared in this study, future investigations need to be carried out addressing the actual daytime of the observed LST and measured T_{air} . Daily LST information from (A)ATSR might become available within the upcoming GlobTemperature program by ESA (European Space Agency) (Kogler et al. 2012). The Integrated Surface Database (ISD), known as Integrated Surface Hourly (ISH), provides, besides the daily mean, information about the exact time of the day of the acquired T_{air} . Thus, a direct connection between the overpass time of the satellite and the acquired T_{air} can be achieved (Smith et al. 2011). This would improve the analysis of comparing remote sensing-based LST and T_{air} measurements from meteorological stations.

3.7 Acknowledgments

The authors want to thank Olivier Arino and Simon Pinnock from ESA ESRIN Frascati (Italy) for providing the LST product from ATSR-1, ATSR-2 and AATSR and allowing the usage for this study. Additional thanks go out to Logan Pryor (University of Lethbridge, Canada) for proofreading this paper.

Chapter 4

Pan-Arctic Climate and Land Cover Trends Derived from Multi-Variate and Multi-Scale Analyses (1981 - 2012)

M. URBAN¹, M. FORKEL², J. EBERLE¹, C. HÜTTICH¹, C. SCHMULLIUS¹ & M. HEROLD³

¹Friedrich-Schiller-University Jena, Department for Earth Observation

²Max Planck Institute for Biogeochemistry, Biogeochemical Model-Data Integration Group

³Wageningen University, Centre for Geo-Information

Published in:

**Remote Sensing - Special Issue "Remote Sensing of Changing
Northern High Latitude Ecosystems"** (2014), 6, 3, 2296-2316

(Received 22 November 2013; Accepted 5 March 2014)

DOI: 10.3390/rs6032296

4.1 Abstract

Arctic ecosystems have been afflicted by vast changes in recent decades. Changes in temperature, as well as precipitation, are having an impact on snow cover, vegetation productivity and coverage, vegetation seasonality, surface albedo, and permafrost dynamics. The coupled climate-vegetation change in the arctic is thought to be a positive feedback in the Earth system, which can potentially further accelerate global warming. This study focuses on the co-occurrence of temperature, precipitation, snow cover, and vegetation greenness trends between 1981 and 2012 in the pan-arctic region based on coarse resolution climate and remote sensing data, as well as ground stations. Precipitation significantly increased during summer and fall. Temperature had the strongest increase during the winter months (twice than during the summer months). The snow water equivalent had the highest trends during the transition seasons of the year. Vegetation greenness trends are characterized by a constant increase during the vegetation-growing period. High spatial resolution remote sensing data were utilized to map structural vegetation changes between 1973 and 2012 for a selected test region in Northern Siberia. An intensification of woody vegetation cover at the taiga-tundra transition area was found. The observed co-occurrence of climatic and ecosystem changes is an example of the multi-scale feedbacks in the arctic ecosystems.

4.2 Introduction

The high latitude regions of the northern hemisphere have been undergoing significant changes during the last few decades (Grace et al. 2002; Moritz et al. 2002; Nelson 2003; Miller et al. 2010). The arctic regions are highly vulnerable to modifications in the climate system and are influenced by changes in temperature and precipitation regimes, as well as snow and vegetation dynamics. Temperature conditions in the arctic regions have never been as high, compared to the last 300 years (Moritz et al. 2002). Predictions from climate models forecast a significant increase in temperature for the upcoming decades (Kaplan and New 2006). These climate trends cause modifications in permafrost soil temperatures, snow cover dynamics, sea ice concentration, vegetation growth, and phenological dynamics (Myneni et al. 1997; Romanovsky et al. 2002; Stow et al. 2004; Post et al. 2009). Among other factors, the increasing greenhouse gas emissions from melting permafrost, as well as the recruitment of woody vegetation species to the northernmost regions are assumed to result in positive feedback mechanisms within the global climate system (Overpeck et al. 1997; Crowley 2000; Serreze et al. 2000; Beringer et al. 2001; Chapin et al. 2005; Blok et al. 2011a; Lorantý et al. 2011; Xu et al. 2013).

The arctic regions are highly vulnerable to climate modifications, therefore the monitoring of land cover changes and triggers are of major importance. Changes in snow cover and sea ice extent have been found to have a critical impact on the environmental and ecological dynamics of the Arctic (Lawrence et al. 2008; Post et al. 2009; Bhatt et al. 2013). In addition to an increase in phenological activity, woody cover vegetation types, which are representing not only trees but also shrubs, have been identified to be expanding in the tundra regions (Bokhorst et al. 2008; Blok et al. 2010; Myers-Smith et al. 2011). Recent publications have emphasized the increase of shrub cover in the pan-arctic area (Tape et al. 2006; Blok et al. 2010; Myers-Smith et al. 2011; Berner et al. 2013). These changes in vegetation dynamics and structure are indicators for present modifications in the arctic climate system (Sturm et al. 2001; Epstein et al. 2004; Bunn and Goetz 2006; Tape et al. 2006), leading to an alternation of the energy budget, the storage capacity, as well as the permafrost dynamics on regional and global scales. The transition zone between the taiga and the tundra has an extent of nearly 13,000 km around the northern hemisphere and is of high importance in climate change studies and climate modeling (Shiyatov 2003; Ranson et al. 2004). The identification and interpretation

of changes in structure, composition and dynamics of different arctic vegetation types, particularly the arctic tree line region, have been highly accentuated in scientific studies during the last decade (Moritz et al. 2002; Harsch et al. 2009; Olthof and Pouliot 2010). The potential for using different earth observation data to monitor the vegetation changes at the taiga-tundra transition zone in northern Siberia has been shown by (Ranson et al. 2004; Kharuk et al. 2006; Sun et al. 2011).

A consistent and operational monitoring of climate variables within the arctic regions is of high importance. Because information from *in situ* measurements is rare in the arctic regions, remote sensing investigation is a useful tool to observe and monitor various essential climate parameters. Long time series on coarse spatial resolution as well as high-resolution remote sensing data for climate research are of high importance. Hence, synergetic multi-scale methodologies for the identification and the analysis of climate parameters derived by Earth observation techniques are required. Various methods for the extraction of trends from time series data are available. A common approach is to calculate linear regressions on time series at different temporal resolutions. The majority of recent trend analyses are based on seasonal and yearly time steps. Trend analyses using monthly resolution time steps, which emphasize the variability within the yearly cycle, are underrepresented in climate change related studies. This paper focuses on the trend analysis from different climate and ecosystem parameters for monthly time series.

However, the changes and trend patterns are not homogeneous over the pan-arctic region. The aim of this paper is to show the variability of findings in temporal and spatial scale for the last 30 years using coarse resolution remote sensing data and additional products. Furthermore, high-resolution Earth observation data, from Landsat and RapidEye, are utilized to measure woody vegetation cover and vegetation structures for a 40-year time span for a selected test region in Siberia. The objectives are to (1) identify areas showing the most significant trends and dynamics, (2) analyze the co-occurrence of different climate and ecosystem parameters, as well as (3) show the synergetic potential of identifying effects of large-scale trend patterns to local scale change. This paper presents monthly trend calculation from maximum snow water equivalent (SWE_{max}), temperature (CRUTemp), precipitation (CRUPrecip), and NDVI (Normalized Difference Vegetation Index—NDVI3g) for the time period of 1981 to 2012. The analysis was done by identifying trend regions using a monthly temporal resolution on pan-arctic scale. A regionalization of the trend findings was done using a biodiversity map defined by the CAFF (Conservation of Arctic Flora and Fauna) (CAFF

(Conservation of Arctic Flora and Fauna) 2010). On a local scale, high-resolution remote sensing data were investigated, using Landsat (1973) and RapidEye (2012) data to monitor woody vegetation cover changes between a 40 year time span at the taiga tundra transition area of the Taymyr peninsula.

4.3 Data and Methods

4.3.1 Maximum Snow Water Equivalent—ESA DUE GlobSnow

The GlobSnow program is a Data User Element (DUE) funded by the European Space Agency (ESA). This project provides information on different snow parameters in near real time, such as snow extent (SE) and snow water equivalent (SWE) for the northern hemisphere. The SWE product covers the time period since 1978 and has a spatial resolution of 25 km in EASE-Grid projection (Equal-Area Scalable Earth Grid). The product is available in daily, weekly and monthly resolutions. In this study, SWE_{max} information has been used for the time series trend analysis. The SWE_{max} information is extracted from the weekly aggregated products (Luo et al. 2011).

The SWE product is derived using remote sensing data from the Scanning Multichannel Microwave Radiometer (SMMR), Special Sensor Microwave/Imager (SSM/I), and Advanced Microwave Scanning Radiometer (AMSR-E). SMMR onboard of the Nimbus-7 satellite covers the time period from 1978 to 1987, SSM/I from 1987 to 2002, and AMSR-E, which is onboard Aqua, since 2002. Additional information about the product development and algorithms, which were used to derive SE and SWE can be found in Pulliainen (2006). Individual studies assessing the quality of the GlobSnow data have proven the good quality of the product with error margins below 40 mm, especially for the derivation of peak accumulation information and seasonal snow dynamics (Takala et al. 2011; Hancock et al. 2013).

4.3.2 Temperature and Precipitation—Climate Research Unit (CRU)

For this study temperature and precipitation measurements from the Climate Research Unit (CRU TS3.2) were utilized (Jones and Moberg 2003). The CRUs provide global gridded information of different climate parameters, such as temperature, precipitation, vapor pressure, cloud cover, *etc.*, which were interpolated from meteorological stations. The input data, derived from climate stations, are collected from different archives coordinated by the World Meteorological Organization (WMO), the National Oceanographic and Atmospheric Administration (NOAA), as well as other data sources (New et al. 2000). In total, the CRUs are based on data from more than 4000 meteorological stations, which are distributed around the globe. However, the amount of meteorological stations in the arctic regions is limited. The interpolation between these stations might introduce

additional errors and need to be taken into account. Based on user requirements from the climatology modeling community, the spatial resolution of the products are defined with 0.5° in latitude and longitude. The time series starts in 1901. Until the early 1980s, the amount of stations has substantially increased (New et al. 1999; New et al. 2000). Temperature and precipitation information from the CRU data archive have been widely used for arctic research studies (Rawlins et al. 2006; Brown et al. 2010; Semenov and Latif 2012; Park et al. 2013).

4.3.3 NDVI3g - GIMMS

The GIMMS NDVI dataset (Global Inventory Modeling and Mapping Studies - Normalized Difference Vegetation Index) from NOAA AVHRR (National Oceanic and Atmospheric Administration—Advanced Very High Resolution Radiometer) have been used in many arctic related climate studies (Slayback et al. 2003; Stow et al. 2004; Tucker et al. 2005; Bunn and Goetz 2006; Piao et al. 2011; Wang et al. 2011; Epstein et al. 2012; Macias-Fauria et al. 2012; Urban et al. 2013b). A new version (NDVI3g) of the long-term time series of GIMMS is available. The GIMMS NDVI3g was re-calibrated for improved usage in high-latitude regions (Xu et al. 2013; Zhu et al. 2013). The dataset covers the time period from July 1981 until December 2011 with a bi-weekly temporal and 8 km spatial resolution. The NOAA satellites are affected by the orbital drift, which causes a delay in overflying time during the life-time of each satellite (Gleason et al. 2002; Julien and Sobrino 2012). These effects have been substantially reduced in the dataset (Tucker et al. 2005; Pinzon 2014).

As the high latitude regions are affected by snow and cloud cover, the GIMMS NDVI3g dataset was pre-processed for the specific requirements of this study. Pixels that were flagged as snow or cloud cover have been excluded from this analysis. The remaining bi-weekly NDVI information was aggregated to a monthly temporal resolution, which is a widely used method to reduce remaining effects from other influencing factors, e.g., haze (Holben 1986).

4.3.4 Arctic Biodiversity Assessment - CAFF

The regionalization of the trend findings was done by using an arctic boundary map produced by the Arctic Biodiversity Assessment as part of the CAFF (CAFF (Conservation of Arctic Flora and Fauna) 2010). The map consists of three classes representing the high and low-arctic areas as well as the sub-arctic regions (shown in

the supplementary material Figure App. 1). The high and low-arctic regions are extracted from the Circumpolar Arctic Vegetation Map (CAVM) by (Walker et al. 2005). The CAVM was divided into two areas. The high-arctic areas are based on the geographic distribution of subzone A, B, and C, whereas subzone D and E are represent the low-arctic regions. The southern limit of the sub-arctic regions is not defined by a specific dataset. Hence, it is representing an approximation of the area covered by the boreal forest (see appendix Figure App. 1). It is planned to update the southern border as soon as the Circumboreal Vegetation Map (CBVM) has been completed (Talbot and Meades 2011).

4.3.5 Trend Analysis

The extraction of trends from time series data can be estimated with different approaches. A common approach is to calculate linear regressions on time series at different temporal resolutions. The resulting slope coefficient from the regression line is used to describe the trend. Many studies have shown the potential of identifying trends in long-term time series (Goetz et al. 2005; de Jong et al. 2011; Piao et al. 2011; Forkel et al. 2013). We computed trends on each month separately, *i.e.*, on 30-year time series with annual resolution. The trend slope was calculated based on ordinary least square regression, while the significance of the trend was assessed by computing the Mann-Kendall trend test (Mann 1945). We used the implementation of trend analysis as described in (Forkel et al. 2013). All input data have been rescaled to a spatial resolution of 0.5°. The trends have been calculated for the entire area covering the regions north of 50-degree latitude.

4.3.6 Vegetation Structure Change Detection Using High Resolution Remote Sensing Data

The observation of vegetation structure at the taiga-tundra transition areas is done for the eastern region of the Taymyr Peninsula in Russia covering approximately 28,800 km². The entire Taymyr peninsula covers an area of about 400,000 km² along the arctic coastline of the Krasnoyarsk Krai in Siberia. The area of investigation is characterized by continental climate conditions and represents the northernmost forest regions (Jacoby et al. 2000), acting as a carbon sink (Shvidenko et al. 2013). Larch (*larix gmelinii*) is the dominant tree species. The Khatanga River represents the border between the taiga and tundra vegetation in the study region (Walker et al. 2005). Growing conditions suitable for woody vegetation are present (Kharuk et

al. 2006). The development and dynamics of the vegetation structure and properties show a strong correlation to the summer temperature trends and growing season length (Kharuk et al. 2005; MacDonald et al. 2008; Shvidenko et al. 2013). Tree ring analysis, based on (Sidorova et al. 2010), has confirmed these findings. Moreover, the start of the growing period has shown to be shifted from June to May. These observations are interpreted to be a start of vegetation activity as soon as the freezing point is reached (Sidorova et al. 2010).

High-resolution land cover change analysis was done using a Landsat MSS (Multispectral Scanner) mosaic, which consists of two images from the same day (26 July 1973) (NASA Landsat Programm 1973a; NASA Landsat Programm 1973b), and two RapidEye scenes from 22 July and 1 September 2012 (40-year time difference). The Landsat MSS images were acquired through the Global Land Cover Facility (USGS). The data were processed with the product generation system (LPGS) into a Level 1 product, where they were geometrically corrected using cubic convolution as the re-sampling method and a terrain correction (L1T) were applied to the raw imagery. The Landsat MSS images have a pixel resolution of 79 m. The RapidEye data were provided by the RapidEye Science Archive (RESA), which is coordinated by the German Aerospace Center (DLR). The images were available in NITF format (National Imagery Transmission Format) including RPCs (Rapid Positioning Capability). Atmospheric effects were reduced using ATCOR2 (Richter 1996). The final RapidEye images have a spatial resolution of 5 m.

In this study an object-oriented supervised classification approach was used. For the identification and extraction of training samples, we used historical topographic and forest maps, Google Earth high-resolution imagery, as well as NDVI profiles. The tree line reference from (Walker et al. 2005) was used as orientation to differentiate the investigation area into tundra and taiga dominated landscapes. The classification results were overlaid by a regular grid with a cell size of 25 km² (5 km by 5 km). For each cell, the percentage cover for each class was calculated. This approach allows retaining the spatial resolution of each dataset. Hence, no downscaling of the spatial high resolution from RapidEye to the Landsat scale was done.

4.4 Results and Discussion

4.4.1 Pan-Arctic Trends on Monthly Scale

The co-occurrence analysis of different climatic and ecosystem parameters suggests the multi-scale feedbacks in the arctic ecosystems (Figures 4.1 – 4.4). The monthly trends were split into positive and negative values. The combination of different trend patterns from different parameters allows identifying regions having congruent and/or divergent trends when separating between positive and negative.

The winter months (Figure 4.1) are dominated by areas showing positive trends in temperature and precipitation in addition to negative SWE_{max} trends. The majority (approx. 40%) of the identified areas are characterized by this trend combination during the time of November to January. The second largest combination during the winter season is characterized by negative temperature and SWE_{max} and positive precipitation trends. However, the increasing precipitation trends are rather low in comparison to the other parameters. Approximately 20% of the significant trend regions are labeled by this type of trend combination.

The proportions of the trend findings remain the same until the end of March, as the area of the major trend combinations increasing towards the end of the winter season. The months of seasonal transition (April and May—Figure 4.2) are dominated by areas showing a decrease in SWE_{max} . This phenomenon can be referred to the early ablation of the snow cover, which also causes the early onset of the vegetation-growing period in these regions (Serreze et al. 2000; Kattsov et al. 2005; Liston and Hiemstra 2011; Loranty et al. 2011). As the positive precipitation trends have their maxima during the summer months and very low trends in the other seasons, decreasing SWE_{max} trends are feasible at the end of the winter season.

During the summer months (Figure 4.3), regions with positive precipitation trends are covering the largest parts of the pan-arctic study area (Kattsov et al. 2005; Peili et al. 2008). The area covered by positive and negative temperature trends is evenly distributed. As expected, no SWE information is available during the summer months June, July, and August. Hence, only temperature, precipitation and the NDVI trends are calculated and therefore displayed in a separate legend. During the months covering all four parameters, areas of negative SWE_{max} and positive temperature trends show an increase in NDVI, especially at the beginning and end of the growing season, which is an indicator for an early onset of the vegetation-growing season (Hüttich et al. 2007; Delbart et al. 2008).

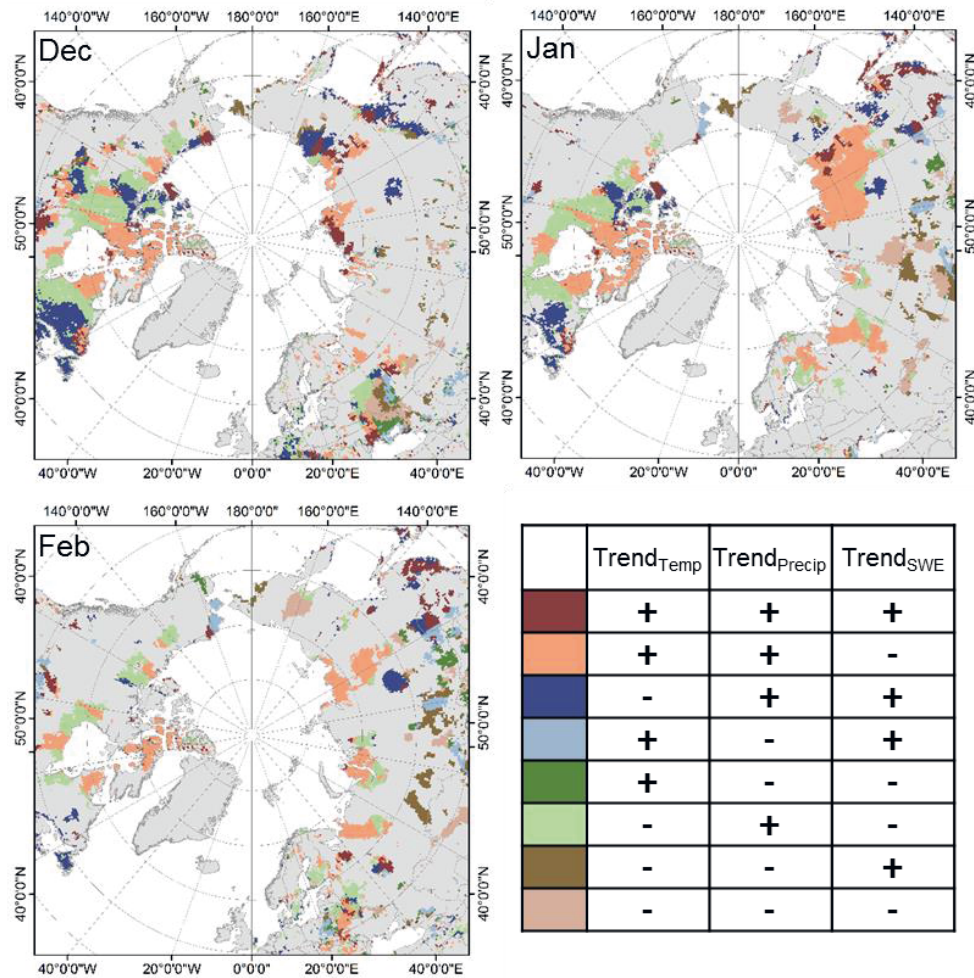


Figure 4.1: Co-occurrence of different climatic and ecosystem trends on pan-arctic scale between 1981 and 2012 (December to February). The trend findings from monthly temperatures, precipitation, SWE_{max} are combined into one information source, which includes all possible combinations of trend patterns. Only areas showing significant trends (p -value < 0.05) are displayed.

At the end of the growing season in September, only few significant trend regions can be identified, which are locally concentrated at the northernmost parts of the pan-arctic region (Figure 4.4). In October, half of the identified trend areas are characterized by rising precipitations and positive SWE_{max} areas are dominant. These trend regions are situated in the northern parts of the high latitudes. Further south, areas showing an opposite trend can be found (Räsänen 2007).

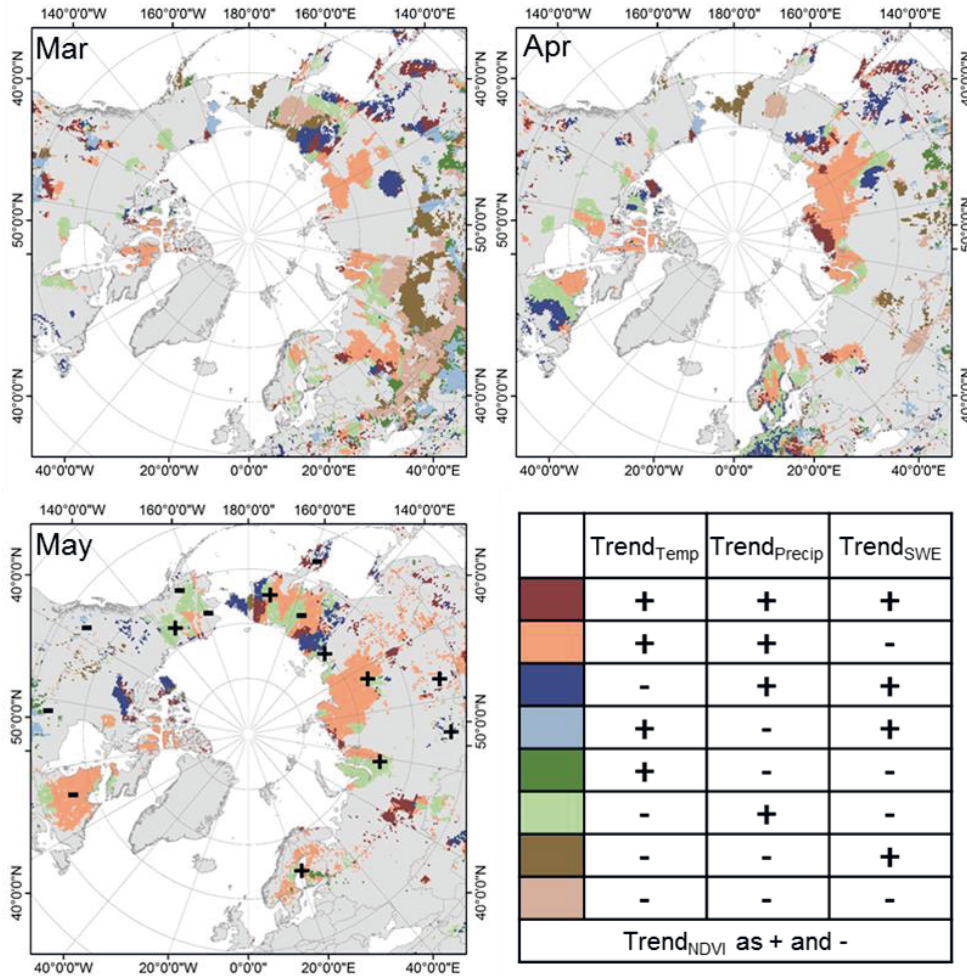


Figure 4.2: Co-occurrence of different climatic and ecosystem trends on pan-arctic scale between 1981 and 2012 (March to May) (for more explanation see Figure 4.1). The NDVI is shown via plus or minus symbols, which are indicating either positive or negative trends at the location.

The increase in early winter temperatures is changing the properties of the snow pack as well as the snow structure. Late fall (Figure 4.4) and early winter are very dynamic, with alternating rain and snow events. This is reducing the snow accumulation at the start of the winter season (Brown et al. 2010). Hence, the SWE_{max} is reduced over time and results in a negative trend. Towards the end of the winter season (Figure 4.2), the negative SWE_{max} trend areas are increasing in size caused by an earlier and faster snow melt in the late winter months (Räisänen 2007; Martin et al. 2009; Brown et al. 2010), accompanied by positive temperature trends. Moreover, the properties of the snowpack are influenced by changes in the frequencies of snow melt during the transition seasons, rain as well as the development of an ice layer on top of the snow pack (Martin et al. 2009).

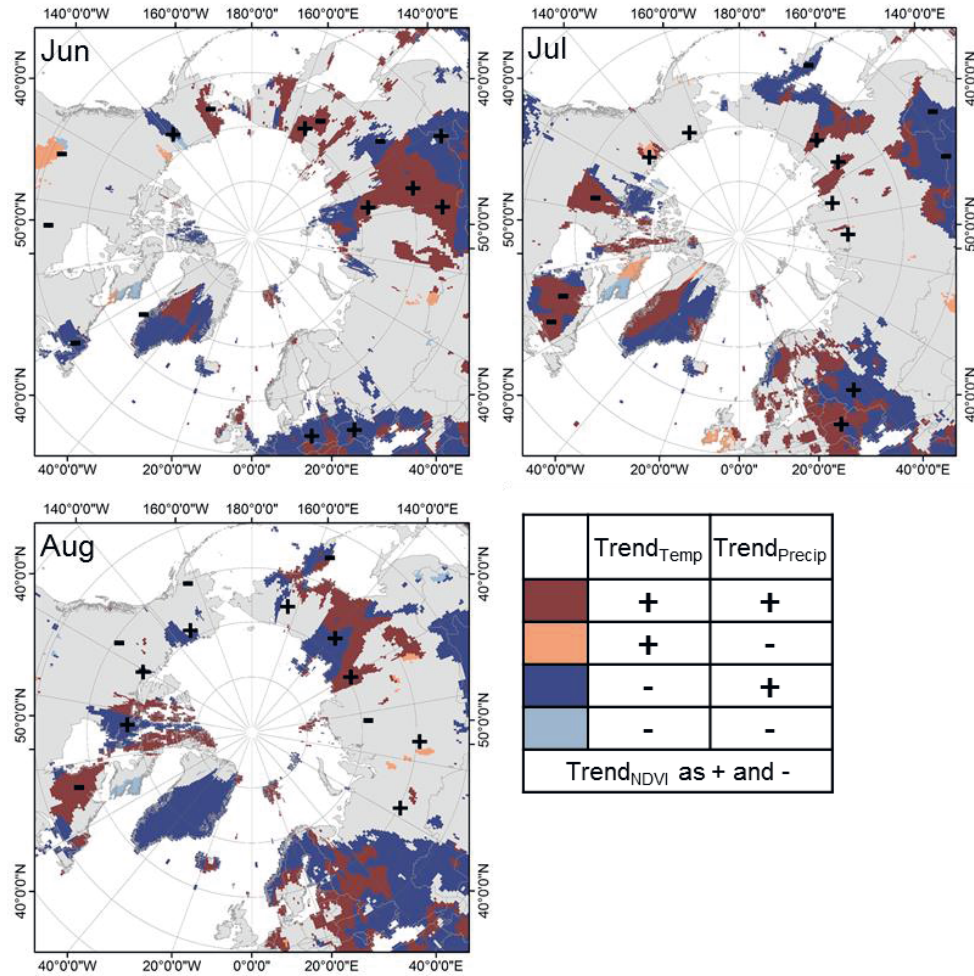


Figure 4.3: Co-occurrence of different climatic and ecosystem trends on pan-arctic scale between 1981 and 2012 (June to August). The trend findings from monthly temperatures and precipitation were combined into one information source. The NDVI is shown via plus or minus symbols, which are indicating either positive or negative trends at the location.

In Siberia, multiple trend combinations are found compared to other regions on pan-arctic scale. Especially in March, the southern parts are dominated by various multivariate trend patterns. During the winter season, Siberia is dominated by an increase in precipitation and temperature, which is accompanied by decreasing SWE_{max} trends. However, the precipitation trends are fairly low compared to the temperature trends. During the summer, larger trend areas are found compared to other regions. In September, at the end of the growing season, no significant trend areas are visible. The NDVI trends are concentrated around the northernmost parts of Siberia. Especially, the Taymyr and Yamal Peninsula show a significant increase in the NDVI signal (Eastman et al. 2013).

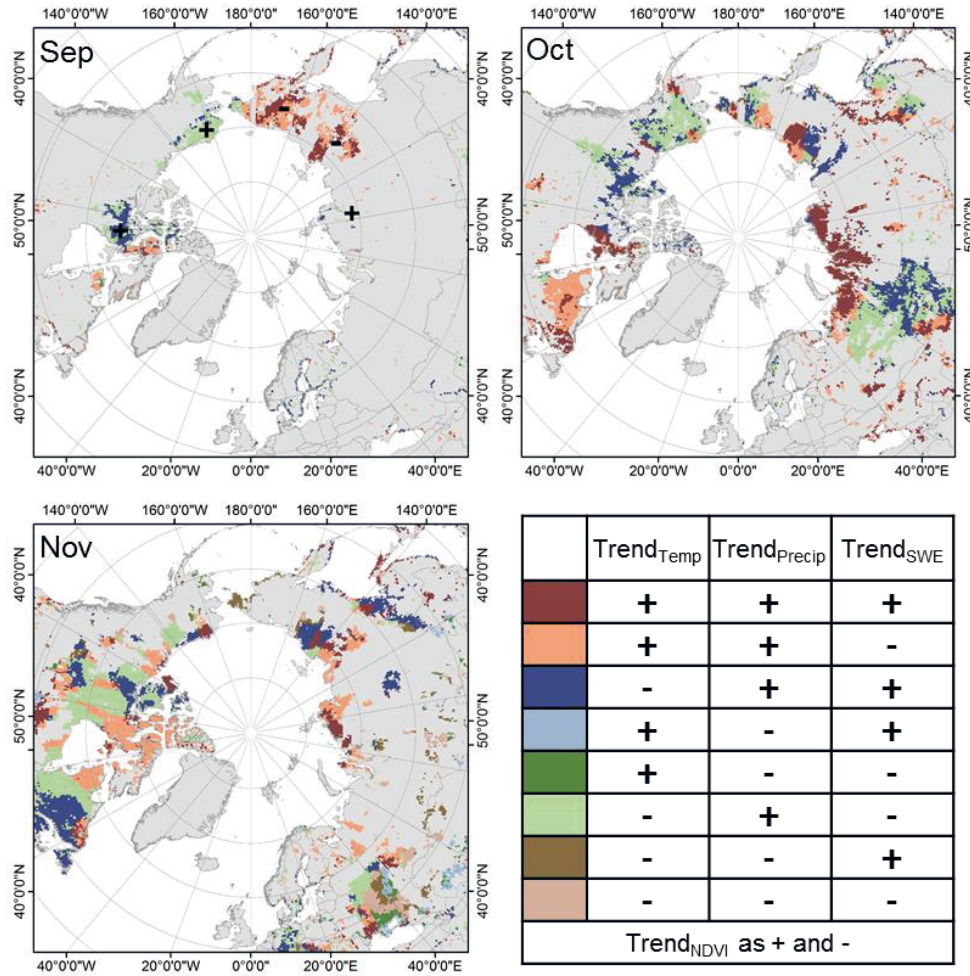


Figure 4.4: Co-occurrence of different climatic and ecosystem trends on pan-arctic scale between 1981 and 2012 (September to November) (for more explanation see Figure 4.1).

In difference to Siberia, the trends around the Bering Strait are dominated by negative precipitation with both positive and negative temperature trends, with all areas showing a negative trend in SWE_{max} . This region is dominated by ocean circulation coming from the northern pacific, the Chukchi Sea as well as the continental territories of Siberia (Callaghan et al. 2011). The most significant trends are found for the transition times after the winter and the summer season. During the summer months, only few significant trend areas are found. Nevertheless, the majority of the area is dominated by increasing trends in all observed parameters. In contrast to all other regions, the Bering Strait shows significant trend areas in September. This month is dominated by increasing precipitation. The North Slope shows some trend patterns during the transition times between the seasons, which have been also described in (Martin et al. 2009). The Hudson Bay region is showing

the same but smaller area trend patterns than the Siberian territories (Gagnon and Gough 2002).

4.4.2 Monthly Inter-Annual Trend Dynamics for Different Arctic Regions

Trend findings have been analyzed for three regions, dividing the pan-arctic regions in high-arctic, the low-arctic, as well as the sub-arctic, according to the CAFF (Conservation of Arctic Flora and Fauna) definition (shown in the supplementary material Figure App. 1). For each parameter the yearly trend dynamics are shown in Figure 4.5. The individual boxplots are showing a monthly summary of the pixel values of each sub region. In comparison to the spatial analysis, the strength, the magnitude, and the dynamics of the trends are displayed.

The SWE_{max} trends are showing high dynamics in March for high and low-arctic regions. In general, variability is increasing while the majority of the SWE_{max} trends are decreasing towards the snow free period. The low-arctic (the median $\emptyset -1.52$ mm/year) and sub-arctic ($\emptyset -1.43$ mm/year) regions are characterized by the largest decline in SWE_{max} trend for April and May. For the time period from January to May, the largest magnitudes of trend findings are found for the low-arctic, indicating these regions to be highly dynamic during the last few decades (Walker et al. 2003; Comiso et al. 2008). Low positive SWE_{max} trends are found at the beginning of the winter season. In September, the high and low-arctic regions are showing a decrease in SWE_{max} (-0.23 mm/year and -0.21 mm/year), which is two times lower than for the sub-arctic regions (-0.12 mm/year). October and November are characterized by positive values ($\emptyset 0.5$ mm/year), whereas the majority of the regions during January to March are showing a decline in the SWE_{max} values ($\emptyset -0.95$ mm/year). The decrease in these snow cover properties will have a direct influence on extreme weather events, as well as the polar jet stream (Francis and Vavrus 2012).

The intra-annual variability of the temperature trends follows a yearly cycle, which is similar for all three regions. In detail, the trend patterns are indicating that the winter season is dominated by larger positive temperature trends in comparison to the summer months. These findings have been also identified by (Semenov and Latif 2012). This is especially true for the high-arctic and low-arctic regions. Compared to Figure 4.1 to 4.4, some parts of the sub-arctic regions are indicating a decline in winter temperatures, which is conform to the analysis of (Cohen et al. 2012). Comparing the summer and winter temperature trends, the majority of the winter trends ($\emptyset 0.13$ °C/year) are nearly twice as high as during the summer

season ($\bar{\Delta} 0.07$ °C/year). The sub-arctic regions are showing a high magnitude in February, indicating declining temperature conditions (-0.10 °C/year). The same month is showing the highest temperature increase in the low-arctic region (0.28 °C/year). In general, the magnitudes of monthly temperature trends during the winter-time are showing the largest variations. The higher temperatures during the cold seasons and in the fall have a direct influence on the dynamics of the SWE_{max} in mid-winter season as well as the snow-melt in late winter (Räsänen 2007; Martin et al. 2009; Brown et al. 2010). Moreover, an increase in winter temperatures was identified to have a large impact on the vegetation structure, as damages maybe caused by the increase of these warming events (Bokhorst et al. 2009).

In comparison to the other parameters, the precipitation trends are rather low. The median values from all months in all three regions range from -0.63 mm/year to 1.03 mm/year. However, the highest dynamics are found for the sub-arctic regions. The other regions have indicated similar trend patterns. From January to May, very low precipitation trends are found for the high-arctic ($\bar{\Delta} 0.08$ mm/year) and low-arctic regions ($\bar{\Delta} 0.12$ mm/year). The median values for the sub-arctic regions are twice as high during the same time period and also show higher dynamics. The largest precipitation trend variability are found in the summer and fall seasons. Especially the sub-arctic regions are showing the highest variability. During the summer season, the high arctic region is characterized by declining precipitation trends. During the fall and the beginning of the winter season, the sub-arctic regions are showing a higher increase in precipitation with a higher range of values when compared to the other parameters.

The monthly inter-annual dynamics of the NDVI trends are rather constant for the low and sub-arctic regions. Larger variability has been found for the high arctic regions. Nevertheless, the high-arctic region is characterized by relatively low vegetation cover. The focus should be more on the dynamics of the other land cover classes, including the taiga-tundra boundary as well as the boreal forest classes. In the perspective of climate change, these regions are of higher interest, as the appearing changes have a larger feedback to the climate system. For the low and sub-arctic higher NDVI trends at the beginning of the growing season are found. This might be an indicator of a shift in the onset of the vegetation-growing period in May, as observed in (Picard et al. 2005). Towards the end of the summer season all regions are showing a decline in positive NDVI trends. Whereas the majority of NDVI trends are still positive for the low and sub-arctic, the high arctic indicates decreasing NDVI trends in October. In addition, a positive median, the sub-arctic

regions are also showing negative NDVI trends in September, which might be referred to the boreal browning, found for some regions on pan-arctic scale (Forkel et al. 2013). Nevertheless, the transition time between the summer and winter months is dominated by areas with increasing NDVI trends. This phenomenon is connected to the enlargement of the vegetation active period in the arctic (Delbart et al. 2008).

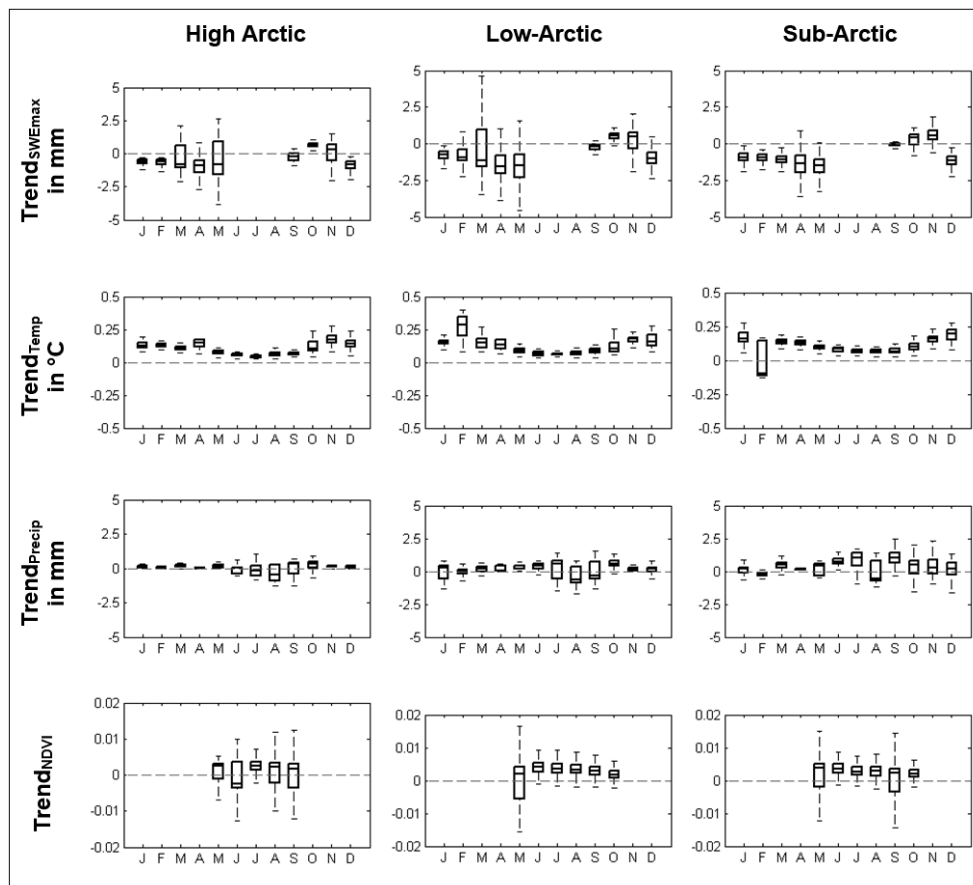


Figure 4.5: Monthly inter-annual variability of the slopes from the multivariate trend calculations. Only trends with a significance level of $p < 0.05$ are shown.

4.4.3 High-Resolution Change Mapping of the Taiga-Tundra Transition Zone in Northern Siberia

The Taymyr peninsula has been found to be one of the regions on pan-arctic scale showing the largest trends in different climate parameters during the last decades (Section 4.4.1). The trend analysis results from the previous section have shown the transition seasons to be characterized by positive temperature trends with a decline in maximum snow water equivalent for the area of the Taymyr peninsula. Daily air

temperature (T_{air}) information from meteorological stations in this region are showing an increase during the last 40 years by approximately 3 °C (Figures 4.6 and Figure App. 2), with an intensification of peak temperature events during the summer months (NCDC 2012; Eberle et al. 2013).

Based on these observations, changes in woody vegetation cover have been analyzed by using historical and recent earth observation data. Figure 4.7 shows the changes of woody vegetation cover between 1973 and 2012. The majority of the cells situated south of the tree line reference, show woody vegetation cover values of greater than 60% for both time steps. The classification result of both time steps highly agrees with the separation of tundra from forested areas defined by the tree line reference from (Walker et al. 2005). Unfortunately, the Landsat MSS mosaic is partly covered by clouds in the south. Both RapidEye images were free of clouds and ice.

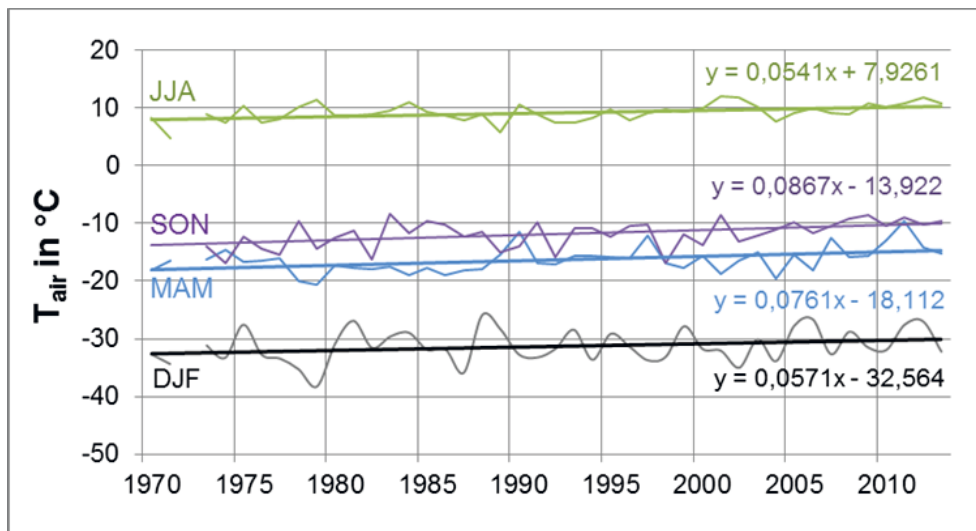


Figure 4.6: Air-Temperature time series divided by seasons (winter—DJF; spring—MAM, summer—JJA and fall—SON) of the meteorological station Khatanga at the Taymyr Peninsula (71.9°N, 102.5°E)—Additional stations are shown in the supplementary material (see appendix Figure App. 2).

When observing the transition zone between taiga and tundra, a decrease of woody vegetation cover percentage towards the northern parts becomes visible. The abrupt change at this vegetation border seems to be stronger in 1973, whereas, the recent years are characterized by a smoother transition. North of the tree line, only single patches of woody vegetation cover are detected. The patches are increasing in size, diameter and distribution in the recent years. Comparing both time steps, an

increase in woody vegetation cover between 1973 and 2012 is obvious. Particularly, the fluvial terraces of the Khatanga river system are characterized by a higher amount of woody vegetation cover percentage in the RapidEye scenes.

The appearance of contiguous patches of woody vegetation north of the tree line is indicating a substantial impact to the ecosystem. This phenomenon is stronger in the eastern region in 2012, as this RapidEye scene is also from the same month as the Landsat MSS data. The western RapidEye scene is from September. Here the increase of woody vegetation patches is not significant, which might be due to the different observation time. When comparing July and September, the vegetation activity is already reduced towards the end of the growing season, which is influencing the ability to detect changes in the classification results.

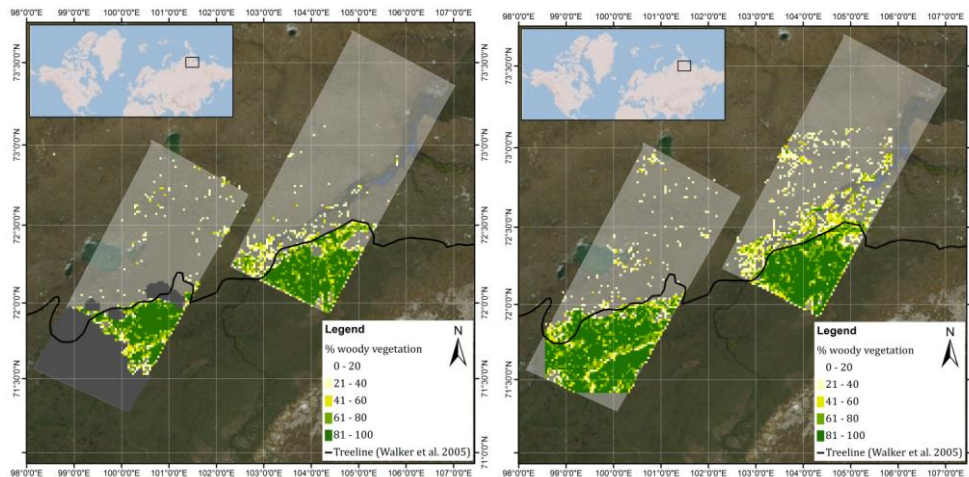


Figure 4.7: Landsat MSS and RapidEye woody vegetation cover (in % per 5 km grid cell) mapping between 1973 (Left) and 2012 (Right)—background based on World Imagery by ESRI. The tree line reference from (Walker et al. 2005) is shown in black. Cloud regions in the Landsat MSS data are shown in grey.

Land cover classification and monitoring in the arctic regions using remote sensing information is a challenging issue due to snow, ice, and cloud cover, as well as the length of growing season (Stow et al. 2004). Temporal variations between different acquisition times within the year need to be minimized when mapping land cover changes over long time periods (Stow et al. 2004). In this study the acquisition times of the high resolution remote sensing data was July, except for one RapidEye scene, which was acquired in September. Hence, we expect the comparison of the western image pair to be affected by uncertainties due to the different acquisition months. Assessing the accuracy of the individual classification results was not

possible, as information from *in situ* measurements is marginally available for the arctic regions. However, tree line change analysis using different data sources have been carried out for a small region in Ary-Mas (360 km²), indicating an encroachment of larch trees into the tundra region between 1973 and 2000 (Kharuk et al. 2006), which increases the confidence of the findings presented in this paper.

4.5 Conclusions

Multi-scale trends in the arctic ecosystems have been observed by analyzing the co-occurrence of climatic and ecosystem changes. The investigation of different spatial and temporal scales has highlighted multiple indicators of land cover changes related to climate-induced trends over the last decades. The highest temperature trends, twice as high as during the summer month, have been found during the winter season. Precipitation trends are rather low compared to the other parameters during the entire year, but considerably higher in summer and fall. The results from SWE_{max} and NDVI analysis have shown substantial modifications during the transition seasons of the year, potentially inducing and reflecting vegetation phenology shifts, resulting in longer vegetation periods and early spring green up. Particularly the low-arctic region, representing the taiga-tundra boundary, has the highest trends in all observed parameters. On a local scale, high-resolution land cover change analysis has shown increasing woody vegetation cover towards the northernmost regions dominated by tundra vegetation indicating a northwards shift of the tree line in a site of Taymyr Peninsula.

The consistent and operational monitoring of different essential climate and ecosystem parameters is of high importance for future arctic research. Earth observation data and techniques from various sources are available to retrieve spatial information and compensate the lack of ground measurements for remote areas. As the coverage of available meteorological stations in the arctic is sparse, the interpolation between the climate stations is introducing uncertainties of unknown magnitude, which needs to be taken into account. Hence, the continuity of satellite observation services for the integration of long-term time series information into climate monitoring and modeling approaches is essential. The synergetic combination of different information sources has shown the potential of identifying the co-occurrence of various climate parameters. Future studies should focus on the integration of data sources from different spatial and temporal scales. Additionally, the assessment of uncertainties and error sources is an essential issue for the investigation of remote sensing products. The identification of trend hot spot regions can create the basis (in terms of detecting regions of above average environmental change) for using observation data with higher spatial resolution. In combination with available ground measurements, the above-shown multi-scale approaches contribute to an increased confidence of land change magnitudes and ensure a high potential for future climate change and land monitoring research in the arctic.

Chapter 5

Synthesis

Concluding Remarks

Future Research Needs

5.1 Concluding Remarks

The pan-arctic ecosystems are subject to significant changes during the last decades and highly vulnerable to modifications in the global climate system. Hence, climate change studies in the high latitude region have become a major focus in Earth system science and climate related research topics. Climate models predict increasing mean temperatures for the upcoming century. Modifications in the temperature as well as precipitation regimes have a significant impact on additional climate and land surface parameters, such as snow cover, vegetation productivity and coverage, vegetation seasonality, surface albedo, greenhouse gas emissions and permafrost dynamics. These coupled climate-land ecosystem changes are thought to foster positive feedbacks in the Earth system, which potentially leads to an acceleration of warming rates on arctic and global scale.

The main goal of this thesis was to analyze spatio-temporal time series information and trends from various climate and land surface parameters on the pan-arctic scale for the last decades using Earth observation data and products as well as ground data from climate stations. The first research question (chapter 1.2) focused on the relationship between land surface temperature (LST) and albedo data from the NOAA AVHRR Polar Pathfinder dataset, which represented the longest time series product for the arctic region (1982 – 2005) (Urban et al. 2013b). The main objective of research question two was to compare different remote sensing derived LST products with air temperature (T_{air}) information from climate stations covering the pan-arctic circle. Moreover, the uncertainties of the LST products have been analyzed with respect to various land cover classes to retrieve information of the bias between LST and T_{air} for different vegetation types and land cover units (Urban et al. 2013a). The third research question focused on multi-scale trend patterns within the arctic ecosystems by analyzing the co-occurrence of climatic and ecosystem changes. The investigation of different spatial and temporal scales has highlighted multiple indicators of land cover changes related to climate-induced trends over the last decades. Beside the coarse scale trend investigation, high spatial resolution remote sensing data have been used to map woody vegetation cover in the taiga tundra transition area of the Taymyr peninsula, which was defined as hot spot region (Urban et al. 2014). The research questions of this dissertation are summarized in the following section.

A) What spatio-temporal dynamics are found in NOAA AVHRR Polar Pathfinder land surface temperature and albedo time series information for northern Siberia between 1982 and 2005?

A.1: What inter-annual temperature and albedo dynamics are found within the taiga-tundra transition zone of northern Siberia?

Land surface temperature (LST) and albedo information derived from the NOAA AVHRR Polar Pathfinder data are highly variable within in the taiga-tundra ecotone of northern Siberia for the month June and September between 1982 and 2005. The time series information has shown temporal intervals, which are characterized by significant increasing and decreasing trends of the two climate parameters during the transition seasons. The LST trends in June are fairly variable a prior to 1992. Subsequently, the time series is characterized by a slight but constant increasing trend towards the year 2005. A reduction in LST trend is found between 1991 and 1992, which might be caused by the atmospheric aerosol contamination from the Pinatubo eruption in 1991, which resulted in a global cooling effect. At the same time, the albedo increases. Strong positive albedo trends in June are found for the years 1984 - 1987 and 1992 - 1996 with peak events in 1987 and 1992.

Significant decreasing LST trends can be associated with positive albedo trends. This negative correlation is representative for snow covered regions, which are characterized by high albedo and low temperatures. June is characterized by larger albedo conditions prior to the year 1997 compared to the years afterwards. Hence, snow cover in June might decrease over time in the taiga-tundra ecotone, which is potentially the result of the enlargement of the snow free period. In general, the taiga-tundra ecotone of northern Siberia is highly dynamic during the transition season. This variability is caused by temporal changes of the onset of snow accumulation and snow melt. The variability of LST and albedo in the taiga-tundra transition area is low and uniform during the summer months.

A.2: How to characterize land surface temperature and albedo trends in northern Siberia during the summer month?

Numerous significant hot spots have been found analyzing LST and albedo trends during the summer season between 1982 and 2005. The Taymyr peninsula, the

Laptev Sea region as well as the Far East territories of Siberia are showing significant decline in albedo and increasing temperatures in June and September. As stated above, this phenomenon might be caused by the absence of snow and/or the shift of the start of the snow season. July and August are characterized by stable LST and albedo conditions with low inter-annual variability. However, a significant hot spot of rising temperatures was found in Central Siberia (Yakutia), where large fire events occurred during 2002 and 2003.

In general, the Taymyr peninsula can be identified as the most significant trend region within the transition times of the summer season. The albedo time series information potentially indicates the enlargement of the snow free period. This would further influence multiple land surface parameters, such as vegetation, permafrost conditions, hydrology, as well as their intra- and inter-annual dynamics in future climate change scenarios and further cause positive feedback mechanism within the arctic environment.

A.3: Is there a connection between land surface temperature and albedo trend findings in selected hot spot regions?

The comparison of significant LST and albedo trends have been carried out for three selected regions showing the most significant trends, e.g. the northern and southern parts of the Taymyr peninsula as well as the Yamal peninsula. In general, positive LST trends are resulting in negative albedo trends and vice versa. Especially, the transition times around the summer season show the highest trends within the hot spot regions. The summer months July and August are found to be characterized by stable conditions. The decrease in albedo and increase in LST are indicators for snow free conditions which are thought to result in an enlargement of the vegetation growing period in northern Siberia. In detail, June shows the most significant increasing land surface trends for all regions. Strong correlations between LST and albedo are found for the southern parts of Taymyr in September, whereas the other hot spot regions show moderate negative correlation.

B) What (dis-)agreements are found comparing satellite derived land surface temperature products from various sources with air temperature measurements from meteorological stations for the pan-arctic region?

B.1: What correlation can be found between remote sensing based land surface temperature and air temperature for the entire time series of each Earth observation product?

Land surface temperature estimates from different Earth observation platforms, e.g. (A)ATSR, AVHRR and MODIS were compared to T_{air} values from climate station covering the entire pan-arctic circle. High correlation between the LST products and T_{air} information has been found for the entire time series of each Earth observation product. (A)ATSR (1991 - 2009) has shown an agreement of 89 %. The AVHRR Polar Pathfinder LST data, which covers the time period between 1981 and 2005, results in an agreement of 90 %. MODIS LST, which is based on AQUA (2002 - 2012) and TERRA (2000 - 2012), has shown the highest agreement in comparison to T_{air} information (95 %).

This study compares two parameters, which are partly linked to each other. In general, LST has slightly different dynamics than T_{air} , which is caused by different physical processes. The ground temperature (LST) describes the emitted incoming solar radiation of the land surface, whereas the temperature at 2 meter height (T_{air}) is influenced by this emission including the circulations of the lower atmosphere. The evaluation and validation of remote sensing derived LST product is suffering from the lack of in-situ data, which are measured by thermal infrared sensors. To overcome this problem, T_{air} from climate stations is a useful variable to retrieve information about the uncertainties and consistencies in remote sensing derived LST products.

However, MODIS LST shows the closest fit to T_{air} measurements. The comparison of T_{air} and LST from (A)ATSR and AVHRR indicates larger uncertainties. Outliers around the freezing point (0 °C) are potentially caused by errors in the algorithms used for the separation of clouds, snow and ice. This results in detection of temperatures from top of cloud or snow and ice covered surfaces, which are colder than the corresponding T_{air} .

B.2: How to characterize the inter-annual variability between different land surface temperature products and air temperature measurements for the time period between 2000 and 2005?

To compare the products among each other, statistical parameters (correlation coefficient, slope and intercept of the regression line, mean difference) have been analyzed for the overlapping time period of all products (2000 - 2005). The correlations range between 60 % and 90 % for all products. Lowest correlations are found in summer, which are caused by turbulences in the lower atmosphere, causing a disagreement between LST and T_{air} . Furthermore, the summer months are characterized by large temperature differences within the diurnal cycle, which cause higher variations in LST products. Lower biases between LST and T_{air} are found during the winter.

(A)ATSR is showing the largest bias between LST and T_{air} . As the product has a monthly resolution, uncertainties might be induced during the temporal aggregation. AVHRR and MODIS result in lower biases when compared to T_{air} . However, AVHRR is characterized by higher amplitudes in the inter-annual cycle, which might be caused by the orbital drift of the sensor resulting in a delay in overflying time. MODIS LST has the closest fit to the 1:1 line, which indicated the high quality of the LST product. However, a slight underestimation of T_{air} is found during winter, whereas an overestimation is found in summer.

Based on the results comparing LST and T_{air} within the yearly cycle, it is possible to provide recommendations to the user community of remote sensing derived LST information, such as climate and ecosystem modelers as well as meteorologist. During fall and winter (September to February) the lowest bias are found in MODIS LST. AVHRR LST has shown the highest agreement to T_{air} during spring (March - May), whereas (A)ATSR seems to have the lowest bias between LST and T_{air} during the summer month (June - August).

B.3: What are the characteristics and differences comparing land surface temperature and air temperature for different land cover types?

The statistical parameters have been analyzed for different land cover types using the global land cover product GLC2000. Only classes with a minimum amount of 20 climate stations have been integrated into this analysis.

All land cover classes resulted in a correlation of higher than 70 %. MODIS has the highest agreement (90 %) with T_{air} for the selected land cover types. Forest classes show the lowest differences between the products. Comparing the standard deviation of the correlation coefficient of all land cover types, (A)ATSR has shown largest variations. Same has found for AVHRR for the parameter mean difference. MODIS has the lowest standard deviation for all land cover types and statistical parameter, which indicates a high quality and valuable consistency of the LST product.

In general, the standard deviation of each statistical parameter is high for low vegetation and non-vegetated areas. Forest classes, which are more homogeneous landscapes compared to the mix of different vegetation species in low vegetation classes, are resulting in lower variations. For the majority of the land cover classes, e.g. needle-leaved evergreen forest, mixed forest, mosaic forest with other natural vegetation, shrubs, herbaceous and sparse vegetation, as well as flooded areas and water bodies, LST values slightly overestimates the corresponding T_{air} .

B.4: What are the spatial patterns of the mean difference parameter on pan-arctic scale?

The spatial distribution of the mean differences has been analyzed for each climate station between 2000 and 2005. The LST products appear to detect colder temperature in comparison to the corresponding T_{air} in coastal and maritime regions. For continental regions, the remote sensing products detect warmer temperature conditions.

The LST from (A)ATSR and AVHRR showing a higher range between positive and negative mean difference values for all regions, indicating larger biases. This is very recent in Europe and the western part of Russia. (A)ATSR detects colder temperatures when compared to T_{air} . However, AVHRR and MODIS TERRA result in lower biases. The spatial patterns of MODIS AQUA are different compared to the other LST products. One reason is that AQUAs acquisition time is in the afternoon, where the temperature conditions have reached a maximum in the diurnal cycle. In North America, (A)ATSR and AVHRR are showing similar characteristics (LST colder than T_{air}). In this region MODIS seems to detect warmer temperature than the corresponding T_{air} . In general, both MODIS products are showing the lowest bias for the entire study area.

C) What information can be extracted from a multi-variate and multi-scale analyses of different land surface and climate parameters for the last decades?

C.1: Which spatio-temporal information can be derived analyzing the co-occurrences of monthly trends from Earth Observation and ground measured parameters?

The trend findings from temperature, precipitation, maximum snow water equivalent (SWE_{max}) as well as vegetation greenness (NDVI) time series information are combined to retrieve multi-variate feedbacks within the arctic ecosystem. The combination of different trends from various parameters allow identifying regions having congruent and/or divergent trend patterns.

The winter season is dominated by positive temperature and precipitation trends in combination with negative SWE_{max} . The increase in precipitation during the last three decades is very low, but significant. During the transition months (April and May), the trend findings show declining SWE_{max} , which indicates an early onset of the snowmelt and start of the growing season. The summer season is characterized by positive temperature, precipitation and NDVI trends. In October, rising precipitation trends are leading to an increase in SWE_{max} . The increase in early winter temperatures is changing the properties of the snow pack as well as the snow structure. The late fall and early winter times are very dynamic, with alternating rain and snow events, which reduces the snow accumulation during the start of the cold season. Hence, SWE_{max} is reduced over time, which is the reason for a negative trend. Towards the end of the winter season, the negative SWE_{max} trend areas are increasing in size caused by an earlier and faster snow melt in the late winter months accompanied by positive temperature trends. Additionally, the properties of the snowpack are influenced by changes in the frequencies of snow melt events during the transition season, rain as well as the development of an ice layer on top of the snow pack.

The spring season is characterized by various multi-variate trend patterns for entire northern Eurasia. The Yamal and Taymyr peninsula have been identified as hot spot regions, due to the strong significant increase in vegetation greenness during the summer season. The Bering Strait is dominated by negative precipitation trends with both positive and negative temperature trend findings as well as declining SWE_{max} . The most significant trends are found during the transition seasons. In comparison to Siberia, similar trends are found for the Hudson Bay

region and central Canada. However, the sizes of the trend patterns are found to be smaller than in northern Eurasia.

C.2: What are the monthly inter-annual trend dynamics for different arctic regions?

Inter-annual trend dynamics have been analyzed for three different arctic zone (high, low and sub-arctic), which were defined by the CAFF (see appendix Figure App. 1). High variability of the SWE_{max} are found for the low and high arctic region during spring. Towards the end of the winter season all regions showing decreasing SWE_{max} trends, largest in March and April. Low positive SWE_{max} trends are recent in all regions in winter. The intra-annual variability of temperature trends are similar for all areas. The winter season is dominated by large positive temperature trends. February is characterized by the highest temperature increase in the low-arctic region as well as the highest magnitude of trends for the sub-arctic. Precipitation trends are rather low and stable in the low and high arctic. However, substantial intra-annual variability are found in the sub-arctic. During winter, higher increasing trends as well as a higher range of trend findings can be observed in the sub-arctic. The NDVI shows a constant inter-annual variability for the low and sub-arctic. Larger variations are found for the high arctic. Moreover, significant increasing NDVI trends are found in the sub-arctic for the start of the vegetation growing period. Negative NDVI trends are found in the sub-arctic in September.

In general, largest dependencies between different climate and land surface parameter in the high latitude regions are found in spring, fall and winter. The largest variations have been identified for the parameter SWE_{max} and temperature. The co-occurrence of these parameters seems to have the largest impact to the arctic environment during the last decades. The sub-arctic regions is characterized by the largest dynamics in all parameters. The low arctic area, which includes taiga-tundra ecotone, has shown the most significant trends in SWE_{max} and temperature. Stable conditions for all parameters have been found in the northernmost parts of the arctic regions.

C.3: What vegetation structure changes at the taiga-tundra transition zone can be identified using high-resolution Earth observation data?

Based on the findings of the multi-variate trend analysis, the Taymyr peninsula has been identified as significant hot spot region. This study area has shown the highest

variability and most considerable trends of various climate related parameters. Temperature time series from climate stations at the Taymyr peninsula have shown an increase of about 3 °C during the last 40 years, with an intensification of the peak temperature events (see appendix Figure App. 2).

Multi-spectral remote sensing data with high spatial resolution have been utilized to map the percentage cover of woody vegetation between 1973 and 2012. The aim was to analyse changes in the vegetation structure within the taiga-tundra ecotone. The southern parts of the tree line are characterized by woody vegetation cover values above 60 %. The classification results are showing a decrease of woody vegetation towards the northern parts, known as the tundra. Few individual patches classified as woody vegetation cover are found inside of the tundra region.

The change analyses have shown a significant intensification of woody vegetation cover between 1973 and 2012 for the study area. This increase in vegetation cover is leading to a smoother transition between forested areas in the south and tundra vegetation in the north. Additionally, an enlargement of individual patches in the tundra dominated regions is observable.

5.2 Future Research Needs

The monitoring and observation of arctic climate and land surface parameters is a challenging issue. As the coverage of field stations from meteorological and climate measurement units in the arctic are sparse, spatial information based on interpolation techniques between the ground stations potentially introduce uncertainties of unknown magnitude. Earth observation information from various sources provides a useful tool to detect and study essential climate and land surface parameters. Remote sensing is an indirect measurement technique allowing the retrieval of spatial information over large areas and compensate for the lack of ground measurements in remote regions, which has gained high importance for climate change related research studies during the last decades. Hence, the continuity of satellite observation services, which are planned and achieved by the ESA Sentinel and NASA MODIS program, are essential and mandatory for the integration of long-term time series information into climate monitoring and modelling approaches to analyze the arctic environment (see chapter 1.6 – Table 1.1 and Table 1.2).

The knowledge about uncertainties in Earth observation data and products, which are due to numerous factors, such as atmospheric influences, land cover changes, sensor errors, etc., are of high importance in remote sensing applications. One of the research questions within this thesis focused on the estimation of uncertainties in satellite derived LST products. The comparison of LST to air temperature from climate stations is a promising method to detect error sources as well as temporal variations of the uncertainties in satellite products. The arctic environment is characterized by thermokarst lakes, non-vegetated surfaces (rocks), as well as snow and ice, which strongly influence emission properties of the earth's surface. Hence, when comparing pixel with point information, different parameters, such as land cover, snow cover, topography, soil moisture and surface water, etc., need to be considered during the analysis (Hachem et al. 2012). Variation in the uncertainties between LST and T_{air} for different land cover classes have also been addressed in this thesis. Furthermore, future validation and evaluation approaches should focus on additional influencing factors, such as soil moisture conditions, atmospheric water content and pollution, as well as topography. The comparison between LST and T_{air} was done using daytime temperature information only. Soliman et al. (2012) has shown high potential of combining day- and nighttime LST, which reduces discrepancies between LST and air temperature measurements.

Variations of temperature conditions within the diurnal cycle are of high importance for studies focusing on arctic climate change. In this respect, knowledge of the accuracies and uncertainties in both day- and nighttime satellite derived temperatures should be subject for future studies. The Integrated Surface Database (ISD) or Integrated Surface Hourly (ISH) provides information about the exact acquisition time of the ground based T_{air} . This allows a direct connection between the overpass time of the satellite and the acquired T_{air} (Smith et al. 2011). This comparison method would significantly increase the expressiveness when comparing remote sensing based LST and T_{air} measurements from climate stations.

The synergetic combination of existing and upcoming LST products is one of the main goal to provide consistent and operational global temperature information derived by various remote sensing satellites (ESA DUE GlobTemperature). Numerous LST data products are available, e.g. orbiting satellite sensors (AVHRR, (A)ATSR, MODIS), as well as geostationary satellites (SEVIRI (Spinning Enhanced Visible and Infrared Imager), GOES (Geostationary Operational Environmental Satellite), MTSAT (Multifunctional Transport Satellites)). The ILST-WG (International Land Surface Temperature working group) was recently formed, which combines the LST community (scientists, institutions, federal agencies, etc.) in order to support future LST research, sharing expertise and increasing the connection between the data providers and the user community. The utilization of LST products is of high relevance for upcoming spatial-temporal investigations, e.g. modelling, time series and trend analysis, focusing on the impact of climate change induced modifications to the arctic environment.

The main focus of this thesis was the analysis of spatial and temporal time series information and trend calculation using coarse resolution Earth observation data as well as ground information. The trends are based on linear regression analysis. With this method it is not possible to separate the time series signal into increasing and decreasing trends. However, the detection of so called breakpoints or turning points is essential for upcoming trend studies. A possibility is to decompose the original time series signal in different components. For example, Wang et al. (2011) and Piao et al. (2011) used a piece-wise linear regression model to detection turning points and trend changes. Another method is called BFAST (Breaks for Additive Seasonal and Trends) (Verbesselt et al. 2010). This algorithm removes seasonal effects and short-term deviations from the time series and estimates breakpoints in the remaining series. Recent software applications for open source programming languages, such as *greenbrown* in R, as described in Forkel et al.

(2013), are using the multiple regression approach of BFAST to derive additional spatial-temporal parameters of time series. The detection of trend breakpoints provide valuable information for the analysis of satellite time series for various applications, such as disturbances, phenological cycle, intra-annual vegetation dynamics, etc. (de Jong et al. 2012). Future developments of methods and applications extracting trends from time series information using various sources needs to be carried out and build on these investigations.

The analyses of multi-scale and multi-variate characteristics of multiple climate and land surface parameters are of high importance for future arctic research. One major issue is to focus on the combination and the co-occurrence of different trends in terms of their spatial and temporal dynamics. The synergetic combination of trend patterns from various information sources has shown high potential in the identification of the co-occurrence of essential climate parameters. Therefore, a consistent and operational monitoring of terrestrial climate and land surface parameters in conjunction with ecosystem modelling is of high importance for the analysis of recent and upcoming global climate conditions. The integration of Earth observation data and products with innovative synergistic and multi-scaling techniques, in order to monitor and detect terrestrial indicators of large and cumulative changes, have to be considered for future studies. The identification of trend hot spot regions are indicators (in terms of detecting regions of above average environmental change) for using observation data with higher spatial resolution. The needs of high spatial resolution data to map land cover changes in regions, which are showing the largest and most significant trends, have been highlighted in this thesis. Combined with available ground measurements, multi-scale approaches contribute to an increased confidence of land change magnitudes and ensure a high potential for future climate change and land monitoring research in the arctic.

The identified hot spot regions in this thesis have shown the need of future investigation focusing on the arctic vegetation transition areas, such as the taiga-tundra ecotone. The arctic tree line is an important ecotone which is sensitive to climate-related ecosystem transitions. The identification and analysis of changes in the tree line area, which is the Earth's greatest vegetation transition zone, is of high importance for future climate research, as changes in this region will have dramatic consequences for the entire arctic ecosystem and global climate by evoking positive feedback mechanisms. Until now, no operational workflow exists for the monitoring of arctic vegetation changes.

Future investigations analyzing climate change induced modifications on a pan-arctic scale will complement various international initiatives and projects. Spatial and temporal dynamics of multiple arctic climate and land surface parameters are of high importance for various initiatives in support of decision makers in international organizations (e.g. IPCC). With respect to future arctic Earth observation investigations, arctic land cover changes are of high relevance for climate related studies (e.g. ESA CCI (Climate Change Initiative), DUE Permafrost, PAGE21). Knowledge and information on structural land surface changes detected on multiple scales within vegetation transition zones using Earth observation data is mandatory for future studies. Moreover, changes in vegetation structure as well as the discrimination between non-forested and forested areas in high latitude regions is of high importance for various land surface processes, such as hydrology and permafrost distribution, as well as additional essential climate variables, such as temperature, albedo, GHG emission, etc.. The knowledge with regard to the impacts and magnitudes of arctic land surface changes is of high importance to the Copernicus Climate Change projects, such as the Climate Change Information Platform for Copernicus (CLIP-C) and Quality Assurance for Essential Climate Variables (QA4ECV).

Earth observation data and techniques are a useful tool with high potential in identifying and monitoring essential climate and land surface variables. The main focus for upcoming research questions should be addressing the estimation of uncertainties in remote sensing data, to assure long-term operational and consistent time series information. Spatial scaling between different Earth observation platforms is of high relevance in the assessment and quantification of land surface changes and ecosystem dynamics in the arctic environment.

References

- ACIA (ARCTIC CLIMATE IMPACT ASSESSMENT). 2004. Impacts of a warming arctic. Arctic Climate Impact Assessment. Cambridge University Press, Cambridge.
- AGUIRRE, M., BERRUTI, B., BEZY, J.-L., DRINKWATER, M., HELIERE, F., KLEIN, U., MAVROCORDATOS, C., AND SILVESTRIN, P. 2007. Sentinel-3 - The ocean and medium-resolution mission for GMES operational services. *ESA Bulletin - European Space Agency* 131, 24 – 29.
- ALBERTZ, J. 2009. Einführung in die Fernerkundung: Grundlagen der Interpretation von Luft-und Satellitenbildern (4th ed., p. 254). WBG (Wissenschaftliche Buchgesellschaft), Darmstadt, Germany.
- ANISIMOV, O.A., AND RENEVA, S. 2006. Permafrost and changing climate: the Russian perspective. *Ambio* 35, 4, 169–175.
- BARTHOLOMÉ, E., AND BELWARD, A.S. 2005. GLC2000: a new approach to global land cover mapping from Earth observation data. *International Journal of Remote Sensing* 26, 9, 1959–1977.
- BARTSCH, A., SABEL, D., NAEIMI, V., PAULIK, C., RESSL, C., NOTEGGER, C., MELZER, T., MISTELBAUER, T., SCHLAFFER, S., RESCHKE, J., ZWIEBACK, S., PARK, S.E., GLIRA, P., WAGNER, W., STROZZI, T., WIESMANN, A., DUGUAY, C., SOLIMAN, A., HACHEM, S., ET AL. 2012. *ESA DUE Permafrost - Final Report Version 2* (p. 143) - http://geo.tuwien.ac.at/permafrost/images/publications/ESA_DUE_Permafrost_Final_report_v2.1_standardsize.pdf (date accessed: 16/12/2013).

-
- BARTSCH, A., WIESMANN, A., STROZZI, T., SCHMULLIUS, C., HESE, S., DUGUAY, C., HEIM, B., AND SEIFERT, F.M. 2010. Implementation of a Satellite Data Based Permafrost Information System - The DUE Permafrost Project. *Proceedings of the ESA Living Planet Symposium 2010*. Bergen, Norway.
- BERINGER, J., TAPPER, N.J., MCHUGH, I., CHAPIN, F.S., LYNCH, A.H., SERREZE, M.C., AND SLATER, A. 2001. Impact of Arctic treeline on synoptic climate. *Geophysical Research Letters* 28, 22, 4247–4250.
- BERNER, L.T., BECK, P.S., BUNN, A.G., AND GOETZ, S.J. 2013. Plant response to climate change along the forest-tundra ecotone in northeastern Siberia. *Global Change Biology* 19, 11, 3449–3462.
- BHATT, U., WALKER, D., RAYNOLDS, M., BIENIEK, P., EPSTEIN, H., COMISO, J., PINZON, J., TUCKER, C., AND POLYAKOV, I. 2013. Recent Declines in Warming and Vegetation Greening Trends over Pan-Arctic Tundra. *Remote Sensing* 5, 9, 4229–4254.
- BLOK, D., HEIJMANS, M.M.P.D., SCHAEPMAN-STRUB, G., KONONOV, A. V., MAXIMOV, T.C., AND BERENDSE, F. 2010. Shrub expansion may reduce summer permafrost thaw in Siberian tundra. *Global Change Biology* 16, 4, 1296–1305.
- BLOK, D., SASS-KLAASSEN, U., SCHAEPMAN-STRUB, G., HEIJMANS, M.M.P.D., SAUREN, P., AND BERENDSE, F. 2011a. What are the main climate drivers for shrub growth in Northeastern Siberian tundra? *Biogeosciences* 8, 5, 1169–1179.
- BLOK, D., SCHAEPMAN-STRUB, G., BARTHOLOMEUS, H., HEIJMANS, M.M.P.D., MAXIMOV, T.C., AND BERENDSE, F. 2011b. The response of Arctic vegetation to the summer climate: relation between shrub cover, NDVI, surface albedo and temperature. *Environmental Research Letters* 6, 1–9.
- BOKHORST, S.F., BJERKE, J.W., BOWLES, F.W., MELILLO, J., CALLAGHAN, T. V., AND PHOENIX, G.K. 2008. Impacts of extreme winter warming in the sub-Arctic: growing season responses of dwarf shrub heathland. *Global Change Biology* 14, 2603–2612.
- BOKHORST, S.F., BJERKE, J.W., TØMMERVIK, H., CALLAGHAN, T. V., AND PHOENIX, G.K. 2009. Winter warming events damage sub-Arctic vegetation: consistent evidence from an experimental manipulation and a natural event. *Journal of Ecology* 97, 6, 1408–1415.

- BONTEMPS, S., DEFOURNY, P., BOGAERT, E. VAN, ARINO, O., KALOGIROU, V., AND PEREZ, J.R. 2011. *GLOBCOVER 2009. Products Description and Validation Report* - http://dup.esrin.esa.it/globcover/LandCover2009/GLOBCOVER2009_Validation_Report_1.0.pdf (date accessed: 14/01/2013).
- BRIFFA, K.R., OSBORN, T.J., SCHWEINGRUBER, F.H., HARRIS, I.C., JONES, P.D., SHIYATOV, S.G., AND VAGANOV, E.A. 2001. Low-frequency temperature variations from a northern tree ring density network. *Journal of Geophysical Research* 106, D3, 2929–2941.
- BROWN, R., DERKSEN, C., AND WANG, L. 2010. A multi-data set analysis of variability and change in Arctic spring snow cover extent, 1967–2008. *Journal of Geophysical Research* 115, D16111, 1–16.
- BROWN, R., AND DERKSEN, C. 2013. Is Eurasian October snow cover extent increasing? *Environmental Research Letters* 8, 1–7.
- BROWN, R., AND ROBINSON, D.A. 2011. Northern Hemisphere spring snow cover variability and change over 1922–2010 including an assessment of uncertainty. *The Cryosphere* 5, 1, 219–229.
- BUNN, A.G., AND GOETZ, S.J. 2006. Trends in Satellite-Observed Circumpolar Photosynthetic Activity from 1982 to 2003: The Influence of Seasonality, Cover Type, and Vegetation Density. *Earth Interactions* 10, 12, 1–19.
- CAFF (CONSERVATION OF ARCTIC FLORA AND FAUNA). 2010. Arctic Biodiversity Trends 2010 - Selected indicators of change. (T. Kurvits, B. Alftan, & E. Mork, eds.) (1st ed.). Akureyri, Iceland.
- CALLAGHAN, T. V., CRAWFORD, R.M.M., ERONEN, M., HOFGAARD, A., PAYETTE, S., REES, W.G., SKRE, O., SVEINBJÖRNSSON, B., VLASSOVA, T.K., AND WERKMAN, B.R. 2002. The Dynamics of the Tundra-Taiga Boundary: An Overview and Suggested Coordinated and Integrated Approach to Research. *Ambio* 12, 3–5.
- CALLAGHAN, T. V., JOHANSSON, M., BROWN, R.D., GROISMAN, P.Y., LABBA, N., RADIONOV, V., BARRY, R.G., BULYGINA, O.N., ESSERY, R.L.H., FROLOV, D.M., GOLUBEV, V.N., GRENFELL, T.C., PETRUSHINA, M.N., RAZUVAEV, V.N., ROBINSON, D.A., ROMANOV, P., SHINDELL, D., SHMAKIN, A.B., SOKRATOV, S.A., ET AL. 2011. The Changing Face of Arctic Snow Cover: A Synthesis of Observed and Projected Changes. *Ambio* 40, 17–31.

-
- CHAPIN, F.S., STURM, M., SERREZE, M.C., MCFADDEN, J.P., KEY, J.R., LLOYD, A.H., MCGUIRE, A.D., RUPP, T.S., LYNCH, A.H., SCHIMEL, J.P., BERINGER, J., CHAPMAN, W.L., EPSTEIN, H.E., EUSKIRCHEN, E.S., HINZMAN, L.D., JIA, G., PING, C.L., TAPE, K.D., THOMPSON, C.D.C., ET AL. 2005. Role of land-surface changes in arctic summer warming. *Science* 310, 5748, 657–660.
- CHRISTENSEN, T., TORBJÖRN, J., AKERMAN, H.H., MASTEPANOV, M., MALMER, N., FRIBORG, T., CRILL, P., AND SVENSSON, B.H. 2004. Thawing sub-arctic permafrost: Effects on vegetation and methane emissions. *Geophysical Research Letters* 31, L04501, 1–4.
- COHEN, J.L., FURTADO, J.C., BARLOW, M.A., ALEXEEV, V.A., AND CHERRY, J.E. 2012. Arctic warming, increasing snow cover and widespread boreal winter cooling. *Environmental Research Letters* 7, 014007, 1–8.
- COLL, C., HOOK, S.J., AND GALVE, J.M. 2009. Land Surface Temperature From the Advanced Along-Track Scanning Radiometer: Validation Over Inland Waters and Vegetated Surfaces. *IEEE Transactions on Geoscience and Remote Sensing* 47, 1, 350–360.
- COMISO, J.C., AND HALL, D.K. 2014. Climate trends in the Arctic as observed from space. *WIREs (Wiley Interdisciplinary Reviews): Climate Change* published by John Wiley & Sons, Ltd. 1–21.
- COMISO, J.C., PARKINSON, C.L., GERSTEN, R., AND STOCK, L. 2008. Accelerated decline in the Arctic sea ice cover. *Geophysical Research Letters* 35, L01703, 1–6.
- CROSSON, W.L., AL-HAMDAN, M.Z., HEMMINGS, S.N.J., AND WADE, G.M. 2012. A daily merged MODIS Aqua–Terra land surface temperature data set for the conterminous United States. *Remote Sensing of Environment* 119, 315–324.
- CROWLEY, T.J. 2000. Causes of Climate Change Over the Past 1000 Years. *Science* 289, 5477, 270–277.
- CUEVAZ-GONZALEZ, M., GERARD, F., BALTZER, H., AND RIANOS, D. 2009. Analysing forest recovery after wildfire disturbance in boreal Siberia using remotely sensed vegetation indices. *Global Change Biology* 15, 3, 561–577.
- CURRY, J.A., ROSSOW, W.B., RANDALL, D., AND SCHRAMM, J.L. 1996. Overview of Arctic cloud and radiation characteristics. *American Meteorological Society* 9, 1731–1764.

- DE JONG, R., DE BRUIN, S., DE WIT, A., SCHAEPMAN, M., AND DENT, D. 2011. Remote Sensing of Environment Analysis of monotonic greening and browning trends from global NDVI time-series. *Remote Sensing of Environment* 115, 2, 692–702.
- DE JONG, R., VERBESSELT, J., SCHAEPMAN, M., AND DE BRUIN, S. 2012. Trend changes in global greening and browning: contribution of short-term trends to longer-term change. *Global Change Biology* 18, 2, 642–655.
- DELBART, N., PICARD, G., LE TOAN, T., KERGOAT, L., QUEGAN, S., WOODWARD, I., DYE, D., AND FEDOTOVA, V. 2008. Spring phenology in boreal Eurasia over a nearly century time scale. *Global Change Biology* 14, 3, 603–614.
- DÉRY, S.J., AND BROWN, R.D. 2007. Recent Northern Hemisphere snow cover extent trends and implications for the snow-albedo feedback. *Geophysical Research Letters* 34, L22504, 1–6.
- DORMAN, J.L., AND SELLERS, P.J. 1989. A Global Climatology of Albedo, Roughness Length and Stomatal Resistance for Atmospheric General Circulation Models as Represented by the Simple Biosphere Model (SiB). *Journal of Applied Meteorology* 28, 9, 833–855.
- DUTRIEUX, L.P., BARTHOLOMEUS, H., HEROLD, M., AND VERBESSELT, J. 2012. Relationships between declining summer sea ice, increasing temperatures and changing vegetation in the Siberian Arctic tundra from MODIS time series (2000–11). *Environmental Research Letters* 7, 044028, 1–12.
- EASTMAN, J.R., SANGERMANO, F., MACHADO, E.A., ROGAN, J., AND ANYAMBA, A. 2013. Global Trends in Seasonality of Normalized Difference Vegetation Index (NDVI), 1982–2011. *Remote Sensing* 5, 10, 4799–4818.
- EBERLE, J., CLAUSNITZER, S., HÜTTICH, C., AND SCHMULLIUS, C. 2013. Multi-Source Data Processing Middleware for Land Monitoring within a Web-Based Spatial Data Infrastructure for Siberia. *ISPRS International Journal of Geo-Information* 2, 3, 553–576.
- EILERS, P.H.C., AND GOEMAN, J.J. 2004. Enhancing scatterplots with smoothed densities. *Bioinformatics* 20, 5, 623–628.
- EPSTEIN, H.E., BERINGER, J., GOULD, W. A., LLOYD, A.H., THOMPSON, C.D., CHAPIN, F.S., MICHAELSON, G.J., PING, C.L., RUPP, T.S., AND WALKER, D. A. 2004. The nature of spatial transitions in the Arctic. *Journal of Biogeography* 31, 12, 1917–1933.

-
- EPSTEIN, H.E., RAYNOLDS, M.K., WALKER, D.A., BHATT, U.S., TUCKER, C.J., AND PINZON, J.E. 2012. Dynamics of aboveground phytomass of the circumpolar Arctic tundra during the past three decades. *Environmental Research Letters* 7, 015506, 1–12.
- FLANNER, M.G., SHELL, K.M., BARLAGE, M., PEROVICH, D.K., AND TSCHUDI, M.A. 2011. Radiative forcing and albedo feedback from the Northern Hemisphere cryosphere between 1979 and 2008. *Nature Geoscience* 4, 3, 151–155.
- FORBES, B.C., FAURIA, M.M., AND ZETTERBERG, P. 2010. Russian Arctic warming and “greening” are closely tracked by tundra shrub willows. *Global Change Biology* 16, 5, 1542–1554.
- FORKEL, M., CARVALHAIS, N., VERBESSELT, J., MAHECHA, M., NEIGH, C., AND REICHSTEIN, M. 2013. Trend Change Detection in NDVI Time Series: Effects of Inter-Annual Variability and Methodology. *Remote Sensing* 5, 5, 2113–2144.
- FOWLER, C., MASLANIK, J., HARAN, T., SCAMBOS, T., KEY, J., AND EMERY, W. 2007. AVHRR Polar Pathfinder Twice-daily 5 km EASE-Grid Composites V003. National Snow and Ice Data Center, Boulder, Digital Media.
- FRANCIS, J.A., AND VAVRUS, S.J. 2012. Evidence linking Arctic amplification to extreme weather in mid-latitudes. *Geophysical Research Letters* 39, L06801, 1–6.
- FREY, C., KUENZER, C., AND DECH, S. 2012. Quantitative comparison of the operational NOAA-AVHRR LST product of DLR and the MODIS LST product. *International Journal of Remote Sensing* 33, 22, 7165–7183.
- FROHN, R.C., HINKEL, K.M., AND EISNER, W.R. 2005. Satellite remote sensing classification of thaw lakes and drained thaw lake basins on the North Slope of Alaska. *Remote Sensing of Environment* 97, 1, 116–126.
- GAGNON, A.S., AND GOUGH, W.A. 2002. Hydro-Climatic Trends in the Hudson Bay Region, Canada. *Canadian Water Resources Journal* 27, 3, 245–262.
- GCOS. 2011. Supplemental details to the satellite-based component of the “Implementation Plan for the Global Observing System for Climate in Support of the UNFCCC (2010 Update).” *GCOS - 154* - <http://www.wmo.int/pages/prog/gcos/Publications/gcos-154.pdf> (date accessed: 28/02/2013).

- GERBER, S., JOOS, F., BRÜGGER, P., STOCKER, T., MANN, M., SITCH, S., AND SCHOLZE, M. 2003. Constraining temperature variations over the last millennium by comparing simulated and observed atmospheric CO₂. *Climate Dynamics* 20, 281–299.
- GLEASON, A.C.R., PRINCE, S.D., GOETZ, S.J., AND SMALL, J. 2002. Effects of orbital drift on land surface temperature measured by AVHRR thermal sensors. *Remote Sensing of Environment* 79, 2-3, 147–165.
- GOETZ, S.J., BUNN, A.G., FISKE, G.J., HOUGHTON, R.A., AND WOODWELL, G.M. 2005. Satellite-observed photosynthetic trends across boreal North America associated with climate and fire disturbance. *Proceedings of the National Academy of Sciences of the United States of America* 102, 38, 13521–13525.
- GRACE, J., BERINGER, F., AND LASZLO, N. 2002. Impacts of Climate Change on the Tree Line. *Annals of Botany* 90, 4, 537–544.
- GREEN, R.M., AND HAY, S.I. 2002. The potential of Pathfinder AVHRR data for providing surrogate climatic variables across Africa and Europe for epidemiological applications. *Remote Sensing of Environment* 79, 2-3, 166–175.
- GUANGMENG, G., AND MEI, Z. 2004. Using MODIS Land Surface Temperature to Evaluate Forest Fire Risk of Northeast China. *IEEE Geoscience and Remote Sensing Letters* 1, 2, 98–100.
- HACHEM, S., DUGUAY, C.R., AND ALLARD, M. 2012. Comparison of MODIS-derived land surface temperatures with ground surface and air temperature measurements in continuous permafrost terrain. *The Cryosphere* 6, 1, 51–69.
- HANCOCK, S., BAXTER, R., EVANS, J., AND HUNTLEY, B. 2013. Evaluating global snow water equivalent products for testing land surface models. *Remote Sensing of Environment* 128, 107–117.
- HARSCH, M.A., AND BADER, M.Y. 2011. Treeline form - a potential key to understanding treeline dynamics. *Global Ecology and Biogeography* 20, 4, 582–596.
- HARSCH, M.A., HULME, P.E., MCGLONE, M.S., AND DUNCAN, R.P. 2009. Are treelines advancing? A global meta-analysis of treeline response to climate warming. *Ecology Letters* 12, 10, 1040–1049.

-
- HENGL, T., HEUVELINK, G.B.M., PERČEC TADIĆ, M., AND PEBESMA, E.J. 2012. Spatio-temporal prediction of daily temperatures using time-series of MODIS LST images. *Theoretical and Applied Climatology* 107, 1-2, 265–277.
- HEROLD, M., MAYAUX, P., WOODCOCK, C.E., BACCINI, A., AND SCHMULLIUS, C. 2008. Some challenges in global land cover mapping: An assessment of agreement and accuracy in existing 1 km datasets. *Remote Sensing of Environment* 112, 5, 2538–2556.
- HINZMAN, L.D., BETTEZ, N.D., BOLTON, W.R., CHAPIN, F.S., DYURGEROV, M.B., FASTIE, C.L., GRIFFITH, B., HOLLISTER, R.D., HOPE, A., HUNTINGTON, H.P., JENSEN, A.M., JIA, G.J., JORGENSEN, T., KANE, D.L., KLEIN, D.R., KOFINAS, G., LYNCH, A.H., LLOYD, A.H., MCGUIRE, A.D., ET AL. 2005. Evidence and Implications of Recent Climate Change in Northern Alaska and Other Arctic Regions. *Climatic Change* 72, 3, 251–298.
- HOLBEN, B.N. 1986. Characteristics of maximum-value composite images from temporal AVHRR data. *International Journal of Remote Sensing* 7, 11, 1417–1434.
- HOLTMEIER, F.-K., AND BROLL, G. 2007. Treeline advance - driving processes and adverse factors. *Landscape Online* 1, 1–33.
- HULLEY, G.C., AND HOOK, S.J. 2009. Intercomparison of versions 4, 4.1 and 5 of the MODIS Land Surface Temperature and Emissivity products and validation with laboratory measurements of sand samples from the Namib desert, Namibia. *Remote Sensing of Environment* 113, 6, 1313–1318.
- HÜTTICH, C., HEROLD, M., SCHMULLIUS, C., EGOROV, V., AND BARTALEV, S.A. 2007. Indicators of Northern Eurasia's land-cover change trends from SPOT-VEGETATION time-series analysis 1998-2005. *International Journal of Remote Sensing* 28, 4199–4206.
- IJIMA, Y., FEDOROV, A.N., PARK, H., SUZUKI, K., YABUKI, H., MAXIMOV, T.C., AND OHATA, T. 2009. Abrupt Increases in Soil Temperatures following Increased Precipitation in a Permafrost Region, Central Lena River Basin, Russia. *Permafrost and Periglacial Processes* 21, 1, 30–41.
- JACOBY, G.C., LOVELIUS, N. V., SHUMILOV, O.I., RASPOPOV, O.M., KARBAINOV, J.M., AND FRANK, D.C. 2000. Long-Term Temperature Trends and Tree Growth in the Taymir Region of Northern Siberia. *Quaternary Research* 53, 3, 312–318.

- JANSEN, E., OVERPECK, J., BRIFFA, K.R.K.R., DUPLESSY, J.-C.C., JOOS, F., MASSON-DELMOTTE, V., OLAGO, D., OTTO-BLIESNER, B., PELTIER, W.R.R., RAHMSTORF, S., RAMESH, R., RAYNAUD, D., RIND, D., SOLOMINA, O., VILLALBA, R., AND ZHANG, D. 2007. Paleoclimate. In: S. SOLOMON, D. QIN, M. MANNING, Z. CHEN, M. MARQUIS, K. B. AERYT, M. TIGNOR, ET AL., EDS., *Climate Change 2007: The Physical Science Basis. Contribution of Working Group I to the Fourth Assessment Report of the Intergovernmental Panel on Climate Change* (pp. 435–497). Cambridge University Press, Cambridge, United Kingdom and New York, NY, USA.
- JIN, M., AND DICKINSON, R.E. 2010. Land surface skin temperature climatology: benefitting from the strengths of satellite observations. *Environmental Research Letters* 5, 044004, 1–13.
- JONES, P., AND MOBERG, A. 2003. Hemispheric and large-scale surface air temperature variations: An extensive revision and an update to 2001. *Journal of Climate* 16, 2, 206–223.
- JONES, P., WIGLEY, T., AND KELLY, P. 1982. Variations in surface air temperatures: Part 1. Northern Hemisphere, 1881-1980. *Monthly Weather Review* 110, 2, 59–70.
- JUDAY, G.P., BARBER, V., DUFFY, P., LINDERHOLM, H., RUPP, S., SPARROW, S., VAGANOV, E., AND YARIE, J. 2005. Forests, Land Management, and Agriculture. In: C. SYMON, L. ARRIS, & B. HEA, EDS., *Arctic Climate Impact Assessment* (pp. 782–854). Cambridge University Press, Cambridge.
- JULIEN, Y., AND SOBRINO, J.A. 2009. The Yearly Land Cover Dynamics (YLCD) method: An analysis of global vegetation from NDVI and LST parameters. *Remote Sensing of Environment* 113, 2, 329–334.
- JULIEN, Y., AND SOBRINO, J.A. 2012. Correcting AVHRR Long Term Data Record V3 estimated LST from orbital drift effects. *Remote Sensing of Environment* 123, 207–219.
- JULIEN, Y., SOBRINO, J.A., AND VERHOEF, W. 2006. Changes in land surface temperatures and NDVI values over Europe between 1982 and 1999. *Remote Sensing of Environment* 103, 1, 43–55.
- KÄÄB, A. 2008. Remote sensing of permafrost-related problems and hazards. *Permafrost and Periglacial Processes* 19, 107–136.

-
- KAPLAN, J.O., AND NEW, M. 2006. Arctic climate change with a 2 °C global warming: Timing, climate patterns and vegetation change. *Climatic Change* 79, 3-4, 213–241.
- KATTSOV, V., KÄLLÉN, E., CATTLE, H., CHRISTENSEN, J., DRANGE, H., HANSENBAUER, I., JÓHANNESSEN, T., KAROL, I., RÄISÄNEN, J., AND SVENSSON, G. 2005. Future Climate Change: Modeling and Scenarios for the Arctic. In: C. SYMON, L. ARRIS, & B. HEA, EDS., *Arctic Climate Impact Assessment* (pp. 100–150). Cambridge University Press, Cambridge.
- KEY, J.R., AND SCHWEIGER, A.J. 1998. Tools for atmospheric radiative transfer: Streamer and FluxNet. *Computers & Geosciences* 24, 5, 443–451.
- KEY, R., COLLINS, J.B., FOWLER, C., AND STONE, R.S. 1997. High-Latitude Surface Temperature from Thermal Satellite Data. *Remote Sensing of Environment* 61, 302 – 309.
- KHARUK, V.I., DVINSKAYA, M.L., RANSON, K.J., AND IM, S.T. 2005. Expansion of Evergreen Conifers to the Larch-Dominated Zone and Climatic Trends. *Russian Journal of Ecology* 36, 3, 164–170.
- KHARUK, V.I., RANSON, K.J., IM, S.T., AND NAURZBAEV, M.M. 2006. Forest-tundra larch forests and climatic trends. *Russian Journal of Ecology* 37, 5, 291–298.
- KNOPF, B., KOWARSCH, M., FLACHSLAND, C., AND EDENHOFER, O. 2012. The 2 °C Target Reconsidered. In: O. EDENHOFER, J. WALLACHER, H. LOTZE-CAMPEN, M. REDER, B. KNOPF, & J. MÜLLER, EDS., *Climate Change, Justice and Sustainability - Linking Climate and Development Policy* (pp. 121–137). Springer Netherlands, Dordrecht.
- KOGLER, C., PINNOCK, S., ARINO, O., CASADIO, S., CORLETT, G., PRATA, F., AND BRAS, T. 2012. Note on the quality of the (A)ATSR land surface temperature record from 1991 to 2009. *International Journal of Remote Sensing* 33, 13, 4178–4192.
- KOZLENKO, N., AND JEFFRIES, M.O. 2000. Bathymetric mapping of shallow water in thaw lakes on the North Slope of Alaska with spaceborne imaging radar. *Arctic* 53, 3, 306–316.
- LAIDLER, G.J., AND TREITZ, P. 2003. Biophysical remote sensing of arctic environments. *Progress in Physical Geography* 27, 1, 44–68.

- LANGER, M., WESTERMANN, S., AND BOIKE, J. 2010. Spatial and temporal variations of summer surface temperatures of wet polygonal tundra in Siberia - implications for MODIS LST based permafrost monitoring. *Remote Sensing of Environment* 114, 9, 2059–2069.
- LANGER, M., WESTERMANN, S., HEIKENFELD, M., DORN, W., AND BOIKE, J. 2013. Satellite-based modeling of permafrost temperatures in a tundra lowland landscape. *Remote Sensing of Environment* 135, 2013, 12–24.
- LAWRENCE, D.M., SLATER, A.G., TOMAS, R.A., HOLLAND, M.M., AND DESER, C. 2008. Accelerated Arctic land warming and permafrost degradation during rapid sea ice loss. *Geophysical Research Letters* 35, L11506, 1–6.
- LEI, Z., YAOMING, M.A., SU, Z., AND SALAMA, S. 2010. Estimation of Land Surface Temperature over the Tibetan Plateau Using AVHRR and MODIS Data. *Advances in Atmospheric Science* 27, 5, 1110–1118.
- LISTON, G.E., AND HIEMSTRA, C. A. 2011. The Changing Cryosphere: Pan-Arctic Snow Trends (1979–2009). *Journal of Climate* 24, 21, 5691–5712.
- LIU, Y., HIYAMA, T., AND YAMAGUCHI, Y. 2006. Scaling of land surface temperature using satellite data: A case examination on ASTER and MODIS products over a heterogeneous terrain area. *Remote Sensing of Environment* 105, 2, 115–128.
- LIU, Y., KEY, J.R., LIU, Z., WANG, X., AND VAVRUS, S.J. 2012. A cloudier Arctic expected with diminishing sea ice. *Geophysical Research Letters* 39, L05705, 1–5.
- LORANTY, M.M., GOETZ, S.J., AND BECK, P.S.A. 2011. Tundra vegetation effects on pan-Arctic albedo. *Environmental Research Letters* 6, 024014, 1–7.
- LOTT, N., VOSE, R., DEL GRECO, S.A., ROSS, T., WORLEY, S., AND COMEAUX, J. 2008. The Integrated Surface Database: Partnerships and Progress. *88th AMS Annual Meeting - American Meteorological Society* (pp. 1–3). New Orleans, Louisiana.
- LU, L., VENUS, V., SKIDMORE, A., WANG, T., AND LUO, G. 2011. Estimating land-surface temperature under clouds using MSG/SEVIRI observations. *International Journal of Applied Earth Observation and Geoinformation* 13, 2, 265–276.

-
- LUCHT, W., PRENTICE, I., MYNENI, R., SITCH, S., FRIEDLINGSTEIN, P., CRAMER, W., BOUSQUET, P., BUERMANN, W., AND SMITH, B. 2002. Climatic control of the high-latitude vegetation greening trend and Pinatubo effect. *Science* 296, 5573, 1687–1689.
- LUOJUS, K., PULLIAINEN, J., TAKALA, M., LEMMETYINEN, J., KANGWA, M., SOLBERG, R., NAGLER, T., ROTT, H., DERKSEN, C., METSÄMÄKI, S., AND WIESMANN, A. 2011. *GlobSnow - Global Snow Monitoring for Climate Research. ESA Study Contract Report* (pp. 1–16) - https://www.wmo.int/pages/prog/www/OSY/Meetings/GCW-IM1/Doc11.1_GlobSnow_Report.pdf (date accessed: 17/10/2013).
- MACDONALD, G.M., KREMENETSKI, K. V, AND BEILMAN, D.W. 2008. Climate change and the northern Russian treeline zone. *Philosophical transactions of the Royal Society of London. Series B.* 363, 2285–2299.
- MACIAS-FAURIA, M., FORBES, B.C., ZETTERBERG, P.P., AND KUMPULA, T. 2012. Eurasian Arctic greening reveals teleconnections and the potential for structurally novel ecosystems. *Nature Climate Change Letters* 2, 613–618.
- MANN, H.B. 1945. Nonparametric tests against trend. *Econometrica* 13, 3, 245–259.
- MANN, M.E., ZHANG, Z., HUGHES, M.K., BRADLEY, R.S., MILLER, S.K., RUTHERFORD, S., AND NI, F. 2008. Proxy-based reconstructions of hemispheric and global surface temperature variations over the past two millennia. *Proceedings of the National Academy of Sciences of the United States of America* 105, 36, 13252–13257.
- MANN, M.E., ZHANG, Z., RUTHERFORD, S., BRADLEY, R.S., HUGHES, M.K., SHINDELL, D., AMMANN, C., FALUVEGI, G., AND NI, F. 2009. Global signatures and dynamical origins of the Little Ice Age and Medieval Climate Anomaly. *Science* 326, 1256–1260.
- MARTIN, P.D., JENKINS, J.L., ADAMS, F.J., JORGENSON, M.T., MATZ, A.C., PAYER, D.C., REYNOLDS, P.E., TIDWELL, A.C., ZELENAK, J.R., JEFFREY, F., ADAMS, J., AND JORGENSON, T. 2009. *Wildlife Response to Environmental Arctic Change: Predicting Future Habitats of Arctic Alaska. Report of the Wildlife Response to Environmental Arctic Change (WildREACH): Predicting Future Habitats of Arctic Alaska Workshop. U.S. Fish and Wildlife Service* (p. 138). Fairbanks, Alaska - http://www.fws.gov/alaska/pdf/wildreach_workshop_report.pdf (date accessed: 25/09/2013).

- MASLANIK, J., FOWLER, I.C., KEY, J., SCAMBOS, T., SON, T., AND EMERYL, W. 1997. AVHRR-based Polar Pathfinder products for Modeling applications. *Annals of Glaciology* 25, 388–392.
- MCBEAN, G., ALEKSEEV, G., CHEN, D., FØRLAND, E., FYFE, J., GROISMAN, P.Y., KING, R., MELLING, H., VOSE, R., AND WHITFIELD, P.H. 2005. Arctic Climate: Past and Present. In: C. SYMON, L. ARRIS, & B. HEA, EDS., *Arctic Climate Impact Assessment* (pp. 22–55). Cambridge University Press, Cambridge, Cambridge.
- MENNE, M., WILLIAMS, C.N., AND VOSE, R.S. 2009. The U.S. Historical Climatology Network Monthly Temperature Data, Version 2. *Bulletin of the American Meteorological Society* 90, 7, 993–1007.
- MILANKOVIĆ, M. 1941. Canon of insolation and the ice-age problem (Special Pu.). Koniglich Serbische Akademie, Belgrade.
- MILDREXLER, D.J., ZHAO, M., AND RUNNING, S.W. 2011. A global comparison between station air temperatures and MODIS land surface temperatures reveals the cooling role of forests. *Journal of Geophysical Research* 116, G03025, 1–15.
- MILLER, G.H., BRIGHAM-GRETTE, J., ALLEY, R.B., ANDERSON, L., BAUCH, H.A., DOUGLAS, M.S.V., EDWARDS, M.E., ELIAS, S.A., FINNEY, B.P., FITZPATRICK, J.J., FUNDER, S.V., HERBERT, T.D., HINZMAN, L.D., KAUFMAN, D.S., MACDONALD, G.M., POLYAK, L., ROBOCK, A., SERREZE, M.C., SMOL, J.P., ET AL. 2010. Temperature and precipitation history of the Arctic. *Quaternary Science Reviews* 29, 15-16, 1679–1715.
- MORITZ, R.E., BITZ, C.M., AND STEIG, E.J. 2002. Dynamics of recent climate change in the Arctic. *Science* 297, 5586, 1497–1502.
- MUTLOW, C., BAILEY, P., BIRKS, A., AND SMITH, D. 1999. *ATSR-1/2 User Guide - A short guide to the ATSR-1 and -2 instruments and their data products* (pp. 1–29) - http://neodc.nerc.ac.uk/docs/atrs/atrs_user_guide_rev_3.pdf (date accessed: 03/03/2013).
- MYERS-SMITH, I.H., FORBES, B.C., WILMKING, M., HALLINGER, M., LANTZ, T., BLOK, D., TAPE, K.D., MACIAS-FAURIA, M., SASS-KLAASSEN, U., LÉVESQUE, E., BOUDREAU, S., ROPARS, P., HERMANUTZ, L., TRANT, A., COLLIER, L.S., WEIJERS, S., ROZEMA, J., RAYBACK, S.A., SCHMIDT, N.M., ET AL. 2011. Shrub expansion in tundra ecosystems: dynamics, impacts and research priorities. *Environmental Research Letters* 6, 045509, 1 – 15.

-
- MYNENI, R.B., KEELING, C.D., TUCKER, C.J., ASRAR, G., AND NEMANI, R.R. 1997. Increased plant growth in the northern high latitudes from 1981 to 1991. *Nature* 386, 698–702.
- NAITO, A.T., AND CAIRNS, D.M. 2011. Relationships between Arctic shrub dynamics and topographically derived hydrologic characteristics. *Environmental Research Letters* 6, 045506, 1–8.
- NASA. 2013. NASA - GISS Surface Temperature Analysis - Station Data - http://data.giss.nasa.gov/gistemp/station_data/ (date accessed: 23/04/2014).
- NASA LANDSAT PROGRAMM. 1973a. Landsat MSS scene LM11590081973207 AAA05, 07/26/1973. USGS, Sioux Falls.
- NASA LANDSAT PROGRAMM. 1973b. Landsat MSS scene LM11590091973207 AAA05, 07/26/1973. USGS, Sioux Falls.
- NAURZBAEV, M.M., VAGANOV, E. A., SIDOROVA, O. V., AND SCHWEINGRUBER, F.H. 2002. Summer temperatures in eastern Taimyr inferred from a 2427-year late-Holocene tree-ring chronology and earlier floating series. *The Holocene* 12, 6, 727–736.
- NCDC. 2012. Global Surface Summary of the Day - GSOD. National Climatic Data Center, Asheville, NC - <http://gcmd.gsfc.nasa.gov/KeywordSearch/Metadata.do?Portal=gosic&MetadataType=0&MetadataView=Brief&KeywordPath=&EntryId=gov.noaa.ncdc.C00516> (date accessed: 21/01/2013).
- NELSON, F.E. 2003. (Un)frozen in Time. *Science* 299, 1673–1675.
- NEW, M., HULME, M., AND JONES, P. 1999. Representing twentieth-century space-time climate variability. Part I: Development of a 1961-90 mean monthly terrestrial climatology. *Journal of Climate* 12, 829–856.
- NEW, M., HULME, M., AND JONES, P. 2000. Representing twentieth-century space-time climate variability. Part II: Development of 1901-96 monthly grids of terrestrial surface climate. *Journal of Climate* 13, 2217–2238.
- OLTHOF, I., AND POULIOT, D. 2010. Treeline vegetation composition and change in Canada's western Subarctic from AVHRR and canopy reflectance modeling. *Remote Sensing of Environment* 114, 4, 805–815.

- OLTHOF, I.A.N., POULIOT, D., LATIFOVIC, R., AND CHEN, W. 2008. Recent (1986 – 2006) Vegetation-Specific NDVI Trends in Northern Canada from Satellite Data. *Arctic* 61, 4, 381–394.
- OUAIDRARI, H., GOWARD, S.N., CZAJKOWSKI, K.P., SOBRINO, J.A., AND VERMOTE, E. 2002. Land surface temperature estimation from AVHRR thermal infrared measurements. An assessment for the AVHRR Land Pathfinder II data set. *Remote Sensing of Environment* 81, 114–128.
- OVERPECK, J., HUGHEN, K., HARDY, D., BRADLEY, R., CASE, R., DOUGLAS, M., FINNEY, B., GAJEWSKI, K., JACOBY, G., JENNINGS, A., LAMOUREUX, S., LASCA, A., MACDONALD, G., MOORE, J., RETELLE, M., SMITH, S., WOLFE, A., AND ZIELINSKI, G. 1997. Arctic Environmental Change of the Last Four Centuries. *Science* 278, 5341, 1251–1256.
- PARK, H., WALSH, J.E., KIM, Y., NAKAI, T., AND OHATA, T. 2013. The role of declining Arctic sea ice in recent decreasing terrestrial Arctic snow depths. *Polar Science* 7, 2, 174–187.
- PEARSON, R.G., PHILLIPS, S.J., LORANTY, M.M., BECK, P.S.A., DAMOULAS, T., KNIGHT, S.J., AND GOETZ, S.J. 2013. Shifts in Arctic vegetation and associated feedbacks under climate change. *Nature Climate Change* 3, 7, 673–677.
- PEDDLE, D.R., FRANKLIN, S., AND FRANKLIN, E. 1993. Classification of permafrost active layer depth from remotely sensed and topographic evidence. *Remote Sensing of Environment* 44, 1, 67–80.
- PEDELTY, J., DEVADIGA, S., MASUOKA, E., BROWN, M., PINZON, J., TUCKER, C., ROY, D., JU, J., SCHAAF, C., LIU, J., VERMOTE, E., PRINCE, S., NAGOL, J., JUSTICE, C., PRIVETTE, J., AND PINHEIRO, A. 2007. Generating a long-term land data record from the AVHRR and MODIS instruments. *IEEE International Geoscience and Remote Sensing Symposium (IGARSS)* (pp. 1021–1025). IGARSS 2007. IEEE International, Barcelona, Spain.
- PEILI, W., HAAK, H., WOOD, R., JUNGCLAUS, J., AND FUREVIK, T. 2008. Simulating the Terms in the Arctic Hydrological Budget. In: R. DICKSON, J. MEINCKE, & P. RHINES, EDS., *Arctic-Subarctic Ocean Fluxes: Defining the Role of the Northern Seas in Climate* (pp. 363–384). Springer.
- PETIT, J., JOUZEL, J., RAYNAUD, D., BARKOV, N., BASILE, I., CHAPPELLAZ, J., RITZ, C., DELMOTTE, M., LEGRAND, M., LORIUS, C., AND PE, L. 1999. Climate and atmospheric history of the past 420,000 years from the Vostok ice core, Antarctica. *Nature* 399, 429–436.

-
- PIAO, S., WANG, X., CIAIS, P., ZHU, B., WANG, T., AND LIU, J. 2011. Changes in satellite-derived vegetation growth trend in temperate and boreal Eurasia from 1982 to 2006. *Global Change Biology* 17, 10, 3228–3239.
- PICARD, G., QUEGAN, S., DELBART, N., LOMAS, M.R., TOAN, T. LE, AND WOODWARD, I. 2005. Bud-burst modelling in Siberia and its impact on quantifying the carbon budget. *Global Change Biology* 11, 2005, 2164–2176.
- PINNOCK, S. 2012. *GlobTemperature - Satellite Land Surface Temperature User Consultation*. Edinburgh, Scotland - http://due.esrin.esa.int/files/m287/GlobT_001_Pinnock.pdf (date accessed: 04/02/2013).
- PINZON, J.E. 2014. Revisiting error, precision and uncertainty in NDVI AVHRR data: development of a consistent NDVI3g time series. *Remote Sensing* in preparation.
- PINZON, J.E., BROWN, M.E., AND TUCKER, C.J. 2005. EMD Correction of Orbital Drift Artifacts in Satellite Data Stream. In: N. HUANG & S. SHEN, EDS., *Hilbert-Huang Transform: Introduction and Applications*. (Interdisci., pp. 167–186). World Scientific Publishing Co. Pte. Ltd., Singapore.
- PISTONE, K., EISENMAN, I., AND RAMANATHAN, V. 2014. Observational determination of albedo decrease caused by vanishing Arctic sea ice. *Proceedings of the National Academy of Sciences of the United States of America* 111, 9, 3322–3326.
- PITHAN, F., AND MAURITSEN, T. 2014. Arctic amplification dominated by temperature feedbacks in contemporary climate models. *Nature Geoscience* 7, 181–184.
- POST, E., FORCHHAMMER, M.C., BRET-HARTE, M.S., CALLAGHAN, T. V., CHRISTENSEN, T.R., ELBERLING, B.B., FOX, A.D., GILG, O., HIK, D.S., HØYE, T.T., IMS, R.A., JEPPESEN, E., KLEIN, D.R., MADSEN, J., MCGUIRE, A.D.D., RYSGAARD, S., SCHINDLER, D.E., STIRLING, I., TAMSTORF, M.P., ET AL. 2009. Ecological dynamics across the Arctic associated with recent climate change. *Science* 325, 5946, 1355–1358.
- PRATA, F. 2002. *Land Surface Temperature Measurement from Space: AATSR Algorithm Theoretical Basis Document* (pp. 1–34). Aspendale, Australia - https://earth.esa.int/pub/ESA_DOC/LST-ATBD.pdf (date accessed: 16/01/2013).

- PULLIAINEN, J. 2006. Mapping of snow water equivalent and snow depth in boreal and sub-arctic zones by assimilating space-borne microwave radiometer data and ground-based observations. *Remote Sensing of Environment* 101, 2, 257–269.
- QU, X., AND HALL, A. 2007. What Controls the Strength of Snow-Albedo Feedback? *Journal of Climate* 20, 15, 3971–3981.
- RÄISÄNEN, J. 2007. Warmer climate: less or more snow? *Climate Dynamics* 30, 2-3, 307–319.
- RANSON, K.J., SUN, G., KHARUK, V.I., AND KOVACS, K. 2004. Assessing tundra–taiga boundary with multi-sensor satellite data. *Remote Sensing of Environment* 93, 3, 283–295.
- RAWLINS, M. A., WILLMOTT, C.J., SHIKLOMANOV, A., LINDER, E., FROLKING, S., LAMMERS, R.B., AND VÖRÖSMARTY, C.J. 2006. Evaluation of trends in derived snowfall and rainfall across Eurasia and linkages with discharge to the Arctic Ocean. *Geophysical Research Letters* 33, L07403, 1–4.
- RAYNOLDS, M.K., COMISO, J.C., WALKER, D.A., AND VERBYLA, D. 2008. Relationship between satellite-derived land surface temperatures, arctic vegetation types, and NDVI. *Remote Sensing of Environment* 112, 4, 1884–1894.
- RICHTER, R. 1996. A spatially adaptive fast atmospheric correction algorithm. *International Journal of Remote Sensing* 17, 6, 1201–1214.
- ROMANOVSKY, V., BURGESS, M., SMITH, S., YOSHIKAWA, K., AND BROWN, J. 2002. Permafrost temperature records: Indicators of climate change. *EOS, Transactions, American Geophysical Union* 83, 50, 589–594.
- ROPARS, P., AND BOUDREAU, S. 2012. Shrub expansion at the forest–tundra ecotone: spatial heterogeneity linked to local topography. *Environmental Research Letters* 7, 015501, 1–9.
- RUFF, T.W., AND NEELIN, J.D. 2012. Long tails in regional surface temperature probability distributions with implications for extremes under global warming. *Geophysical Research Letters* 39, L04704, 1–6.
- SAVTCHENKO, A., OUZOUNOV, D., AHMAD, S., ACKER, J., LEPTOUKH, G., KOZIANA, J., AND NICKLESS, D. 2004. Terra and Aqua MODIS products available from NASA GES DAAC. *Advances in Space Research* 34, 4, 710–714.

-
- SCARPINO, M., AND CARDACI, M. 2009. *Envisat-1 product specifications, Vol. 7, AATSR products specifications, ESA Doc Ref. PO-RS-MDA-GS-2009* (pp. 1–42) - http://envisat.esa.int/pub/ESA_DOC/ENVISAT/Vol07_Aatsr_4A.pdf (date accessed: 11/12/2012).
- SCHUUR, E.A.G., BOCKHEIM, J., CANADELL, J.G., EUSKIRCHEN, E., CHRISTOPHER, B., GORYACHKIN, S. V., HAGEMANN, S., KUHR, P., LAFLEUR, P.M., LEE, H., NELSON, F.E., RINKE, A., ROMANOVSKY, V.E., SHIKLOMANOV, N., TARNOCAI, C., VENEVSKY, S., VOGEL, J.G., ZIMOV, S.A., FIELD, C.B., ET AL. 2008. Vulnerability of Permafrost Carbon to Climate Change: Implications for the Global Carbon Cycle. *BioScience* 58, 8, 701–714.
- SEIDEL, D.J., AND FREE, M. 2005. Diurnal cycle of upper-air temperature estimated from radiosondes. *Journal of Geophysical Research* 110, D09102, 1–13.
- SEMENOV, V., AND LATIF, M. 2012. The early twentieth century warming and winter Arctic sea ice. *The Cryosphere* 6, 1231–1237.
- SERREZE, M.C., WALSH, J.E., OSTERKAMP, T.E., DYURGEROV, M., ROMANOVSKY, V.E., OECHEL, W.C., MORISON, J., ZHANG, T., AND BARRY, R.G. 2000. Observational evidence of recent change in the northern high-latitude environment. *Climatic Change* 46, 159–207.
- SHIYATOV, S. 2003. Rates of change in the upper treeline ecotone in the Polar Ural Mountains. *Pages News* 11, 1, 8–10.
- SHVIDENKO, A.Z., GUSTAFSON, E., MCGUIRE, A.D., KHARUK, V.I., SCHEPASCHENKO, D.G., SHUGART, H.H., TCHEBAKOVA, N.M., VYGODSKAYA, N.N., ONUCHIN, A.A., HAYES, D.J., MCCALLUM, I., MAKSYUTOV, S., MUKHORTOVA, L. V, SOJA, A.J., BELELLI-MARCHESINI, L., KURBATOVA, J.A., OLTCHEV, A. V, PARFENOVA, E.I., AND SHUMAN, J.K. 2013. Terrestrial Ecosystems and Their Change. In: P. Y. GROISMAN & G. GUTMAN, EDS., *Regional Environmental Changes in Siberia and Their Global Consequences*, Springer Environmental Science and Engineering (pp. 171–249). Springer Netherlands, Dordrecht.
- SIDOROVA, O. V., SIEGWOLF, R.T.W., SAURER, M., NAURZBAEV, M.M., SHASHKIN, A. V., AND VAGANOV, E.A. 2010. Spatial patterns of climatic changes in the Eurasian north reflected in Siberian larch tree-ring parameters and stable isotopes. *Global Change Biology* 16, 3, 1003–1018.

- SIMMS, É., AND WARD, H. 2013. Multisensor NDVI-Based Monitoring of the Tundra-Taiga Interface (Mealy Mountains, Labrador, Canada). *Remote Sensing* 5, 3, 1066–1090.
- SLAYBACK, D.A., PINZON, J.E., LOS, O.S., AND TUCKER, C.J. 2003. Northern hemisphere photosynthetic trends 1982–1999. *Global Change Biology* 9, 1, 1–15.
- SMITH, A., LOTT, N., AND VOSE, R. 2011. The Integrated Surface Database: Recent Developments and Partnerships. *Bulletin of the American Meteorological Society* 92, 6, 704–708.
- SMITH, D.L. 2006. *Update on AATSR Visible Channel Long Term Trends -Doc No PO-TN-RAL-AT-0552* (pp. 1–11) - https://earth.esa.int/pub/ESA_DOC/ENVISAT/AATSR/Visible_Channel_Update_TN-0552.pdf (date accessed 11/12/2012).
- SNYDER, W.C., AND WAN, Z. 1998. BRDF models to predict spectral reflectance and emissivity in the thermal infrared. *IEEE Transactions on Geoscience and Remote Sensing* 36, 1, 214–225.
- SOBRINO, J.A., JULIEN, Y., AND MORALES, L. 2006. Multitemporal analysis of PAL images for the study of land cover dynamics in South America. *Global and Planetary Change* 51, 3-4, 172–180.
- SOLIMAN, A., DUGUAY, C., SAUNDERS, W., AND HACHEM, S. 2012. Pan-Arctic Land Surface Temperature from MODIS and AATSR: Product Development and Intercomparison. *Remote Sensing* 4, 12, 3833–3856.
- STOW, D.A., HOPE, A., MCGUIRE, D., VERBYLA, D., GAMON, J., HUENNRICH, F., HOUSTON, S., RACINE, C., STURM, M., TAPE, K., HINZMAN, L., YOSHIKAWA, K., TWEEDIE, C., NOYLE, B., SILAPASWAN, C., DOUGLAS, D., GRIFFITH, B., JIA, G., EPSTEIN, H., ET AL. 2004. Remote sensing of vegetation and land-cover change in Arctic Tundra Ecosystems. *Remote Sensing of Environment* 89, 3, 281–308.
- STROEVE, J.C., BOX, J.E., FOWLER, C., HARAN, T., AND KEY, J. 2001. Intercomparison between In Situ and AVHRR Polar Pathfinder-Derived Surface Albedo over Greenland. *Remote Sensing of Environment* 75, 3, 360–374.

-
- STURM, M., DOUGLAS, T., RACINE, C., AND LISTON, G. 2005. Changing snow and shrub conditions affect albedo with global implications. *Journal of Geophysical Research* 110, G01004, 1–13.
- STURM, M., RACINE, C.H., TAPE, K.D., CRONIN, T.W., CALDWELL, R.L., AND MARSHALL, J. 2001. Increasing shrub abundance in the Arctic. *Nature* 411, 546–547.
- SUN, G., RANSON, K., AND KHARUK, V. 2011. Characterization and monitoring of tundra-taiga transition zone with multi-sensor satellite data. In: G. GUTMAN & A. REISELL, EDS., *Eurasian Arctic Land Cover and Land Use in a Changing Climate* (pp. 53–77).
- SUN, J., AND MAHRT, L. 1995. Determination of Surface Fluxes from the Surface Radiative Temperature. *Journal of the Atmospheric Sciences* 52, 8, 1096–1106.
- SUTTLES, J.T., GREEN, R.N., MINNIS, P., SMITH, G.L., STAYLOR, W.F., WIELICKI, B.A., WAKER, I.J., YOUNG, D.F., TAYLOR, V.R., AND STOWE, L.L. 1988. *Angular Radiation Models for Earth-Atmosphere System. Volume 1: Shortwave Radiation* (pp. 1–144). NASA Reference Publication 1184 - <http://ntrs.nasa.gov/archive/nasa/casi.ntrs.nasa.gov/19880018293.pdf> (date accessed 06/12/2013).
- TAKALA, M., LUOJUS, K., PULLIAINEN, J., DERKSEN, C., LEMMETYINEN, J., KÄRNÄ, J.-P., KOSKINEN, J., AND BOJKOV, B. 2011. Estimating northern hemisphere snow water equivalent for climate research through assimilation of space-borne radiometer data and ground-based measurements. *Remote Sensing of Environment* 115, 12, 3517–3529.
- TALBOT, S., AND MEADES, W. 2011. *Circumboreal Vegetation Map (CBVM) Mapping the Concept Paper. CAFF Strategy Series Report No. 3. CAFF Flora Group (CFG)*. CAFF International Secretariat, Akureyri, Iceland - http://www.caff.is/publications/doc_download/50-circumboreal-vegetation-map-cbvm-mapping-the-green-halo-concept-paper (date accessed: 24/10/2013).
- TAPE, K., STURM, M., AND RACINE, C. 2006. The evidence for shrub expansion in northern Alaska and the Pan-Arctic. *Global Change Biology* 12, 4, 686–702.
- TUCKER, C.J., PINZON, J.E., AND BROWN, M.E. 2004. *Global Inventory Modeling and Mapping Studies*. Global Land Cover Facility, University of Maryland, College Park, Maryland - <http://glcf.umd.edu/data/gimms/> (date accessed: 06/03/2013).

- TUCKER, C.J., PINZON, J.E., BROWN, M.E., SLAYBACK, D.A., PAK, E.W., SLAYBACK, A., MAHONEY, R., VERMOTE, E.F., EL SALEOUS, N., AND SALEOUS, N.E.L. 2005. An extended AVHRR 8-km NDVI dataset compatible with MODIS and SPOT vegetation NDVI data. *International Journal of Remote Sensing* 26, 20, 4485–4498.
- TUCKER, C.J., SLAYBACK, D.A., PINZON, J.E., LOS, S.O., MYNENI, R.B., TAYLOR, M.G., AND RANGA, S.O.L. 2001. Higher northern latitude normalized difference vegetation index and growing season trends from 1982 to 1999. *International Journal of Biometeorology* 45, 4, 184–190.
- URBAN, M., EBERLE, J., HÜTTICH, C., SCHMULLIUS, C., AND HEROLD, M. 2013a. Comparison of Satellite-Derived Land Surface Temperature and Air Temperature from Meteorological Stations on the Pan-Arctic Scale. *Remote Sensing* 5, 5, 2348–2367.
- URBAN, M., FORKEL, M., EBERLE, J., HÜTTICH, C., SCHMULLIUS, C., AND HEROLD, M. 2014. Pan-Arctic Climate and Land Cover Trends Derived from Multi-Variate and Multi-Scale Analyses (1981–2012). *Remote Sensing - Special Issue Remote Sensing of Changing Northern High Latitude Ecosystems* 6, 3, 2296–2316.
- URBAN, M., FORKEL, M., SCHMULLIUS, C., HESE, S., HÜTTICH, C., AND HEROLD, M. 2013b. Identification of land surface temperature and albedo trends in AVHRR Pathfinder data from 1982 to 2005 for northern Siberia. *International Journal of Remote Sensing* 34, 12, 4491–4507.
- VARDAVAS, I., AND TAYLOR, F. 2012. Radiation and Climate: Atmospheric energy budget from satellite remote sensing (p. 512). Oxford University Press, Oxford.
- VAUGHAN, D.G., COMISO, J.C., ALLISON, I., CARRASCO, J., KASER, G., KWOK, R., MOTE, P., MURRAY, T., PAUL, F., REN, J., RIGNOT, E., SOLOMINA, O., STEFFEN, K., AND ZHANG, T. 2013. Observations: Cryosphere. In: T. F. STOCKER, D. QIN, G.-K. PLATTNER, M. TIGNOR, S. K. ALLEN, J. BOSCHUNG, A. NAUELS, ET AL., EDS., *Climate Change 2013: The Physical Science Basis. Contribution of Working Group I to the Fifth Assessment Report of the Intergovernmental Panel on Climate Change*. Cambridge University Press, Cambridge, Cambridge, United Kingdom and New York, NY, USA.
- VERBESSELT, J., HYNDMAN, R., NEWNHAM, G., AND CULVENOR, D. 2010. Detecting trend and seasonal changes in satellite image time series. *Remote Sensing of Environment* 114, 1, 106–115.

-
- WALKER, D.A., JIA, G.J., EPSTEIN, H.E., RAYNOLDS, M.K., CHAPIN III, F.S., COPASS, C., HINZMAN, L.D., KNUDSON, J., MAIER, H., MICHAELSON, G.J., NELSON, F., PING, C.L., ROMANOVSKY, V.E., AND SHIKLOMANOV, N. 2003. Vegetation-soil-thaw-depth relationships along a low-arctic bioclimate gradient, Alaska: synthesis of information from the ATLAS studies. *Permafrost and Periglacial Processes* 14, 2, 103–123.
- WALKER, D.A., RAYNOLDS, M.K., DANIELS, F.J.A., EINARSSON, E., ELVEBAKK, A., GOULD, W.A., KATENIN, A.E., KHOLOD, S.S., MARKON, C.J., MELNIKOV, E.S., MOSKALENKO, N.G., TALBOT, S.S., YURTSEV, B.A., DONALD, A., MARTHA, K., FRED, J.A., WILLIAM, A., ADRIAN, E., SERGEI, S., ET AL. 2005. The Circumpolar Arctic vegetation map. *Journal of Vegetation Science* 16, 3, 267–282.
- WAN, Z., AND LI, Z. 1997. A Physics-Based Algorithm for Retrieving Land-Surface Emissivity and Temperature from EOS / MODIS Data. *IEEE Transactions on Geoscience and Remote Sensing* 35, 4, 980–996.
- WANG, X., AND KEY, J.R. 2005. Arctic surface, cloud, and radiation properties based on the AVHRR Polar Pathfinder dataset. Part II: Recent trends. *American Meteorological Society* 18, 14, 2575–2593.
- WANG, X., PIAO, S., CIAIS, P., LI, J., FRIEDLINGSTEIN, P., KOVEN, C., AND CHEN, A. 2011. Spring temperature change and its implication in the change of vegetation growth in North America from 1982 to 2006. *Proceedings of the National Academy of Sciences of the United States of America* 108, 4, 1240–1245.
- WHITE, M., BEURS, D., KIRSTEN, M., DIDAN, K., INOUE, D.W., RICHARDSON, A.D., JENSEN, O.P., O'KEEFE, J., ZHANG, G., NEMANI, R.R., VAN LEEUWEN, W.J.D., BROWN, J.F., DE WIT, A., SCHAEPMAN, M., LIN, X., DETTINGER, M., BAILEY, A.S., KIMBALL, J., SCHWARTZ, M.D., ET AL. 2009. Intercomparison, interpretation, and assessment of spring phenology in North America estimated from remote sensing for 1982–2006. *Global Change Biology* 15, 10, 2335–2359.
- WINTON, M. 2006. Amplified Arctic climate change: What does surface albedo feedback have to do with it? *Geophysical Research Letters* 33, L03701, 1–4.
- WOODHOUSE, I. 2006. Introduction to microwave remote sensing (p. 370). CRC Press - Taylor and Francis, Boca Raton, FL, USA.

- XU, L., MYNENI, R.B., CHAPIN III, F.S., CALLAGHAN, T. V., PINZON, J.E., TUCKER, C.J., ZHU, Z., BI, J., CIAIS, P., TØMMERVIK, H., EUSKIRCHEN, E.S., FORBES, B.C., PIAO, S.L., ANDERSON, B.T., GANGULY, S., NEMANI, R.R., GOETZ, S.J., BECK, P.S. A., BUNN, A. G., ET AL. 2013. Temperature and vegetation seasonality diminishment over northern lands. *Nature Climate Change Letters* 3, 581–586.
- YI, S., WOO, M., AND ARAIN, M.A. 2007. Impacts of peat and vegetation on permafrost degradation under climate warming. *Geophysical Research Letters* 34, 16, 1–5.
- ZENG, H., JIA, G., AND EPSTEIN, H. 2011. Recent changes in phenology over the northern high latitudes detected from multi-satellite data. *Environmental Research Letters* 6, 045508, 1–11.
- ZENG, N. 2003. Glacial-interglacial atmospheric CO₂ change - The glacial burial hypothesis. *Advances in Atmospheric Sciences* 20, 5, 677–693.
- ZHANG, W., HUANG, Y., YU, Y., AND SUN, W. 2011. Empirical models for estimating daily maximum , minimum and mean air temperatures with MODIS land surface temperatures. *International Journal of Remote Sensing* 32, 24, 9415–9440.
- ZHU, Z., BI, J., PAN, Y., GANGULY, S., ANAV, A., XU, L., SAMANTA, A., PIAO, S., NEMANI, R., AND MYNENI, R. 2013. Global Data Sets of Vegetation Leaf Area Index (LAI)3g and Fraction of Photosynthetically Active Radiation (FPAR)3g Derived from Global Inventory Modeling and Mapping Studies Normalized Difference Vegetation Index (NDVI3g) for the Period 1981 to 2011. *Remote Sensing* 5, 2, 927–948.

Appendix



Figure App.1: Arctic boundary map produced by the Arctic Biodiversity Assessment as part of the CAFF (Conservation of Arctic Flora and Fauna), 2010.

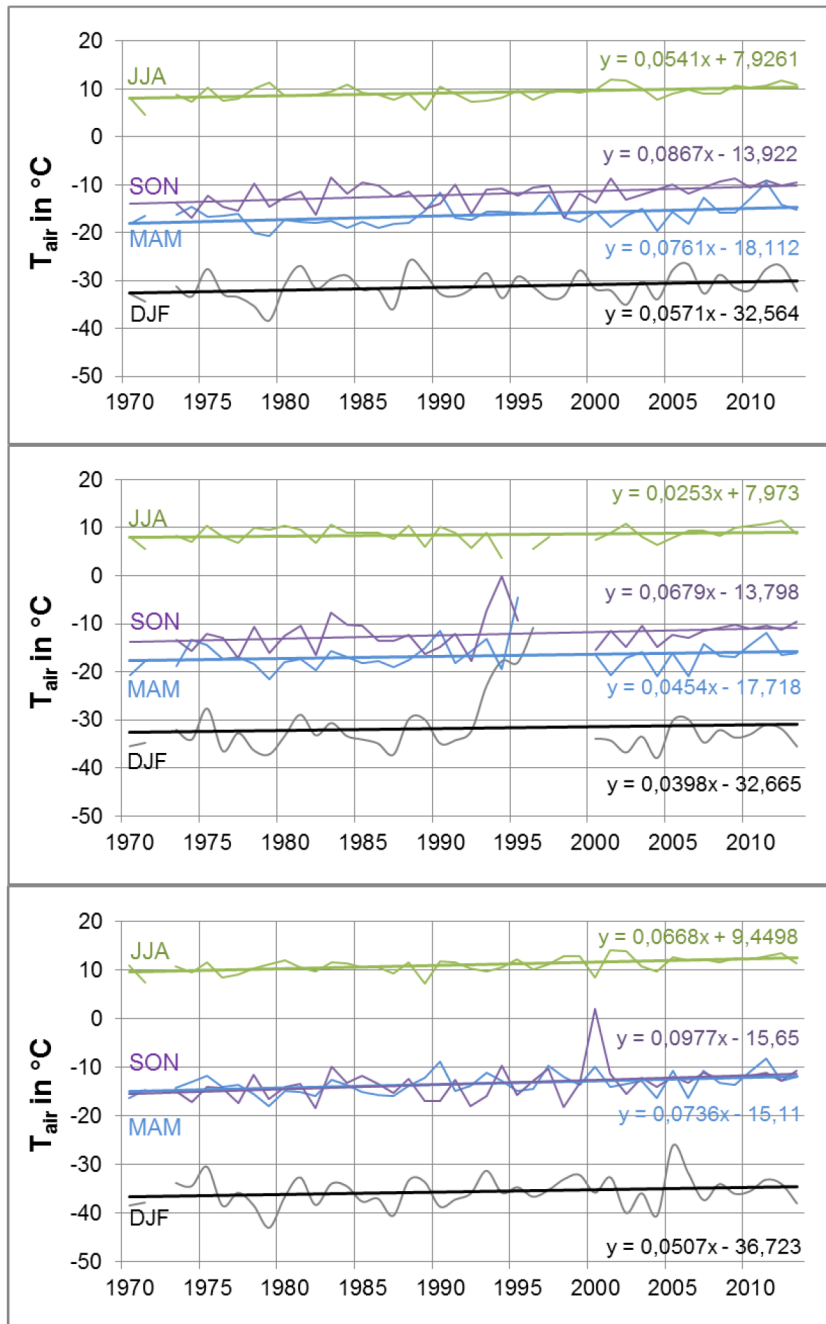


Figure App.2: Air-Temperature time series divided by seasons (winter - DJF; spring - MAM, summer - JJA and fall - SON) of meteorological stations at the Taymyr Peninsula (top: Lake Taymyr (74.5° N, 102.5° E); middle: Saskylah (71.9° N, 114.1° E); bottom: Dzalinda (70.1° N, 113.9° E)).

Acknowledgement

I would like to express my utmost gratitude to Prof. Dr. Christiane Schmullius for the supervision of this dissertation and her enthusiastic encouragement, guidance and valuable critiques during the entire doctoral program. I would also like to extend my gratitude to Prof. Dr. Martin Herold for his intensive supervision and willingness to review my dissertation. Moreover, I would like to thank him for his motivation and inspiration during the last years. I am deeply grateful to both supervisors, who offered and expressed their confidence and trust for my research interests and activities.

In addition to my efforts, this dissertation depends on the support and contribution of several other people as well. I herewith express my sincere thanks to Dr. Christian Hüttich, who gave me the required assistance for all kinds of issues during my research work. In addition, I would like to thank Matthias Forkel (Max Planck Institute for Biogeochemistry, Jena) for the valuable scientific discussions during the preparation and writing phase of the paper. I am particularly grateful for the assistance given by Jonas Eberle for supporting me with numerous computer programming and informatics issues.

Furthermore I would like to express my sincere appreciation to Olivier Arino, Simon Pinnock and Frank-Martin Seifert from ESA ESRIN (Frascati, Italy) for hosting me for three month in 2012 and allowing the usage of land surface temperature data from ATSR-1, ATSR-2 and AATSR within this dissertation. In the same context I would like to thank Prof. Dr. Claude Duguay from the University Waterloo (Waterloo, Canada), for supporting my research in the field of arctic land surface temperature analysis and the productive discussions we had during my time in ESA ESRIN. Additional thanks goes out to Dr. Jan Verbesselt from the Centre for Geoinformation (Wageningen, Netherlands), for the help with

challenging issues during trend and time series analysis as well as valuable scientific discussions during my visit.

I would like to thank the group of the Nansen International Environmental and Remote Sensing Center (St. Petersburg, Russia) for hosting me and for our valuable discussions. Further acknowledgement goes out to the head of the Department Leonid Bobylev as well as Dmitry Pozdnyakov and Lyudmila Lebedeva.

Special thanks goes out to Logan Pryor (Lethbridge, Canada), Jonas Eberle, Robert Eckardt, Tim Robin van Doorn and Dr. Christian Hüttich for proofreading this dissertation and helping me with formatting and design issues. Additionally, I would like to express my thanks to the entire staff of the Department of Earth Observation of the Friedrich-Schiller-University Jena.

Special thanks goes out to my friends and band members from the True Colors, Christian, Christian and Steffen, for the inspiring time we had during our rehearsals and concerts. I would also like to thank all my friends for having a great time here in Jena.

Finally, I express my sincere thanks to my parents Monika and Gerd Urban, for their motivation and support during the entire time of the dissertation and my studies at the Friedrich-Schiller-University Jena. Special credits goes out to my mother for creating the artwork of the cover page. Additional, I would like to thank my sisters Daniela and Kerstin Urban for their support in all kind of situations.

Last but not least, I express my deepest gratitude to my fiancée Maria Palme, who always supported me with valuable discussions and appreciated critics. Thank you for believing in me, laughing with me, your patience and giving me so much love. This dissertation is dedicated to you!

Jena, August 2014

Marcel Urban

Curriculum Vitae

PERSONAL DATA

Surname, Given name: Urban, Marcel
Date and place of birth: 31st May in 1983, Bad-Saarow
Marital Status: unmarried
Nationality: German
E-mail address: Marcel.Urban@uni-jena.de / Marcel.Urban@gmail.com

PROFESSIONAL DEVELOPMENT

01/2011 – 08/2014 PhD student at the Department of Earth Observation at the Friedrich Schiller University, Jena
06/2012 – 08/2012 German Trainee at ESA – ESRIN in Frascati, Italy
08/2009 – 01/2011 research assistant at the Department of Earth Observation at the Friedrich Schiller University, Jena - ESA Data User Element (DUE) Permafrost
11/2007 – 07/2009 research assistant at the Department of Earth Observation at the Friedrich Schiller University, Jena - GOFC-GOLD, Tutorial for students (Image Processing)
05/2007 – 10/2007 research assistant at the Smithsonian Conservation and Research Center in Front Royal, Virginia, USA
12/2006 – 04/2007 research assistant at the Department of Earth Observation at the Friedrich Schiller University, Jena - Vanuatu Carbon Credits Project

05/2006 – 02/2007 student assistant at the Department of Earth Observation at the Friedrich Schiller University, Jena - Development of a database for satellite imagery, Tutorial for students (Image Processing)

UNIVERSITY EDUCATION

2009 – 2010 Master of Science in Geoinformatics (Ø 1.1 - ETCS: A)
M.Sc. Thesis (Ø 1.0 - written in german)

2007 – 2009 Study of Geoinformatics at the Friedrich-Schiller-University Jena (M.Sc.) – Remote Sensing

2006 Bachelor of Science in Geography (ECTS: B) - B.Sc. Thesis (Ø 1.3 - written in german)

2003 – 2006 Study of Geography at the Friedrich-Schiller-University Jena (B.Sc.) – Remote Sensing and Geoinformatics

INTERNSHIPS AND PRACTICAL EXPERIENCES

2012 German Trainee at ESA – ESRIN in Frascati, Italy (3 month)

2011 ESA Summer School Land Training Course 2011, Krakow, Poland (1 week)

2011 Summer School on Climate and Environmental Change, St. Petersburg, Russia (1 week) (practical lecture given on data processing in ENVI IDL)

2010 Internship at “Max Planck-Institut Biogeochemie (MPI-BGC)”, Jena (8 weeks)

2009 Field Campaign: Hyperspectral work, Thuringian Forest, Germany

2006 Internship at “Thüringer Landesvermessungsamt”, Erfurt (6 weeks)

2006 Field Campaign: AGRISAR, Demmin, Germany (1 week)

SOCIAL CIVIL SERVICE

2002 – 2003 „Helios Klinikum“, Bad-Saarow

SCHOOLING

2002 Abitur at the „Geschwister-Scholl-Gymnasium“, Fürstenwalde

MISCELLANEOUS QUALIFICATIONS

Computer literacy: ENVI, Trimble eCognition, ERDAS Imagine, PCI Geomatica, ArcGIS, GAMMA RS

Programming Skills: IDL, MATLAB, R, Java, Microsoft Office Processing (Microsoft Word, Excel, PowerPoint, Outlook etc.)

Further education: Workshop 2004 – Science and Applications of Hyperspectral Data (Dipl. Geol. Andreas Müller, DLR – German Aerospace Center)

Workshop 2008 – Interferometric SAR Processing (Dr. Maurizio Santoro, GAMMA Remote Sensing AG)

Workshop 2009 – Modular Programming using IDL (Dipl.-Inf. Martin Habermeyer, DLR – German Aerospace Center)

Linguistic proficiency: English - fluent
 French - moderate

PUBLICATIONS LIST

2014

- Eberle, J., **M. Urban**, A. Homolka, C. Hüttich & C. Schmullius (2014): Multi-Source Data Integration and Analysis for Land Monitoring in Siberia. – Book Chapter (in Review).
- Semenova, O., L. Lebedev, N. Volkova, I. Korenev, M. Forkel, J. Eberle & **M. Urban** (2014): Detecting immediate wildfire impact on runoff in a poorly-gauged mountainous permafrost basin. – Hydrological Sciences Journal (accepted).
- Urban, M.**, M. Forkel, J. Eberle, C. Schmullius & M. Herold (2014): Pan-arctic climate and land cover trends derived from multi-variate and multi-scale analysis (1981 - 2012). – Remote Sensing - Special Issue on Remote Sensing of Changing Northern High Latitude Ecosystems, 6, 3, 2296-2316.
- Urban, M.**, M. Voltersen, S. Pöcking, S. Hese, M. Herold & C. Schmullius (2014): Multi-Scale Vegetation and Water Body Mapping of the Northern Latitudes in Siberia with Optical Remote Sensing. – Book Chapter (in Review).

2013

- Urban, M.**, J. Eberle, C. Hüttich, C. Schmullius & M. Herold (2013): Comparison of satellite derived Land Surface Temperature and Air Temperature from meteorological station on pan-arctic scale. – Remote Sensing, 5, 2348-2367.
- Urban, M.**, M. Forkel, C. Schmullius, S. Hese, C. Hüttich & M. Herold (2013): Identification of Land Surface Temperature and Albedo Trends in AVHRR Pathfinder data from 1982 to 2005 for northern Siberia. – International Journal of Remote Sensing, 34, 12, 4491-4507.

2012

- Urban, M.** et al. (2012): A fractional vegetation cover remote sensing product on pan-arctic scale - Dataset #779575 - PANGAEA - Data Publisher for Earth & Environmental Science.
- Hese, S., M. Voltersen & **M. Urban** (2012): High Resolution Land Cover Mapping and the Arctic Thermokarst Lake Change Monitoring in the DUE Permafrost Project. In: Borg, E., H. Daedelow & R. Johnson (Hrsg.): RapidEye Science Archive (RESA): Von Algorithmus zum Produkt. 4. RESA Workshop. Berlin: GITO, 257-274.
- Hese, S. & **M. Urban** (2012): Water Body and Tree Line Change Mapping. In: Borg, E., H. Daedelow & R. Johnson (Hrsg.): RapidEye Science Archive (RESA): Von Algorithmus zum Produkt. 4. RESA Workshop. Berlin: GITO, 311-319.

Pinnock, S., O. Arino, **M. Urban** & C. Duguay (2012): GlobTemperature. Proceedings of the 3rd MERIS/(A)ATSR and OCLI-SLSTR (Sentinel-3) Preparatory Workshop, Frascati, Italy, 15 - 19 October 2012, ESA Special Publication SP-708 (CD-ROM).

2011

Urban, M., C. Schmullius, S. Hese & M. Herold (2011): Using Coarse Resolution Land Surface Temperature Time Series Data for Vegetation Analysis in the Taiga Tundra Transition Zone. A Case Study for Yamal, Krasnoyarsk Krai and Yakutia. – AGU Fall Meeting 2011, San Francisco, California, USA. (oral presentation)

Voltersen, M., **Urban, M.**, S. Hese & C. Schmullius (2011): High resolution monitoring of lake object structure changes in arctic permafrost regions. – AGU Fall Meeting 2011, San Francisco, California, USA. (poster presentation)

2010

Urban, M., S. Hese, M. Herold, S. Pöcking & C. Schmullius (2010): Pan-Arctic Land Cover Mapping and Fire Assessment for the ESA Data User Element Permafrost. – PFG Photogrammetrie, Fernerkundung, Geoinformation, 4, 283-293.

Urban, M., M. Herold, S. Hese, S. Pöcking & C. Schmullius (2010): Synergistic Analysis of Coarse Resolution Vegetation and Land Cover Data for Permafrost Monitoring. – Proceedings of the ESA Living Planet Symposium, 28 June - 2 July 2010, Bergen, Norway.

Pöcking, S., S. Hese, **M. Urban**, M. Herold & C. Schmullius (2010): High Resolution Vegetation and Water Body Mapping in Arctic Permafrost Regions. – Proceedings of the ESA Living Planet Symposium, 28 June - 2 July 2010, Bergen, Norway.

2009

Urban, M., M. Herold, C. Schmullius & S. Bartalev (2009): Synergistic analysis of global land cover data sets indicating area of loss in Russian agriculture between 1992 - 2001. – Proceedings of 33rd ISRSE, 4 - 8 May 2009, Stresa, Italy.

Berger, C., **M. Urban** & M. Herold (2009): Accuracy assessment for estimating historical forest area changes - a REDD case study for Pacific island state of Vanuatu. – Proceedings of 33rd ISRSE, 4 - 8 May 2009, Stresa, Italy.

Sambale, J., M. Herold, R. Eckardt & **M. Urban** (2009): Developing national forest monitoring capacities for REDD participation of Vanuatu. – Proceedings of 33rd ISRSE, 4 - 8 May 2009, Stresa, Italy.

2008

Urban, M., M. Herold, S. Bartalev & C. Schmullius (2008): Synergistic analysis of global land cover data sets indicating areas of loss in Russian agriculture between 1992 – 2001. – Poster presentation at the EGU General Assembly April 2008, Vienna, Austria.

2007

Herold, M., J. Sambale, M. Lindner, **M. Urban** & S. Weaver (2007): Satellite based monitoring of the national forest resources in the pacific island state of Vanuatu. – Proceedings of the Tri-National Conference 2007 of the Swiss, Austrian and German Society for Photogrammetry and Remote Sensing, 19 -21 June 2007, Basel, Switzerland, 319-398.

Jena,

Ort, Datum

Marcel Urban

Statement of Authorship

Selbstständigkeitserklärung:

Ich erkläre, dass ich die vorliegende Arbeit selbstständig und unter Verwendung der angegebenen Hilfsmittel, persönlichen Mitteilungen und Quellen angefertigt habe.

Jena,

Ort, Datum

Marcel Urban